CENTRE D'HYDROGÉOLOGIE
UNIVERSITÉ DE NEUCHÂTEL

Use of stable isotope analysis to assess biodegradation of volatile organic compounds in the unsaturated subsurface

PhD thesis presented to the faculty of Sciences of the University of Neuchâtel to satisfy the requirement for the degree of Doctor of Philosophy in Science

by

Daniel Bouchard

Thesis defence date: January 29th 2007
Public presentation date: February 23rd 2007

Ph.D thesis evaluation committee:

Daniel Hunkeler, Associate professor (thesis director), University of Neuchâtel, Switzerland
Patrick Höhener, Professor (thesis co-director), University of Provence (Aix-Marseille I), France
Stefano M. Bernasconi, Senior scientist, ETH Zürich, Switzerland
Pierre Perrochet, Professor, University of Neuchâtel, Switzerland
Peter Kjeldsen, Associate professor, Technical University of Denmark

Université de Neuchâtel

FACULTE DES SCIENCES
Secrétariat-Décanat de la faculté
- Rue Emile-Argand 11
- CP 158
- CH-2009 Neuchâtel

IMPRIMATUR POUR LA THESE

Use of stable isotope analysis to assess biodegradation of volatile organic compounds in the unsaturated subsurface

Daniel BOUCHARD

UNIVERSITE DE NEUCHATEL

FACULTE DES SCIENCES

La Faculté des sciences de l'Université de Neuchâtel,
sur le rapport des membres du jury

MM. D. Hunkeler (directeur de thèse),
P. Perrochet, S. Bernasconi (ETH Zürich),
P. Kjeldsen (DTU, Danemark)
et P. Höhener (Marseille)

autorise l'impression de la présente thèse.

Neuchâtel, le 22 février 2007

Le doyen :
T. Ward

UNIVERSITE DE NEUCHATEL
FACULTE DES SCIENCES
Secrétariat-décanat de la faculté
Rue Emile-Argand 11 - CP 158
CH-2009 Neuchâtel

Table of contents

Préface

Assis devant l'ordinateur, prêt à entamer la rédaction des remerciements symbolisant la dernière phase de ce travail, et ce après 4 années de gros efforts, je me demande si je dois me réjouir ou laisser la nostalgie s'emparer de moi…

Je voudrais tout d'abord exprimer mes meilleurs remerciements à Dr. Daniel Hunkeler, directeur de cette thèse. J'ai arrêté de compter les nombreuses heures passées dans son bureau à discuter, et ce même par les soirs et les jours de week-end, mais surtout à m'enseigner toute l'exactitude requise pour devenir un homme de science et à m'expliquer un des nombreux phénomènes naturels en relation avec les isotopes. Mère nature est bien compliquée parfois à comprendre, mais Daniel a toujours apporté solutions à mes problèmes (que je croyais être un vrai Problème), parfois avec une aisance déconcertante. Egalement, mes remerciements vont à Dr. Patrick Höhener pour son rôle de co-directeur, pour son soutient constant tout au long de ce travail, par l'apport de ses idées et de longues discussions enrichissantes. Malgré la distance qui séparait nos bureaux respectifs, bien des fois j'avais l'impression que Patrick était dans le même bâtiment que moi.

Ce travail de doctorat fut réalisé grâce à la contribution financière de l'Office fédéral suisse pour l'Education et la Recherche dans le cadre du plan d'action de recherche européen COST 629. Egalement, ce projet a été enrichi par la collaboration d'un autre projet européen : le projet GRACOS. Ainsi, je tiens à remercier tous les collaborateurs à ce projet et plus spécialement l'équipe du Danish Technical University, du Danemark, sous la direction du Prof. Peter. Kjeldsen. Une dernière collaboration, et non la moindre, a permis à cette étude d'atteindre ses objectifs par l'ajout de modélisations numériques. Mes remerciements vont de ce fait à Dr. Petros Gaganis, de l'Université Aegean en Grèce, pour avoir maîtrisé ce code numérique à ma place et me sauvant ainsi de nombreuses heures de casse-tête.

Dans la même lancée, je remercie Dr. Fabien Cornaton de m'avoir présenté Pierre-Simon Laplace et aussi Dr. Richard Baltensperger de m'avoir présenté Paul Dirac, mais surtout pour leur aide combien pertinente concernant les formulations mathématiques contenu dans le présent document et l'explication approfondie de certains phénomènes physiques. Je tiens à

remercier Prof. Pierre Perrochet également pour son aide concernant la phase mathématique de ce travail et de sa présence parmi le jury de thèse, ainsi que les autres membres externes du jury, soit le Prof Peter Kjelsen et le Dr. Stefano Bernasconi.

Mes longues heures passées au laboratoire auraient été monotones sans la présence des autres membres du « Hunke's group » (Yumiko, Barbara, Ludovic et Marie-Eve), pour parler bien sûr, mais bien souvent aussi pour m'aider pendant des expériences en cours ou pour régler ce GC-MS quelques fois capricieux.

Un long travail nécessite obligatoirement de bonnes pauses afin de recharger les batteries et de repartir de plus belle le temps (le lundi matin…) venu. Plus des amis que des collègues de travail, les nombreuses heures passées à discuter, à jaser, à parler, à « déparler », à « s'astiner » et à rire autour d'un bon jus de pomme avec les collaborateurs du CHYN seront pour moi de très doux souvenirs. Sans s'en rendre compte, d'autres personnes ont grandement contribué à m'aider à garder le moral par moments difficiles, en l'occurrence la gang de chums de Fribourg et du Jura, mes amis au Québec, « mon » équipe de basket, et bien sûr, ma famille.

Je ne s'aurais passer sous silence le douloureux évènement survenu au cours de ce travail de 4 ans, où la Mort est venu chercher la vie de mon petit frère de 25 ans. Etant donné l'incertitude du temps qui nous est alloué de vivre, c'est avec l'appui ressenti de mon petit frère que je me suis déterminé à mener à terme ce travail dans l'optique que les résultats de recherche pourront aider mon prochain. On va se revoir mon Juss, mais pas tout de suite…

Abstract

The general aim of the project is to evaluate the feasibility of using compound-specific isotope analysis (CSIA) to assess biodegradation of petroleum hydrocarbons in the unsaturated zone.

The first objective was to quantify the isotope enrichment factors during biodegradation of several volatile organic compounds (VOCs) commonly found on petroleum hydrocarbon contaminated sites. These microcosm experiments were carried out with unsaturated soil sediments under aerobic conditions. The results confirmed the possibility to monitor an isotope enrichment in the remaining VOCs in the air phase. The magnitude of isotope enrichment factors was small for carbon and large for hydrogen.

A column experiment was then carried out to investigate the possible role played by diffusion in the isotope fractionation of migrating VOC vapours. A 1.06 m long column filled with alluvial sand was used with a VOC source. During an initial period after source emplacement, the heavy isotope ^{13}C became increasingly depleted with distance from the source. This observation can be explained by the faster diffusion of molecules containing ^{12}C and was confirmed by analytical simulations that attributed different diffusion coefficients to molecules with a different isotopic composition. Later, the isotope profile levelled out and for some compounds an enrichment of ^{13}C with distance was observed indicating biodegradation. However, some compounds were also affected by an enrichment of ^{13}C at the source as the compounds were depleting form the source. It was shown that the source isotope evolution of these compounds followed a Rayleigh trend with the ratio of diffusion coefficients for molecules with a different isotopic composition as isotope fractionation factor.

A highly-controlled field experiment conducted in Denmark as part of the GRACOS project provided a unique opportunity to evaluate if similar isotope trends also occur at the field scale. The experiment consisted of burying an artificial fuel source in the unsaturated zone of a sandy aquifer. Indeed, a similar isotope evolution as in the column study was observed with an initial depletion of ^{13}C with distance followed by a levelling out of the isotope profile and enrichment of ^{13}C. To evaluate the relative contribution of diffusion and biodegradation on

isotope shifts in more detail, the concentration and isotope ratio evolution was simulated using a modified numerical code (MOFAT). It was possible to reproduce the observed trends using independently estimated biodegradation rates and isotope enrichment factors for biodegradation and diffusion.

Finally, based on the knowledge gained on isotope fractionation with the previous experiments, the expected isotope evolution was simulated for VOC sources with different geometries (e.g. point source, floating pool). The simulations demonstrated that a linear relationship between the ln of the mass flux and the isotope changes can be observed in a diffusion controlled system under steady state conditions analogous to the Rayleigh equation. However, the slope of the relationship is smaller than the isotope enrichment factor again illustrating the importance of the diffusion isotope effect.

In conclusion, the study demonstrates that assessment of biodegradation in the unsaturated zone is more complex than in the saturated zone because the diffusion process influences isotope ratios as well. However, under steady state conditions and as long as the compound does not significantly deplete, isotope data can provide qualitative and possible quantitative information on the degree of biodegradation. While the substantial shift of isotope ratios during source depletion complicates the identification of biodegradation trends, it may help to identify the final stage of the evolution of a VOC source.

Keywords

Biodegradation; natural attenuation; petroleum hydrocarbons; stable isotopes; unsaturated zone.

Résumé

L'objectif premier de ce projet consiste à évaluer la faisabilité d'utiliser l'analyse isotopique spécifique à chaque composé afin de démontrer la biodégradation des hydrocarbures pétroliers dans la zone non saturée.

Le premier objectif était de quantifier le facteur d'enrichissement isotopique pendant la dégradation de plusieurs composés organiques volatiles (COVs) communément retrouvés sur des sites contaminés. Ces expériences en microcosmes ont été menées avec des sédiments de sol non saturés et sous des conditions aérobiques. Les résultats ont confirmé la possibilité d'observer un enrichissement isotopique dans la fraction restante du COV en phase gazeuse. La magnitude du facteur d'enrichissement isotopique mesurée était faible pour le carbone et nettement plus élevée pour l'hydrogène.

Une expérience en colonne a été réalisée pour investiguer sur le rôle possiblement joué par le processus de diffusion dans le fractionnement isotopique. Une colonne longue de 1,06 m et remplie de sable alluvial fut utilisée et une source liquide de plusieurs COVs fut placée à une extrémité. Pendant la période initiale peu après la mise en place de la source, une diminution croissante du carbone lourd ^{13}C avec la distance était notable. Cette observation peut être expliquée par une diffusion plus rapide des molécules ne contenant que des ^{12}C ; hypothèse par la suite confirmée par des simulations analytiques qui attribuèrent différents coefficients de diffusion aux molécules de composition isotopique différente. Par la suite, le ratio isotopique s'est uniformisé indépendamment de la distance. Cependant, quelques composés ont été affectés par un enrichissement en ^{13}C à la source pendant que ce dernier s'épuisait de la fraction liquide. Il fut montré que l'évolution isotopique de ces composés à la source suivait une tendance dite de Rayleigh et que le ratio des deux coefficients de diffusion dû à des molécules isotopiquement différentes indique le facteur d'enrichissement.

Une expérience terrain avec un dense réseau de points de prélèvement a été réalisée au Danemark dans le cadre du projet GRACOS et a procurée une chance unique d'évaluer si des tendances similaires occurrent également à plus grande échelle. L'expérience consistait à enterrer une source artificielle de fuel dans la zone non saturée d'un aquifère sableux. Telle

qu'attendue, une évolution isotopique similaire à celle observée pendant l'expérience en colonne fut mesurée, avec une phase initiale d'appauvrissement en ^{13}C avec la distance, suivie par une uniformisation du ratio, et se terminant par un enrichissement en ^{13}C. Afin d'évaluer la contribution relative de la diffusion et de la biodégradation sur le shift isotopique plus en détail, l'évolution des concentrations et du ratio isotopique a été simulée à l'aide d'un code numérique modifié (MOFAT). Il a été possible de reproduire les tendances observées en utilisant la vitesse de biodégradation évaluée de façon indépendante ainsi que les facteurs d'enrichissement reliés à la biodégradation et à la diffusion.

Finalement, en se basant sur les connaissances développées sur le fractionnement isotopique par les expériences préalables, l'évolution isotopique attendue par d'autres sources de COV ayant une géométrie différente a été simulée (par ex. : une source flottante sur la nappe phréatique). Les simulations ont démontré qu'une relation linéaire entre le ln du flux de masse et le changement isotopique peut être observée lors de diffusion des COVs en régime permanent, analogiquement à l'équation de Rayleigh. Cependant, l'enrichissement isotopique net est plus petit que le facteur d'enrichissement, ceci démontrant encore une fois l'importance de la présence d'un isotope lourd dans la molécule.

En conclusion, l'étude montre que l'obtention de preuve de la biodégradation des COVs dans la zone non saturée par l'analyse isotopique est plus complexe que dans la zone saturée, car l'effet de diffusion affecte également le ratio isotopique. Cependant, sous régime permanent et aussi longtemps que le composé reste en quantité suffisante à la source, le ratio isotopique peut fournir des informations autant qualitatives que quantitatives sur le degré de biodégradation. Pendant que le shift substantiel du ratio isotopique à la source complique l'identification des tendances reliées à la biodégradation, ceci aide néanmoins à l'identification de l'étape finale de l'évolution du COV à la source.

Mots clés

Biodégradation; atténuation naturelle; hydrocarbures pétroliers; isotopes stables; zone non saturée.

Chapter 1

General introduction

1.1 Behaviour of volatile organic compounds in the unsaturated zone

The wide use of petroleum hydrocarbons as primary source of energy unfortunately leads to frequent spills of these non aqueous phase liquids (NAPLs) to soils. Spilled NAPLs migrate downward through the unsaturated zone resulting in subsurface contamination. Due to interfacial tension, a fraction of the spilled NAPL is retained in the pores of the unsaturated zone and creates a long term source of contaminants from which volatile organic compounds (VOCs) are volatilizing for potentially long periods. In the unsaturated zone, migration by vapour phase diffusion was shown to be the predominant transport process of VOCs under natural conditions and consequently creates a vapour phase contaminant plume in the soil gas (Baehr & Corapcioglu, 1987; Christophersen *et al.*, 2005; Conant *et al*., 1996; Jury *et al*., 1984; Pasteris *et al.,* 2002; Silka, 1988). This gaseous transport of VOCs has been largely recognized as a mechanism for groundwater contamination even if the NAPL has not reached the water table (Baehr, 1987; Baehr *et al.,* 1999; Falta *et al.,* 1989). The vapour phase diffusion is strongly influenced by the partitioning of VOCs between the gas, the water and the solid phase and by the geometry of the soil pores. In addition to diffusion, density-driven forces and gas-pressure gradient was shown in some cases to significantly contribute to expand the size of the plume (Conant *et al*., 1996; Costanza-Robinson & Brusseau, 2002; Smith *et al.,* 1996), whereas several studies demonstrated that biodegradation restrains the spreading of contaminants.

1.2 Monitoring biodegradation during natural attenuation of contaminants

Natural attenuation is a widely applied strategy to restore petroleum hydrocarbon contaminated sites that is increasingly accepted by regulators (Mulligan & Yong, 2004; Rittmann, 2004; Sondermann & Knorpp, 2004). The strategy relies on the capacity of indigenous microorganisms to eliminate contaminants from the subsurface under natural conditions and thus tries to limit the use of engineering technologies. Over the past decade,

this remedial strategy became an attractive alternative to engineered remediation as it was shown to reduce the risk of impacts on man and environment to an acceptable level at several petroleum hydrocarbon contaminated sites with limited economical investments (Hinchee *et al.*, 1995; NRC, 2000). However, to make this strategy reliable, it is imperative to demonstrate that biodegradation of hydrocarbons are actually occurring at the site. Microbial breakdown is usually the only process to decompose the compound into CO_2 and clear evidence must be provided that the VOC concentration depletion is linked to the microbial activity and not to physical processes like sorption, dilution and dispersion, which is challenging. It is important to predict the transport and fate of the contaminant in the soil air in order to assess health risks to communities in the area of the contaminated site or to evaluate the threat of a contamination of nearby public water wells. A brief overview of common methods used to demonstrate in situ biodegradation of contaminants is given in the following section.

1.2.1 Common methods

The most common methods to demonstrate biodegradation of VOCs in the unsaturated zone and their advantages and disadvantages are summarized in Table 1.1. A number of studies assessed *in situ* biodegradation in the unsaturated zone by monitoring the depletion of both molecular oxygen (O_2) and VOC concentration and the increase of carbon dioxide (CO_2) concentration in the soil gas (Dakhel *et al.,* 2003; Franzmann *et al.*, 1999; Hers *et al.,* 2000; Kaufmann *et al.,* 2004; Ostendorf & Kampbell, 1991). However, O_2 and VOC concentrations can be highly variable at a seasonal scale due to moisture variations by infiltrating rainwater. The recharge of water in pores decreases the O_2 diffusion and thus limits VOCs biodegradation (Davis *et al.*, 2000). Moreover, interpretation of CO_2 and VOC concentration can be impeded by vapour phase transport due to water table fluctuations, barometric pressure variation and rain water infiltrations (Parker, 2003). In addition, CO_2 can also originate from other sources such as root respiration, oxidation of soil organic matter and dissolution of carbonate minerals (Franzmann *et al.*, 1999). Finally, concentrations of CO_2 do not provide clear evidence for degradation of a specific compound within a mixture.

Table 1.1

Advantages and limitations of some common methods used to assess biodegradation of VOCs in the unsaturated zone.

	Advantage	Limitation/disadvantage
VOC concentration	Information about single compound	Concentration variations can be due to other processes than biodegradation Interpretation depends on the analytical procedure used
O_2 concentration	Simple, easy and inexpensive.	No information about which compound is degraded
CO_2 concentration	Simple, easy and inexpensive.	No information about which compound is degraded. Various possible origins: VOC, organic matter, carbonate. Measurement influenced by soil water content.
CH_4 concentration	Reliable if no other source of methane	No information about which compound is degraded. Methanogenesis may not be related to compound loss
^{13}C in CO_2	Can be inexpensive.	Requires complete mass balance.
	Additional information about origin of CO_2.	No information about which compound is degraded. Various possible origins: VOC, organic matter, carbonate.
^{14}C in CO_2	Clear evidence for complete mineralization of petroleum hydrocarbons.	Expensive.
		No information about which compound is degraded
Modelling	Links concepts of biodegradation with field observations	No ready-to-use model: must be validated for each site. Time-consuming. Large data requirement.
Microbial count	Direct correlation with occurrence of biodegradation	Microbial enumeration is complicated. Heterogeneous distribution in the subsurface. Expensive and time-consuming. Difficult to relate microbial abundance to degradation rate.
Biomolecular/nucleic acid-based method	Analysis preserve the in situ metabolic status and community composition	Inefficiency extraction of cells, DNA and RNA. Possible variation in nucleotide sequences. Difficult to relate microbial parameters to degradation rate.

Ref: Madsen (1991), Riser-Roberts (1998) and Wiedemeier *et al.* (1999)

The use of stable isotope analysis to demonstrate biodegradation in the unsaturated zone are mainly applied to $\delta^{13}C$ of soil gas CO_2 (Aggarwal & Hinchee, 1991; Conrad & DePaolo, 2004; Feng *et al.*, 2000; Jackson & Pardue, 1999; Suchomel *et al.*, 1990). However, $\delta^{13}C$

variations in CO_2 can also be due to soil organic matter degradation, and sometimes the ^{14}C measurements were used to distinguish between CO_2 from recent soil organic matter or from fossil petroleum (Kirtland *et al.*, 2005).

1.2.2 Compound-specific isotope analysis

Compound-specific isotope analysis (CSIA) has recently been shown to be an effective tool to confirm in situ biodegradation by the indigenous microbial population. Therefore, the method is increasingly used to assess and sometimes to quantify *in situ* biodegradation of various types of organic contaminants in the saturated zone (Beneteau *et al.*, 1999; Chu *et al.*, 2004; Griebler *et al.*, 2004; Hunkeler *et al.*, 2005; Hunkeler *et al.*, 1999; Kelley *et al.*, 1997; Kirtland *et al.*, 2003; Kolhatkar *et al.*, 2002; Mancini *et al.*, 2002; Meckenstock *et al.*, 2002; Morrill *et al.*, 2005; Richnow *et al.*, 2003a; Richnow *et al.*, 2003b; Sherwood Lollar *et al.*, 2001; Song *et al.*, 2002; Steinbach *et al.*, 2004; Sturchio *et al.*, 1998). The isotopic method is based on the occurrence of different reaction rates for molecules with light and heavy isotopes, respectively. The presence of a ^{13}C atom in the bond that is broken in the initial enzymatic transformation step can slightly slow down the biodegradation rate (for more information see section 1.4). As a consequence, ^{13}C–compounds accumulate in the remaining contaminant pool over time. A growing body of literature has described how isotope data can be used to assess and quantify biodegradation in the saturated zone of the subsurface (see recent reviews by Elsner *et al*. (2005), Meckenstock *et al.* (2004) and Schmidt *et al,* (2004)).

However, there is little information for using CSIA in the unsaturated zone. Preliminary attempts to monitor compound-specific $\delta^{13}C$ values of organic compounds in the unsaturated zone provided optimistic results. A significant ^{13}C enrichment in the remaining TCE and DCE in the air phase with respect to the original isotopic signature of PCE was observed by Kirtland *et al.* (2005) while Stehmeier *et al.* (1999) monitored a ^{13}C enrichment for an undetermined contaminant.

1.3 Aims and approach of the study

In contrast to the saturated zone, biodegradation is still difficult to prove in the unsaturated zone due to a lack of appropriate assessment methods and because VOC concentrations can be highly variable in space and time. Given that CSIA can provide evidence for biodegradation of individual compounds, which is difficult to achieve with other methods,

there is a high interest to apply the method also in the unsaturated zone. Therefore, the investigations carried out in the framework of this thesis aim to evaluate whether CSIA can be used to demonstrate biodegradation of volatile organic compounds in the unsaturated zone. To achieve the goal, experiments at different scale were carried out, from the batch to the field scale to investigate isotope fractionation due to transport and biodegradation under unsaturated conditions. The experiments were completed by analytical and numerical calculations to gain additional insight into factors controlling the observed isotope evolution and to evaluate in more detail the possibilities and limits of the isotope approach. Each type of experiment is related to a chapter that is intended, except for chapter 1, to be published in international scientific journals.

Chapter 1:

The following sections of chapter 1 introduce some important concepts and terms about stable isotopes, discuss the origin of isotope fractionation during biodegradation and factors that influence its magnitude. In addition, it is demonstrated how isotope fractionation is incorporated into analytical and numerical reactive transport calculations that are carried out in chapters 3 to 5.

Chapter 2:

Existing data on carbon isotope fractionation for VOC biodegradation were mainly determined for anaerobic, saturated conditions. Therefore, in this chapter, microcosm studies were carried out under aerobic, unsaturated conditions to quantify isotope fractionation factors during biodegradation of typical gasoline components. The effect of molecules size and structure on the magnitude of isotope fractionation was also evaluated. The obtained isotope fractionation factors were used in subsequent studies for data interpretation and modelling.

Chapter 3:

The laboratory column experiment investigated the expected diffusion effect on isotope ratios of VOCs in the migrating vapour. In addition, the evolution of the isotope ratio of VOCs at the NAPL source was evaluated. A mathematical model was developed that incorporates isotope fractionation due to diffusion and biodegradation to reproduce the observed isotope

evolution. The detailed data set provided a good basis to test the modelling approach as a basis for further application in the field study.

Chapter 4:

The fourth chapter focuses on a field experiment that was conducted in Denmark in order to evaluate the fate of 13 volatile organic compounds (VOCs) that were buried as an artificial fuel spill in the unsaturated zone. This field experiment aimed to confirm the processes controlling the isotope ratio observed in the laboratory and to gain a better understanding of their evolution at a field scale. The measured isotope ratios were reproduced by means of numerical modelling. To separate the influence of diffusion and biodegradation, isotope fractionation associated with each process was simulated individually. In addition, the field experiment intends to evaluate the potential of CSIA to assess the occurrence of biodegradation in the unsaturated zone.

Chapter 5:

Based on the knowledge gained in the previous chapters, the expected isotope evolution was simulated for VOC sources of different configuration (e.g. point source, floating pool) and for different phases of source evolution and VOC transport. The aim of these studies was to gain additional insights under what conditions isotopes can be used to assess biodegradation and whether quantitative information can be derived.

Chapter 6:

Finally the last chapter synthesizes the findings of the different studies and draws general conclusions about the applications of CSIA in unsaturated zone studies.

1.4 Theory on stable isotopes

1.4.1 Origin of the isotope effect

The total mass of an atom is essentially concentrated in the nucleus which is composed of protons and neutrons. The number of protons defines the element and the number of neutrons defines the isotope. The predominant form of carbon atoms (C), the nucleus contains 6 protons and 6 neutrons, and is conventionally given as ^{12}C (carbon-12). The carbon atom with

a 7th neutron is conventionally denoted as ^{13}C and commonly termed heavy isotope as the atom is now 1g per mol heavier than the predominant ^{12}C. For the predominant hydrogen atom (H), the nucleus is uniquely composed of 1 proton. With the presence of a neutron, the heavy isotope is termed ^{2}H or more frequently deuterium (D). Heavy isotopes naturally occur in nature and the abundance differs for each element. The mean global abundance of ^{13}C is 1.11%, whereas the abundance of D is 0.015% compared to their lighter counterpart (IUPAC, 1991).

The presence of a supplemental neutron in the nucleus of an atom confers slightly different physical properties to the molecule containing that atom. For instance, it was shown by Narten & Kuhn (1961) that ^{13}C-benzene had a higher vapour pressure than ^{12}C-benzene, and later indirectly confirmed by Bartell & Roskos (1966) when demonstrating a greater surface tension (intermolecular attraction) for the lighter compounds. A smaller lipophilicity was observed for molecules including heavy isotopes such as labelled aromatic compounds (El Tayar *et al.*, 1984). Finally, diffusion (Müller & Wienholz, 1967) and carrier-gas transport (Craig, 1968; Hoering & Moore, 1958) were shown to change the isotope composition during migration of natural gases.

The presence of a supplemental neutron does not create any additional electrical charges and thus the potential energy surface characterizing the chemical bond is invariable. However, the increase in nucleus mass directly affects the vibrational energy of molecules. The vibration frequency of a bond is given by (Melander & Saunders, 1980):

$$\nu = \frac{1}{2\pi}\sqrt{\frac{\kappa}{\mu}} \qquad (1.1)$$

where ν is the frequency of vibration of two atoms, κ is a constant force of the bond and μ is the reduced mass given by:

$$\mu = \frac{M_{w1} M_{w2}}{M_{w1} + M_{w2}} \qquad (1.2)$$

where M_{w1} and M_{w2} are the different masses of the atoms involved. As the κ value is independent of the isotope and thus remains constant when either ^{12}C or ^{13}C is involved, only the change in mass can influence the frequency of vibration in equation 1.1. The frequency of vibration influences the level of free energy required for a reaction to proceed. Therefore, the

small distinction in frequency of vibration between chemical species isotopically different is sufficient to create two different levels of activation energy required for the reaction to proceed. Because of the inverse relationship of v and μ, the heavier atomic mass of ^{13}C lowers the vibrational energy and hence increases the energy difference between product and transition state. In a more practical sense, it means that chemical bonds between two light isotopes are more rapidly broken compared to bonds between a light and a heavy isotope.

1.4.2 Factors regulating the magnitude of isotope fractionation during enzymatic processes

The variation in reaction rate between molecules with ^{12}C and ^{13}C is termed as kinetic isotope effect (KIE). Using k to represent the degradation rate coefficient, KIE is defined as:

$$KIE = {}^{l}k / {}^{h}k \qquad (1.3)$$

where l and h stand for light and heavy isotope, respectively. The magnitude of isotope fractionation depends on the nature of the broken bond (e.g. for carbon, C-Cl is larger than C-H) (Cook, 1991), the reaction mechanism (e.g. S_N1 vs S_N2 hydrolysis), and the extent of bond cleavage in the transition state. Since different biodegradation pathways of organic compounds may involve different bonds and reaction mechanisms, the magnitude of the fractionation factor frequently varies depending on the degradation pathway (Cook, 1991; Hall *et al*., 1999; Hirschorn *et al*., 2004; Hunkeler *et al.*, 2005; Morasch *et al.*, 2001; Morasch *et al*., 2002). For instance, oxidation reactions are expected to generate large H and small C isotope effects whereas hydrolytic dehalogenation reactions usually generate the opposite extent, showing larger C isotope effect than H (Westerway, 1987). During the cleavage of the C-Cl bond in the latter pathway, only a small secondary hydrogen isotope effect can be expected.

Additionally, the position of the heavy isotope in the molecule is also important. A significant isotope effect during biodegradation of a molecule is observed only when the heavy isotope is located where the initial enzymatic bond transformation takes place (Cook, 1991; Galimov, 1985; Melander & Saunders, 1980). This position in the molecule is termed reactive position (rp). When the heavy isotope is located elsewhere, i.e. on a non-reactive position (nrp), no significant isotope effect is generally expected and the molecule is degraded at a normal rate. The same molecule can have different reactive positions when degraded by different enzymes.

For compounds such as ^{13}C-methane ($^{13}CH_4$) and ^{13}C-tetrachloromethane ($^{13}CCl_4$), the ^{13}C is always involved in the initial enzymatic bond cleavage. However, this might not be the case for molecules of two carbon atoms or more. Therefore, the size of the molecule is also likely to influence the isotope enrichment. The larger the molecule, the more likely is the heavy isotope at a non-reactive position leading to no isotope effect. Consequently, these ^{13}C "hide" from potential isotope effects and thus tend to diminish the isotope effect, an effect that is sometimes referred to as "dilution". In addition, during enzymatic processes binding steps that proceed bond cleavage can be rate limiting. Therefore, the actually observed isotope effect (denoted as apparent kinetic isotope effect, AKIE) is frequently lower than the KIE. Elsner *et al*. (2005) proposed an equation to correct for the effect of non-reactive positions and to calculate the AKIE:

$$AKIE \approx \frac{1}{1+n\varepsilon/1000} \tag{1.4}$$

where n is the number of atoms of interest composing the molecule and ε is the enrichment factor (and is defined in section 1.4.3). This equation makes it possible to compare KIE between different molecules, independently of their size. However, the equation is only valid if the initial transformation step only involves a single atom of the element of interest.

1.4.3 Notation for isotope ratios and isotope fractionation

Usually isotope data are reported as isotope ratios in the δ notation relative to the VPDB standard according (Clark & Fritz, 1997):

$$\delta C = \left(\frac{R_{sample}}{R_{reference}} - 1 \right) 1000 \tag{1.5}$$

where R_{sample} and $R_{reference}$ is the $^{13}C/^{12}C$ ratio of the measured sample and the reference material, respectively. The magnitude of isotope fractionation between can be expressed by an isotope fractionation factor (α):

$$\alpha = {}^{h}k /{}^{l}k \tag{1.6}$$

The fractionation factor indicates the degree of separation of the isotope ratio between substrate and product and is usually less than one for bond-breaking reactions to indicate a

^{13}C enrichment in the substrate (thus inversely expressed than KIE). The relationship between substrate concentration change and isotope fractionation allows quantifying the fractionation factor. The common equation that describes this progressive partitioning of the isotopic composition of the substrate is (Clark & Fritz, 1997):

$$R = R_0 f^{(\alpha-1)} \quad (1.7)$$

where R and R_0 are the ratio and the initial ratio of heavy to light isotope of the contaminant, respectively, f is the remaining fraction of the contaminant. The derivation of equation 1.7 is based on the classical Rayleigh equation which describes fractional distillation of mixed liquids. The equation 1.7 is only valid for low abundance of the heavy isotope (Hunkeler *et al.*, 2002). The fractionation factor is more conveniently expressed as enrichment factor (ε) according to:

$$\varepsilon = (\alpha - 1) * 1000 \quad (1.8)$$

1.5 Incorporating isotopes into reactive-transport models

1.5.1 Analytical diffusion models

The diffusive transport of dilute VOCs in the unsaturated zone is traditionally modelled by Fick's law (Abriola & Pinder, 1985a; Abriola & Pinder, 1985b; Baehr & Bruell, 1990; Jury *et al.*, 1983) and the model described hereafter relies on the validity of Fick's law as well. Fick's first law in 1 dimension simply reads:

$$F_i = -D\frac{\partial C_i}{\partial x} \quad (1.9)$$

where F is the mass flux (g $m^{-2}d^{-1}$), D is the molecular diffusion coefficient (m^2d^{-1}) and C_i is the concentration of compound i (g m^{-3}). Fick's law is suitable to describe diffusion of dilute species responding to a concentration gradient in a bulk phase, and is commonly utilized in environmental sciences (Scanlon *et al.*, 2000). The validity of the law is restricted in some cases, such as for soil vapour plumes with chlorinated solvents or gasoline, when the vapours created are considerably denser than the surrounding soil gas. In this case, the application of the Stefan-Maxwell equations may be necessary for modelling gas-phase diffusion (Baehr & Bruell, 1990 In the absence of pressure gradient, diffusive transport of gaseous compounds is

assumed to dominate over advective transport, and therefore the latter is frequently neglected. The effective gas diffusion coefficient in the soil air is dependent on the increased mean path length travelled by VOCs, termed the tortuosity factor (τ), and also dependent on either the physical properties of the compound or the volume of voids. Because only the mass fraction of organic molecules in the soil air phase is relevant for mass transport, partitioning of the compound between the different phases composing the system (air, water and solid, eventually liquid NAPL if present) influences diffusion rates. During transient-state diffusion, the sorption-affected diffusion coefficient (D_s) has to be used which is given by (Werner & Höhener, 2003):

$$D_s = f_a \tau D_m \tag{1.10}$$

where D_m (m^2d^{-1}) is the diffusion coefficient in the air phase, τ is the tortuosity factor and f_a is the mass fraction of the compound in the soil air and calculated by (Werner & Höhener, 2003):

$$f_a = \frac{1}{1 + \frac{K_d \rho_s (1-\theta_t) + \theta_w}{H \theta_a}} \tag{1.11}$$

where θ_a, θ_w and θ_t denote the air-filled, water filled and total porosity, respectively, ρ_s denote the density of the solids (g/m^3), H is the air-water partitioning coefficient (or Henry's coefficient) and K_d is the water-solid partitioning coefficient. To simplify the calculations, instantaneous and linear equilibrium are generally assumed. When a steady-state diffusion regime is reached, soil water and sorption surfaces are now saturated (partitioning processes in equilibrium) and VOC diffusion is now only affected by the volume of voids. Consequently, the effective diffusion coefficient (D_e) given by Werner & Höhener (2003) has to be used:

$$D_e = \theta_a \tau D_m \tag{1.12}$$

Biodegradation of VOCs is another process typically included in models. In the unsaturated zone, biodegradation of VOCs occurs only in the aqueous phase and can be described by a variety of kinetic models (zero-order, first-order or Monod kinetics). Höhener *et al* (2003) gave an outline of the possible relationships between the biodegradation rate and the concentration of the volatile compound in soil gas, which involve Henry's law. As VOCs are

mostly present in small aqueous concentrations (especially those with high Henry coefficients), it is therefore justified to use first-order kinetics in reactive models for the unsaturated zone. This has been experimentally shown in laboratory microcosm and column experiments (Höhener *et al.*, 2003; Jin *et al.*, 1994; Jury *et al.*, 1983), in a lysimeter study (Pasteris *et al.*, 2002) and in the field (Höhener *et al.*, 2006). The biodegradation rate (d^{-1}) occurring in the aqueous phase can be expressed as an apparent biodegradation rate occurring in the air phase (k_{app}) using the identity from Pasteris *et al*, (2002):

$$^{l}k_{app} = \frac{^{l}k_w \theta_w}{H} \tag{1.13}$$

For simplicity, the apparent biodegradation rate in the air phase will be denoted as k in the text. Other processes can also be included in models such as density-driven flow and deposition on the air-water interface, but their pertinence varies depending on the type of contaminant. Density-driven flow was concluded to be significant for highly volatile compounds with high vapour density, especially in highly permeable soils (Falta *et al.*, 1989) and observed to be appreciable only during summer's high vapour concentration gradients (Conant *et al.*, 1996). For deposition on the air-water interface, interfacial partitioning is mainly dependent on the hydrophobicity of the contaminant (Hoff *et al.*, 1993).

If only diffusion and biodegradation affect the fate of VOCs, the following partial differential equation that describes the spreading of VOCs can be formulated Werner & Höhener (2003):

$$\frac{\partial C_a}{\partial t} = \nabla.\left(f_a \tau D_m \nabla C_a \right) - f_w k_w C_a \tag{1.14}$$

where ∇ denotes the Laplace operator, f_w and k_w are the fraction of VOC and the biodegradation rate in the water, respectively. The f_w can be simply converted to f_a using the relationship (Werner & Höhener, 2003):

$$f_a = \frac{f_w H \theta_a}{\theta_w} \tag{1.15}$$

When the transport of VOC has reached a steady state regime, the partial differential equation 1.14 can be rearranged based on Höhener *et al* (2003):

$$\frac{\partial C_a}{\partial t} = \nabla.\left(\theta_a \tau D_m \nabla C_a\right) - \frac{\theta_w k_w C_a}{H} \qquad (1.16)$$

1.5.2 Tracing the carbon isotope ratio in the unsaturated zone

Several models using the mathematical approach outlined above were shown to consistently reproduce measured concentrations in column (Jin *et al.*, 1994), lysimeter (Karapanagioti *et al*., 2004) and field (Gaganis *et al*., 2004) studies. These established models can be modified to simulate carbon isotope ratio in addition to concentration. To achieve this link, a single species (for instance *n*-hexane) needs to be decomposed into subspecies according to the presence of a heavy isotope in the molecule. Concentration distribution of the subspecies over space and time can then be independently estimated accounting for the different behaviour of each subspecies.

The factors influencing the behaviour of the subspecies must be carefully determined in order to suitably reproduce the evolution of the isotope ratio. In addition to the well-known isotope effect during biodegradation (see above), diffusion may lead to isotope fraction and must be evaluated. Several experimental works have demonstrated the occurrence of isotope fractionation during migration of methane through different media (Galimov, 1967; Pernaton *et al*., 1996; Prinzhofer & Pernaton, 1997; Stahl *et al*., 1981; Zhang & Krooss, 2001) and for ethane, propane and butane diffusing through either solution or sediments (Reitsema *et al.*, 1981). Also, theoretical (Craig, 1953; Jost, 1960) and field (Cerling *et al.*, 1991) studies demonstrated carbon isotope fractionation during transport of CO_2 in the air phase of the unsaturated zone. Due to the presence of a heavy isotope in the molecule, $^{13}CO_2$ was found to diffuse slower than $^{12}CO_2$ which caused isotope fractionation over distance. Since the main transport of VOCs in the unsaturated zone is by diffusion and since some of the considered molecules have a quite low molecular weight, carbon isotope fractionation during gas phase diffusion of VOCs is likely to occur.

Based on the literature, the carbon isotope fractionation due to sorption and volatilisation processes is very small. At equilibrium, negligible isotope fractionation was observed for halogenated and aromatic hydrocarbons sorption onto activated carbon, lignite coke and lignite (Schüth *et al.*, 2003) and onto activated carbon and graphite (Slater *et al.*, 2000) in single step experiments. In contrast, observations by Kopinke *et al.* (2005) suggest non negligible carbon isotope fractionation during sorption of benzene and toluene onto humic

acid in a multi-step column experiment approach. During equilibrium liquid/vapour volatilisation, negligible fractionation for aromatic compounds was observed (Harrington *et al.*, 1999; Slater *et al.*, 1999), whereas considerable fractionation was observed for chlorinated solvents (Hunkeler & Aravena, 2000). Density-driven advection is not expected to influence isotope ratios since both isotopes are transported at the same rate. However, it may perturb isotope profiles established by other processes.

In the modelling concept, only biodegradation and diffusion were taken into account to cause isotope fractionation. Partitioning processes (sorption and volatilisation) were assumed to lead to no significant isotope fractionation.

1.5.3 Division into 2 subspecies: Approximation method

A division of the species into different subspecies is required to simulate the behavior of different isotopes due to diffusion and biodegradation. In case of an isotope that is present at low abundance, such as carbon, the simplest approach is to distinguish between two subspecies. Subdivision into two subspecies is demonstrated using *n*-hexane as an example (Figure 1.1). Subspecies I contains six ^{12}C and subspecies II contains five ^{12}C and one ^{13}C, no matter the location of ^{13}C in the molecule. Molecules with more than one ^{13}C are neglected since they are very rare.

A degradation rate coefficient is also attributed to each subspecies. Since subspecies I is by far the most abundant, its biodegradation rate can be approximated by the overall rate. The subspecies II degrades at a slower rate, denoted ${}^{h}k_{2sp}$ that is related to the biodegradation rate of subspecies I by:

$$\alpha = \frac{{}^{h}k_{2sp}}{{}^{l}k} \qquad (1.17)$$

where α is the fractionation factor and ${}^{l}k$ and ${}^{h}k_{2sp}$ are the biodegradation rates of subspecies I and II, respectively. The fractionation factor (α) of the compound can easily be determined with classical microcosm experiments. Usually the fractionation factors relate the temporal evolution of concentrations ^{13}C and ^{12}C atoms rather than the evolution of subspecies I and II. However, when isotope ratios are transformed into subspecies ratios before calculating α, it corresponds to the ratio of degradation rates given above.

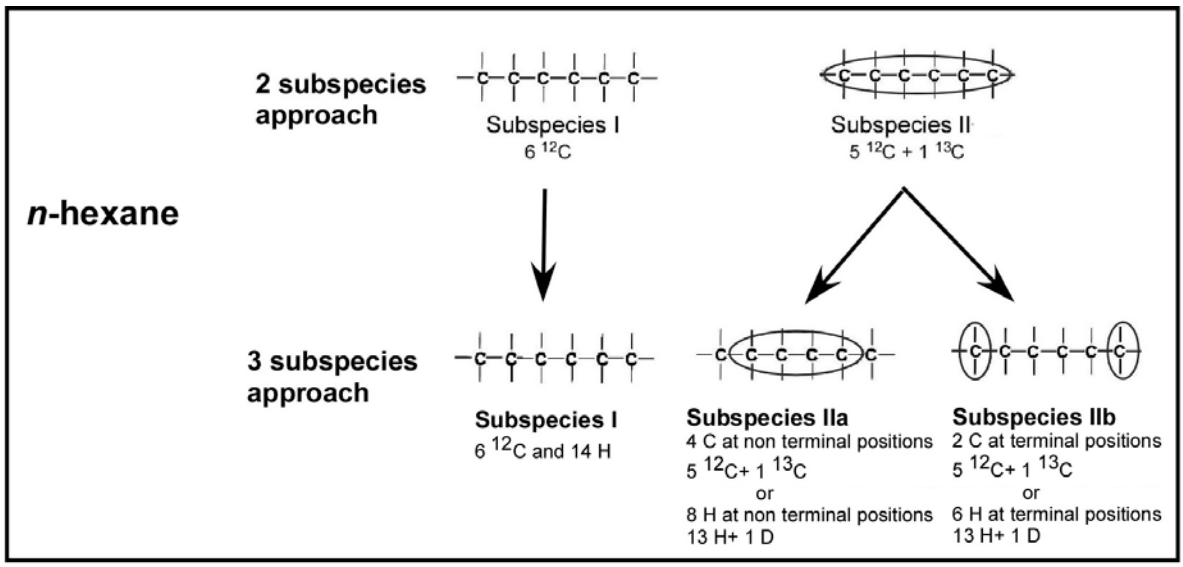

Figure 1.1: Division of *n*-hexane into 2 subspecies according to the presence of ^{13}C in the molecule (upper row) and division into 3 subspecies according to the presence and the location of ^{13}C or D in the molecule (lower row). The circles identify the possible location of a ^{13}C or D in the molecule.

1.5.4 Division into 3 subspecies: Reference method

When the biodegradation pathway is well identified as for instance for *n*-hexane, where biodegradation is generally initiated by an enzymatic bond cleavage involving the carbon at a terminal position (Atlas, 1981), the molecule of interest can be divided into three subspecies (Figure 1.1). A differentiation is first made between molecules composed of only ^{12}C from those containing one ^{13}C atom. Subsequently, ^{13}C-molecules with a ^{13}C at the reactive position can be separated from those having a ^{13}C at the non reactive position. This specific subdivision of ^{13}C-molecules into subspecies IIa and IIb requires fundamental knowledge on the enzymatic mechanism occurring during contaminant degradation. Therefore, the second subdivision is only justified if the exact degradation mechanism is known as it is the case for short *n*-alkanes.

In this approach, subspecies I and IIa degrade at a rate ${}^{l}k$ (the same rate as the previous subspecies I in the 2 subspecies approach) and subspecies IIb degrades at a slower rate, denoted ${}^{h}k_{3sp}$, which is lower than ${}^{h}k_{2sp}$. The degradation rate ${}^{h}k_{3sp}$ is related to the degradation rate ${}^{h}k_{2sp}$ by:

$$ {}^{h}k_{2sp} = f_{IIa}\,{}^{l}k + f_{IIb}\,{}^{h}k_{3sp} \qquad (1.18) $$

where f_{IIa} and f_{IIb} are the fraction of subspecies IIa and IIb, respectively within the total quantity of subspecies II. Assuming that the ^{13}C is statistically distributed in the molecules, the equation 1.18 transforms to:

$$ {}^{h}k_{2sp} = {}^{l}k\,\frac{n-b}{n} + {}^{h}k_{3sp}\,\frac{b}{n} \qquad (1.19) $$

where *n* is the number of carbon atoms in the molecule and *b* is the number of reactive positions (terminal positions in the case of *n*-hexane). If ^{13}C is not distributed statistically, any other values for the abundance of the two subspecies can be inserted into equation 1.19, if known.

1.5.5 Advantage/disadvantage

The decision whether to model 2 or 3 subspecies depends on the knowledge of the biodegradation pathway. When the biodegradation pathway is not fully identified or when initial transformation can occur at different location in a molecule, the 2 subspecies approach is imposed. The approach with 2 subspecies differentiates the molecules according to the presence or not of a ^{13}C only and is indicated to be the procedure to follow for some common contaminants (for instance toluene and methyl-cyclopentane). Consequently, the subdivision into two subspecies avoid false hypothesis about the biodegradation mechanism, but on the other hand, has limitations in its accuracy to approximate the isotope ratio.

The similarity of the two approaches (equation 1.18) relies on the accuracy of ${}^{h}k_{2sp}$ rate to represent the weighted average of ${}^{l}k$ and ${}^{h}k_{3sp}$ rates. However, equivalence of equation 1.19 holds true only at the beginning of the degradation process. As degradation proceeds, the fraction of subspecies IIa and IIb begins to slightly deviate from those initially given in equation 1.19 because subspecies IIa is degraded faster than subspecies IIb. Hence, given that ${}^{l}k$ and ${}^{h}k_{3sp}$ are constant, the ${}^{h}k_{2sp}$ is expected to slightly decrease as degradation proceeds, which is not taken into account when the two subspecies approach is used.

In order to better appreciate the discrepancy in the $\delta^{13}C$ introduced by the approximate 2 subspecies approach, Figure 1.2 illustrates the evolution of the $\delta^{13}C$ for *n*-hexane over time independently calculated by the two different approaches with a first-order kinetic model. It can be noted from the figure that the 2 subspecies approach systematically underestimates the extent of isotope fractionation. As subspecies IIa degrades slightly faster than IIb, more subspecies IIb remains to be degraded at longer time. This accumulation of subspecies IIb slightly decreases the overall biodegradation rate of ^{13}C-molecules. Consequently, with an enrichment factor that increases slightly as biodegradation proceeds, the shift towards positive delta is larger and explains the more positive values predicted by the 3 subspecies approach. The change in proportion of subspecies IIa and IIb is not taken into account when the species is subdivided into two subspecies as the subspecies II is degrading at a fixed averaged rate. For this reason, the approximation of equation 1.19 holds true until the proportion of subspecies IIa and IIb in the remaining substrate has significantly changed compared to the initial proportion, thus establishing the limit of the 2 subspecies approach. In this specific case, if one assumes analytical error ranging from 0.2 to 0.5, the equation 1.19 is appropriate during 20 days. Obviously, the limit in time will vary according to the enrichment factor and the biodegradation rate.

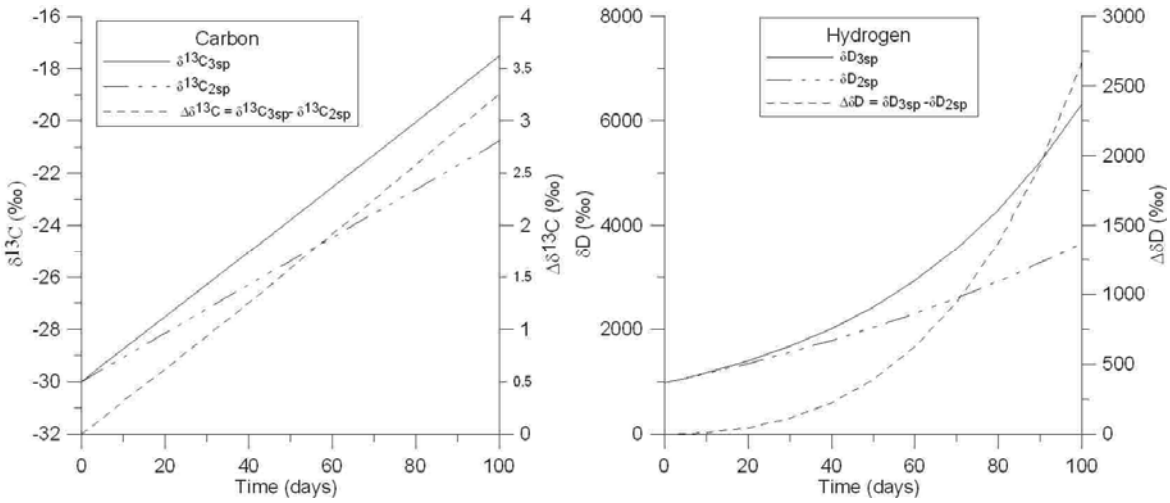

Figure 1.2: Evolution of $\delta^{13}C$ and δD for *n*-hexane estimated by the 2 and the 3 subspecies approach (left y axis) and the discrepancy between the two different approaches (right y axis) over time. A first-order decay model was used with a biodegradation rate of 0.065 d^{-1} and an enrichment factor for C and H of -2.3 ‰ and -132 ‰, respectively.

1.5.6 Division into 3 subspecies for hydrogen

For hydrogen isotope effect, only the primary isotope effect is considered. Although a secondary isotope effect (due to a presence of D adjacent to a broken bond) may be significant in some cases, it will be neglected in this study. For hydrogen, *n*-hexane can be subdivided into the following 3 subspecies:

- Subspecies I: Molecules with H only
- Subspecies IIa: Molecules with one D within the molecule (position C2, C3, C4 or C5)
- Subspecies IIb: Molecules with one D at a terminal position (position C1 or C6)

As for carbon, subspecies with more than one D are neglected. Accordingly, *n*-hexane accounts for 6 terminal position and 8 non terminal positions (Figure 1.1). Figure 1.2 also illustrates the discrepancy between the two approaches created over time in δD values for *n*-hexane. Once again, the approach with 2 subspecies under estimated the extent of isotope fractionation. Compared to carbon, the approach with 2 subspecies approximates for a shorter time the value calculated by the 3 subspecies approach due to the larger fractionation factor. Using the analytical uncertainty found in this study (15 ‰), the approximation is valid during only the first 10-12 days. Later, the discrepancy evolves much faster that for carbon due to a very large isotope fractionation factor for H. The same equations as developed for C to calculate the $^{h}k_{3sp}$ are used for H.

Chapter 2

Evaluation of enrichment factors

Abstract

Microcosm experiments were conducted to measure the carbon isotope fractionation during aerobic biodegradation of *n*-alkanes (from C_3 to C_{10}) and monoaromatic hydrocarbons in a sandy soil under unsaturated conditions. Individual measurements of *n*-alkanes obtained the largest enrichment factor was obtained for propane (-10.8 ± 0.7‰). As expected, the magnitude of the enrichment factor decreased with increasing number of carbon atoms from propane to *n*-decane (-0.2 ± 0.1‰), due to a "dilution" effect from non-reactive isotopes. However, the apparent kinetic isotope effects obtained from the *n*-alkane series point out an additional isotope fractionation occurring during the multi-step process of biodegradation. For aromatic compounds individually tested, the enrichment factor measured for benzene (B) was the largest (-1.4 ± 0.1‰), followed by toluene (T) (-0.8 ± 0.1‰) and *m*-xylene (X) (-0.6 ± 0.1‰). Enrichment factors for BTX were systematically smaller than for *n*-alkanes with equivalent number of carbons, likely related to different biodegradation mechanisms. Enrichment factors for *n*-alkanes, toluene and *m*-xylene were found to be equivalent when individually tested or tested as a mixture. Benzene behaved differently since its enrichment factor was larger when tested in presence of *n*-alkanes and TX.

Bouchard D, Höhener P and Hunkeler D: **Carbon isotope fractionation during aerobic biodegradation of *n*-alkanes and aromatic compounds under unsaturated soil conditions**

To be submitted to Organic Geochemistry.

2.1 Introduction and aims

In a contaminated saturated zone with petroleum hydrocarbons, rapid depletion of oxygen usually occurs due to microbial activity and a large proportion of the compounds are thus degraded under anoxic conditions. Consequently, several microcosm or column studies were carried out to determine the enrichment factors during degradation of benzene, toluene and xylene (BTX) using anaerobic enrichment cultures under saturated conditions or pure strains (see Elsner *et al.*, (2005), Meckenstock *et al.*, (2004) and Schmidt *et al.*, (2004) for extensive reviews). Moreover, less data are available on isotope fractionation during biodegradation of short chain alkanes (C_3 to C_9), which are common gasoline constituents (Riser-Roberts, 1998). A ^{13}C enrichment during biodegradation of short *n*-alkanes (C_1 and C_3) has first been observed by Lebedew *et al*., (1969) and later by Stahl (1980) for chain lengths from C_3 to C_6 and by George *et al*. (2002) for chain lengths from C_5 to C_9. However, neither the reported data in the latter two studies allow calculating enrichment factors for individual compound. Studies that quantify isotope fractionation of individual compounds have either focussed on methane or on *n*-alkanes with chain lengths $\geq C_{13}$ (Mansuy *et al.*, 1997; Mazeas *et al.*, 2002). The isotope enrichment factors reported during aerobic oxidation of methane were found to be dependent on temperature (Coleman *et al*., 1981; King *et al*., 1989) and on soil water content (Tyler *et al*., 1994).

The aim of this study was to determine the carbon isotope enrichment factors during aerobic degradation of several aliphatic hydrocarbons (from C_3 to C_{10}) in soil microcosms with an indigenous microbial population under unsaturated experimental conditions, and to evaluate how isotope enrichment factors vary as a function of chain length. Enrichment factors for BTX, methyl-cyclopentane (MCP), methyl-cyclohexane (MCH) and 3-methylpentane (3MP) compounds were also determined to compare the variations in carbon isotope fractionation involving C-H bonds between saturated and non saturated hydrocarbons having the same number of carbons. Unsaturated conditions were chosen due to the low solubility of the compounds and in view of using the isotopic enrichment studies for evaluation of biodegradation in the unsaturated zone of contaminated sites. Finally, hydrogen enrichment factors were determined for *n*-pentane and *n*-hexane to investigate on the degree of magnitude.

2.2 Material and methods

2.2.1 Microcosm experiments

Biodegradation of organic contaminants was carried out in serum bottles of 63 ml volume closed with Teflon Mininert® valves (VICI, Schenkon, Switzerland). An alluvial sand from lake Geneva near the Rhone river delta, Switzerland, which had been shown to degrade diverse petroleum hydrocarbons (Höhener *et al.*, 2003), was used. The microbial and physical properties of this sand have been previously described (Pasteris *et al*., 2002). Prior to the experiments, the sand was amended with NH_4NO_3 and K_2HPO_4 (Fluka, Buchs, Switzerland) to make sure that the nutrients were not rate-limiting based on C:N and C:P ratios of 25:1 and 250:1, respectively (Zhou & Crawford, 1995). The soil water content was kept lower than 10 % w/w. The sand was compacted as much as possible in the bottles and experiments were carried out at 23°C.

2.2.2 Compounds

The gaseous compounds propane (C_3) and *n*-butane (C_4) were obtained from Messer (Lenzburg, Switzerland). All other liquid compounds were obtained from Fluka in their purest form. Biodegradation of *n*-alkanes (C_3, C_4, C_5, C_6, C_7, C_8 and C_{10}) and BTX was first tested individually in flasks containing the compound of interest and a tracer in order to check for gas leaks. For C_3 and C_4 *n*-alkanes, 0.5 mg of compounds was injected simultaneously with methane, which was previously shown not to degrade within the time frame of the experiments. For longer *n*-alkanes (C_5 to C_8), 0.6 mg of gaseous compound was injected simultaneously with isooctane (2,2,4,-trimethylpentane) as a slowly degradable tracer. The quantity of C_{10} was 0.1 mg due to its low vapour pressure. Injections and sampling were performed using gastight syringes (VICI, Schenkon, Switzerland). Each compound was tested in duplicate and repeated twice.

In addition, biodegradation experiments with two different hydrocarbon mixtures were carried out. The mixture 1 (called the 5-compound mixture) consisted of five typical constituents of gasoline (*n*-hexane, *n*-octane, benzene, toluene, *m*-xylene) and the mixture 2 (called the *n*-alkane mixture) consisted of four *n*-alkane compounds (*n*-pentane, *n*-hexane, *n*-octane and *n*-decane). Both liquid mixtures were prepared in flasks with a large headspace. The proportion of compounds in the liquid phase was chosen such that equal pressures of each compound in

the gas phase were obtained. Ten ml of vapour of each mixture was taken from the headspace and injected in the microcosm along with a tracer. Approximately 0.2 mg of each compound was added in the microcosm with the 5-compound mixture and, due to the low vapour pressure of *n*-decane, only 0.1 mg of each compound was added with the *n*-alkane mixture. Experiments were conducted in duplicate and repeated twice for each mixture. For control microcosms, the same procedure as described above was carried out with sand autoclaved three times at 120 ^{0}C for 20 minutes within a three day period, and with an additional 2 ml of NaN_3 (10% solution) to ensure total inhibition of microbial activity. Two control microcosms were prepared for each type of incubation to determine whether processes other then biodegradation can change the isotope ratio.

2.2.3 Concentration and isotope analysis

Gas samples were periodically taken from the microcosms and the δ^{13}C and δD values of the compounds were determined using a TRACE™ gas chromatography (GC) coupled to an isotope ratio mass spectrometer (IRMS) via a ThermoFinnigan™ GC combustion III interface. Injections were performed using a loop injector and varied from 10 to 250 *u*l to insure a minimum delivery of 1 *n*mol of C and 10 *n*mol of H to the column. The carrier gas was helium with a flow rate of 1.7 ml min^{-1}. For C analysis, the oxidation and reduction reactors were set to 940 ºC and 650 ºC, respectively. For H analysis, the oxidation reactor was set to 1400 °C. Concentrations of the biodegradable substrate and the tracer were determined based on the combined peak area of all three CO_2 mass ions (44, 45 and 46) for every sample. Concentrations of biodegradable substrate were then normalised with respect to the concentration of the tracer. Reproducibility of concentration measurements was ± 5%. The average standard uncertainty for carbon isotope ratio was ± 0.2 ‰ (n=12) and for H isotope ratio was 15‰ (n=10). Measurements were performed until less than 10 % of the compound was remaining in the microcosm for pure compound experiments (< 30% for propane) and less than 20% for mixture experiments. Isotope enrichment factors were quantified using the Rayleigh type evolution model for closed system according to (Clark & Fritz, 1997):

$$R_{sample} = R_0 \left(C_{sample} / C_0 \right)^{\alpha-1} \quad (2.1)$$

Rearrangement of equation 2.1 yields:

$$\ln\left(R_{sample}/R_0\right) = \left(\alpha - 1\right) \ln \left(C_{sample}/C_0\right) \quad (2.2)$$

where R_0 is the initial $^{13}C/^{12}C$ ratio, α is the fractionation factor, C_0 and C_{sample} is the initial concentration and the remaining concentration at time *t*, respectively. The fractionation factor is obtained by plotting ln (R_{sample}/R_0) versus ln (C_{sample}/C_0), which yields α–1 as the slope of the linear regression.

2.3 Carbon enrichment factor

2.3.1 Results

2.3.1-A Biodegradation of compounds

The concentrations decrease during aerobic biodegradation of *n*-alkanes (C_3, C_4, C_5, C_6, C_7, C_8 and C_{10}), aromatic compounds (BTX) and cyclic compounds (MCH and MCP) in single compound microcosms are presented in Figure 2.1 for one representative repetition. The initial concentration corresponds to the moment when the compound has diffused evenly inside the microcosm. The concentration decrease is approximately linear for most of the compounds, suggesting zero order kinetics.

The evolution of concentrations for the microcosms receiving either the 5-compound mixture or the *n*-alkane mixture undergoing aerobic biodegradation is presented in Figure 2.2. The biodegradation of each compound in both mixtures follows approximately a zero-order rate law and a sequential uptake was observed over the course of both experiments. After an acclimation period during the first series of tests (lag phase before occurrence of biodegradation), the 5-compound mixture was degraded with preferential utilization in the following order: *n*-octane > *n*-hexane > aromatic compounds. In the *n*-alkane mixture, a sequential degradation was also observed. The concentrations of *n*-decane and *n*-octane decreased to zero within the first 400 minutes, during which the concentration of the other compounds varied little. Thereafter 400 minutes, *n*-hexane started to decrease quickly, followed by *n*-pentane.

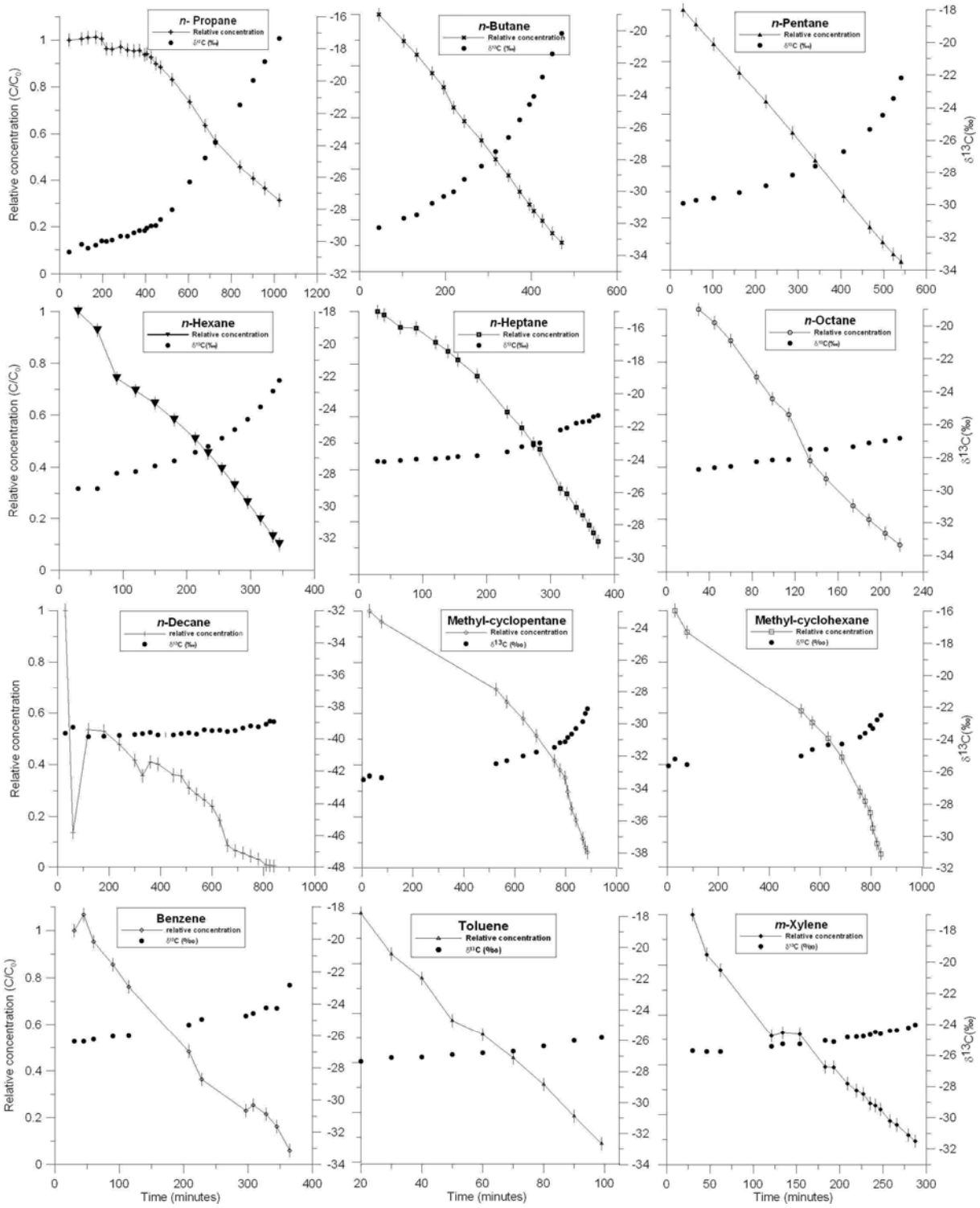

Figure 2.1: Relative concentration and evolution of the $\delta^{13}C$ values of the remaining substrate occurring over time during aerobic biodegradation of different *n*-alkane and aromatic compounds in microcosms.

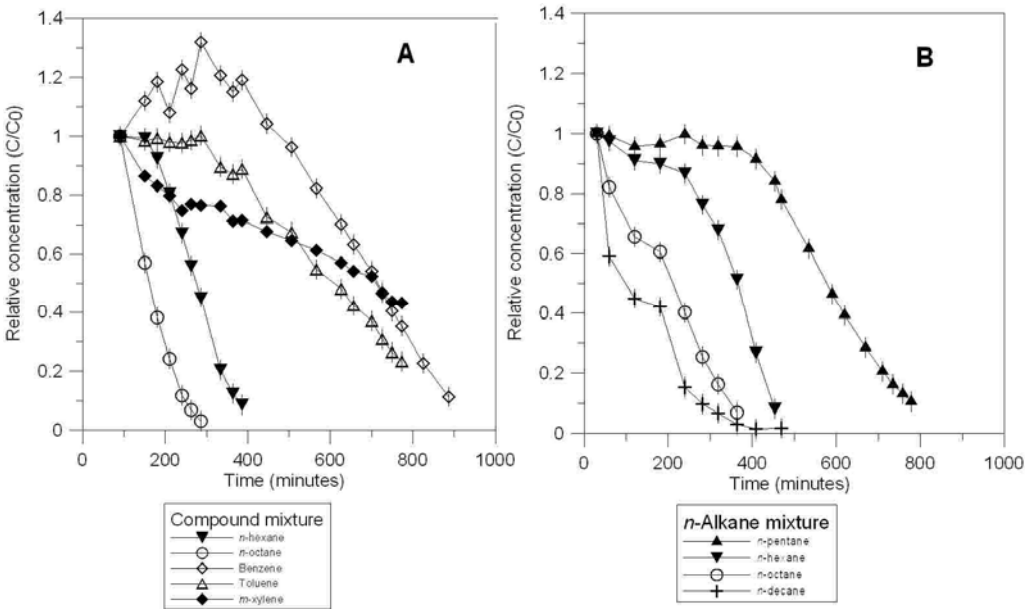

Figure 2.2: Concentration evolution of hydrocarbon compounds during aerobic biodegradation of the 5-compound mixture (A) and the n-alkanes mixture (B). Compound concentration data are corrected relatively to the tracer.

2.3.1-B Isotope fractionation (including sterile micrcosm)

For *n*-alkanes, the maximal shift in $\delta^{13}C$ decreases with increasing chain length (Figure 2.1). The carbon isotope enrichment factors were calculated using equation 2.2 (Table 2.1). For *n*-alkanes tested individually, the largest enrichment factor was obtained for the shortest *n*-alkane chain, propane (-10.8 ‰). With increasing chain length, the enrichment factors decreased. The enrichment factor of -0.2 ‰ obtained for *n*-decane is still significantly different from a slope of zero, with 99% of confidence according to the Student test. The carbon isotope enrichment factors obtained for *n*-alkanes were found to be linearly related on a natural logarithmic scale to the number of carbon atoms in the molecule (Figure 2.3). For individually tested compounds, the value for *n*-pentane (-2.4 ‰) is slightly smaller than the linear trend (Figure 2.3A), while it follows the trend in the microcosm with *n*-alkane mixture (-3.4 ‰, Fig. 2.3B). For the aromatic compounds tested individually, benzene showed the largest enrichment factor (-1.4 ‰) and *m*-xylene the smallest (-0.6 ‰) (Table 2.1). In the case of cycloalkane, a fractionation was observed for methylcyclopentane and methylcyclohexane and carbon isotope enrichment factors were -1.5‰ and -1.1‰. The carbon isotope enrichment measured for 3MP was -1.1‰. Finally, in sterile microcosms, no significant isotopic changes were observed due to air-water or air-solid partitioning for the 5-compound mixture (Figure 2.4).

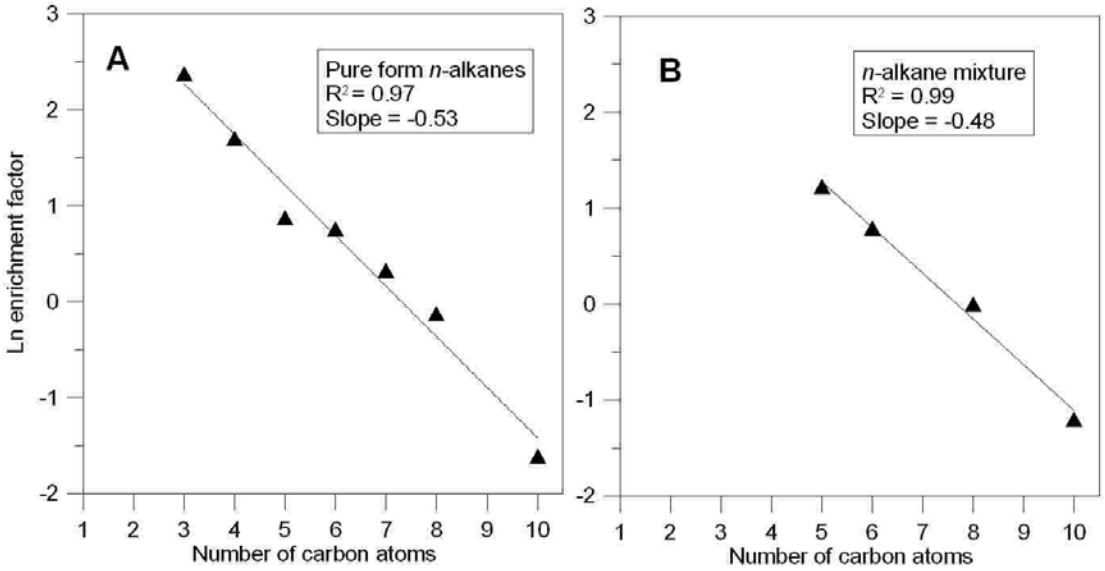

Figure 2.3: Relationships between the natural logarithm of the enrichment factors and the number of carbon atoms included in the *n*-alkane chain for experiment with individual compounds (A) and for the *n*-alkane mixture (B).

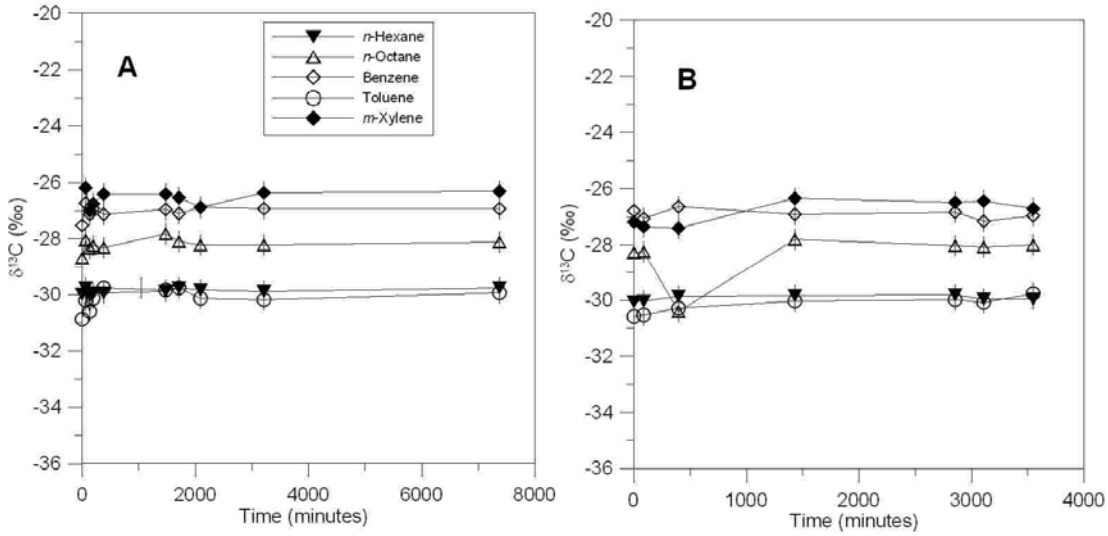

Figure 2.4: Evolution of the $\delta^{13}C$ for the 5-compound mixture with sterilized sand in function of time for two replicates.

Table 2.1

Carbon and hydrogen isotope enrichment factors obtained during the biodegradation of saturated and aromatic hydrocarbons under oxic conditions in microcosms.

Compound	**C enrichment factors (‰)**			**H enrichment factors (‰)**
	5-compound mixt.[1]	*n*-alkane mixt.[1]	Pure compound[1]	*n*-alkane mixt
Propane	nd	nd	-10.8 +/- 0.7	nd
n-Butane	nd	nd	-5.6 +/- 0.1	nd
n-Pentane	nd	-3.8 +/- 1.3	-2.4 +/- 0.2	-97 ± 8 (n=2)
n-Hexane	-2.2 +/- 0.4	-2.4+/- 0.3	-2.3 +/- 0.6	-132 ± 15 (n=2)
n-Heptane	nd	nd	-1.4 +/- 0.1	nd
n-Octane	-0.7 +/- 0.2	-1.1+/- 0.1	-0.9 +/- 0.1	nd
n-Decane	nd	-0.3+/- 0.1	-0.2 +/- 0.1	nd
Benzene	-2.1 +/- 0.1	nd	-1.4 +/- 0.1	nd
Toluene	-0.7 +/- 0.1	nd	-0.8 +/- 0.1	nd
m-Xylene	-0.8 +/- 0.1	nd	-0.6 +/- 0.1	nd
MCP	nd	nd	-1.53 +/-0.04 (n=2)	nd
MCH	nd	nd	-1.1 +/-0.1 (n=2)	nd
3MP	nd	nd	-1.09 +/-0.03 (n=3)	nd

[1] Mean of 4 repetitions +/- standard deviation

2.3.2 Discussion

2.3.2-A Degradation rates and kinetics

The preferential utilization of *n*-alkanes over aromatic compounds observed in this study is in agreement with previous studies (Bailey *et al*., 1973; Milner *et al.*, 1977; Stahl, 1980) as well as for the preferential uptake of long *n*-alkane chains over short chains (Stahl, 1980). An increase in biodegradation rates with increasing number of carbon atoms for gaseous *n*-pentane to *n*-decane was observed in previous laboratory (Höhener *et al*., 2003; Ostendorf *et al*., 2000) and field studies (Höhener *et al.*, 2006; Pasteris *et al.*, 2002), where first order

kinetics were observed when compounds were at low concentrations. In order to have enough substrate for isotope analysis, experiments in this study were performed with high initial vapour concentrations. Thus, zero-rate order rate kinetics were expected since maximum specific substrate utilization rates are reached when the vapour concentration C_a is much larger than HK_s (Höhener *et al.,* 2003), where H is the Henry's coefficient, and K_s is the half-saturation constant in the aqueous phase (more often called Monod constant). *n*-Alkanes have very low K_s (Höhener *et al*., 2003), and thus although they have high H's, the product HK_s is small.

2.3.2-B Alkane isotope analysis

Enrichment factors obtained for *n*-alkanes tested either as single compound or in a mixture provided similar values suggesting a relative similarity between the active microbial populations of both microcosms. The decrease of enrichment factors with increasing number of carbon atoms in the molecule (Figure 2.4) is partially explained by the "dilution" effect. With increasing number of carbon atoms, a ^{13}C is less likely to be involved in the initial enzymatic bond cleavage, which is required to cause an isotope effect. The dilution effect was suggested in George *et al.* (2002) and now experimentally demonstrated. When correcting for the number of carbon atoms, a relatively large range of AKIE values reaching from 1.002 to 1.033 is obtained (Table 2.2). This indicates that other factors than dilution of the isotope effect by non-reactive positions are responsible for the observed trend to smaller isotope enrichment factors for larger molecules. For small molecules the AKIE corresponds well to the expected KIE, which is in the range of 1.021 for C-H bond cleavage according to the Streitwieser approximation (Elsner *et al*., 2005). However, the AKIE values for larger molecules are significantly lower. Microbial oxidation reactions are catalysed either by P450 monooxygenase or by multiprotein monooxygenase systems (Berthe-Corti & Fetzner, 2002) and a direct H abstraction mechanism is expected for saturated hydrocarbons (Yoshizawa, 2002).

Table 2.2

Apparent kinetic isotope effect calculated for results of this study and from Anderson *et al.,* (2004).

Compound	**AKIE**	**AKIE**
	This study	**Anderson *et al*., (2004)**
n-Ethane	nd	1.017
n-Propane	1.033	1.014
n-Butane	1.022	1.013
n-Pentane	1.019*	1.014
n-Hexane	1.013	1.021
n-Heptane	1.010	1.017
n-Octane	1.007	1.017
n-Decane	1.002	

*Using value obtained with *n*-alkane mixture

The trend to smaller AKIE for larger molecules could be due to rate limiting steps before the actual transformation step. Enzymatic reactions during biological degradation of compounds is a multi-step procedure (O'Leary & Yapp, 1978), which includes transport of the compound into the cell (step 1), binding of the substrate to the enzyme (step 2), transformation at the reaction centre (step 3) and finally, dissociation of the product with the enzyme (step 4). Although transport and binding steps are generally assumed not to be associated with significant carbon isotope fractionation, they influence the AKIE value indirectly. If the actual bond cleavage step is fast compared to the proceeding transport steps (high commitment to catalysis), nearly each molecule that reaches the enzyme is transformed irrespectively of its isotopic composition and no isotope fractionation is apparent. In contrast, if reversible transport and binding is fast compared to bond cleavage (low commitment to catalysis), the isotope discrimination associated with bond cleavage becomes apparent outside of the cell. Hence, the different AKIE values for different molecules could reflect a different degree of commitment to catalysis. Larger compounds show a higher commitment to catalysis which could be due to either a slower transport of the molecule or to its binding to the enzyme.

Unlike biological, homogeneous chemical processes have no potentially slow step preceding the initial bond cleaving step (Paneth, 1994) and hence should be less affected by molecule size effects other than dilution. To evaluate this hypothesis, the enrichment factors of this study were compared with those measured during gas phase reactions with OH radicals.

Enrichment factors obtained by chemical reactions (reported in ‰ according to $\varepsilon = (k_{13}/k_{12}-1)*1000$) were decreasing from C_2 (-8.57 ‰) to C_8 (-2.13 ‰) (Anderson *et al.*, 2004). Once transformed AKIEs, the new values show relatively good homogeneity without the trend seen with the AKIE values for biological process (Table 2.2). This comparison of results emphasizes the indirect effect of transport and binding steps in biological processes on the observed isotope fractionation. Similar studies with whole cells and cell extracts for toluene (Morasch *et al.*, 2001) and tetrachloroethene (Nijenhuis *et al.*, 2005) biodegradation demonstrated that isotope fractionation tends to be somewhat larger when cell walls no longer limit the uptake of substrates.

The relationship between carbon isotope enrichment factors and carbon number observed in this study (Figure 2.3) is consistent with previous observations for methane and longer chain alkanes. When extrapolation to methane, values of -27.9 ‰ and -24.3 ‰, respectively, are obtained, similar as those observed in previous studies with environmental samples (Table 2.3). The extrapolation toward longer chains (Figure 2.3) provides enrichment factors close to zero for chain $\geq C_{11}$, in agreement with previous studies that reported absence of measurable isotope fractionation during biodegradation of *n*-alkanes $\geq C_{13}$ (Mansuy *et al.*, 1997) and *n*-alkanes $\geq C_{14}$ (Mazeas *et al*., 2002).

Table 2.3

Observed enrichment factors during aerobic oxidation of methane with soil indigenous microbial population.

Enrichment factor (‰)	**soil**	**Reference**
-22.0 to -28.0	Forest soil	Tyler *et al.* (1994)
-21.5 to -24.4	Forest soil	Reeburgh *et al.* (1997)
-24.4	Laboratory culture	Coleman *et al.* (1981)
-16.0 to -27.0	Tundra soil	King *et al.* (1989)
-27.9	Lake sediment	Extrapolation from this study (Fig. 2.3A)
-24.3	Lake sediment	Extrapolation from this study (Fig. 2.3B)

2.3.2-C BTX isotopes analysis

The values obtained for benzene in this study are intermediate with respect to the values reported by Hunkeler *et al.,* (2001) for two pure cultures (-1.4 and -3.5 ‰). For toluene, a relatively small isotope enrichment factor was observed (Table 2.1). Under oxic conditions, the biodegradation of toluene can be initiated by a variety of oxygenase reactions and a study has shown diverse enrichment factors related with different enzyme mechanisms (Morasch *et al*., 2002). The use of pure strains allowed observing enrichment factor of -3.3‰ for a methyl monooxygenase reaction and enrichment factors of -1.1‰ and -0.4‰ for a ring monooxygenase and a ring dioxygenase reaction, respectively. Measured values in this study (-0.7 and -0.8‰) strongly suggest a domination of the ring transformation mechanism in the active soil population. This ring oxygenation domination is also in agreement with works of Keener *et al*. (2001), which reported that the majority of isolates from a contaminated aquifer proceeded via the toluene 3-monooxygenase pathway to degrade toluene. For *m*-xylene, the enrichment factor observed in this study is much smaller than the value observed (-1.7‰) for a pure strain culture with initial bond cleavage on the methyl group (Morasch *et al*., 2002). Thereby, data reported herein for *m*-xylene also suggest a ring oxygenation.

Isotope enrichments factors for BTX were systematically smaller than for *n*-alkanes with equivalent number of carbons (C_6, C_7 and C_8, respectively) (Table 2.1). The smaller isotope enrichment factors are likely related to the difference in reaction mechanism. In contrast to degradation of *n*-alkanes that implies a C-H bond cleavage in the initial step, the presence of π electrons in the aromatic ring allows the formation of an arene oxide without breaking the C-H bond (Tomaszewski *et al*., 1975; Wilkins *et al*., 1994). This type of mechanism without H abstraction alters less the strength of bonds involving carbon during formation of the transition state. This lesser extent in the bond cleavage leads to a smaller isotope effect than for *n*-alkanes.

No difference in the enrichment factors were measured for toluene and *m*-xylene when individually tested or mixed with other compounds. However, results showed larger enrichment factors for benzene when included in a mixture (Table 2.1). Several studies reported enhanced biodegradation of benzene in presence of toluene, thus conferring to toluene a role of enzyme inducer (Alvarez & Vogel, 1995; Arvin *et al.,* 1989; Chang *et al.,* 1993; Gülensoy & Alvarez, 1999). As a result, the presence of toluene in the 5-compound

mixture would induce the activity of some enzymes that were not active during single degradation of benzene.

2.3.2-D MCH, MCP and 3MP isotopes analysis

Enrichments factors for MCP and MCH were systematically smaller than for *n*-alkanes with equivalent number of carbons (C_6 and $C_{7,}$ respectively) and larger than aromatic compounds (benzene and toluene) (Table 2.1). These observed enrichment factors located between two compound families would imply a third enzyme mechanism perhaps specific for saturated alicyclic compounds. The enrichment factor for 3MP is slightly smaller than expected when compared to other compounds with equivalent number of carbons (*n*-hexane and benzene).

2.4 Hydrogen enrichment factor

2.4.1 Results

2.4.1-A *n*-Alkanes isotope fractionation

In the *n*-alkane experiment for hydrogen enrichment, both compounds were simultaneously added in the microcosm. Figure 2.5 illustrates the evolution of δD during biodegradation of *n*-pentane and *n*-hexane until less than 20% of the compound remained. *n-H*exane was degraded preferentially and *n*-pentane started to degrade only when less than 25% of *n*-hexane left in the microcosm. Large hydrogen enrichment factors were observed for both compounds and were -132 ‰ and -97 ‰ for *n*-hexane and *n*-pentane, respectively (Table 2.1).

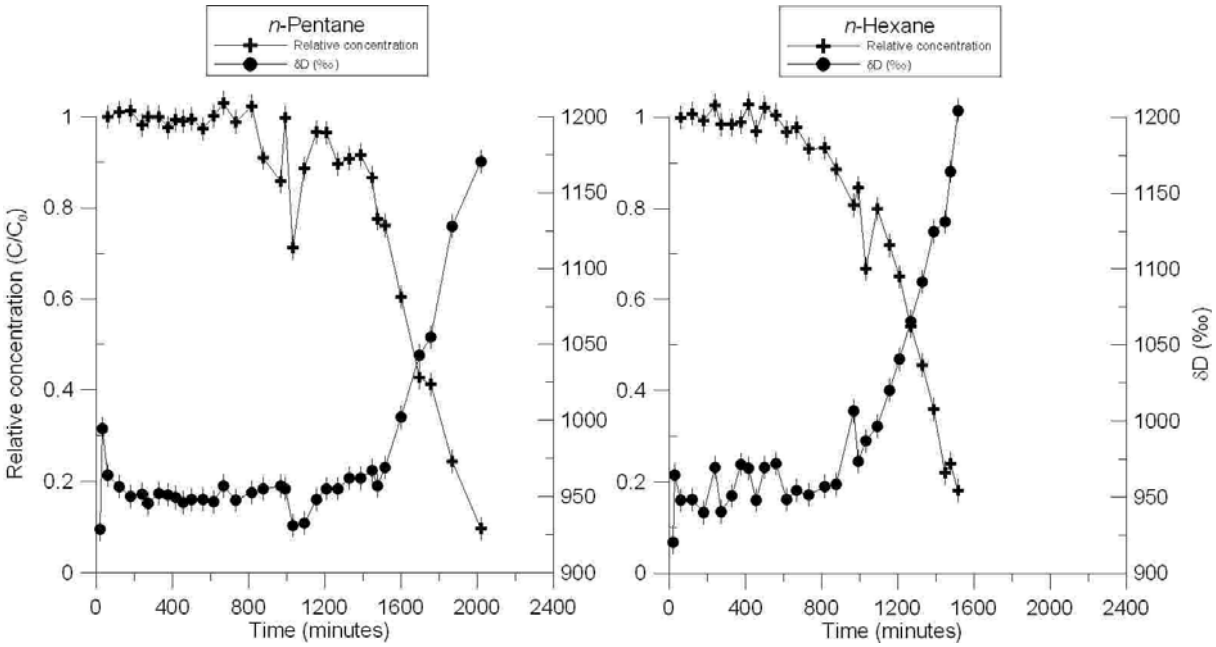

Figure 2.5: Relative concentration and evolution of the δD values of the remaining substrate occurring over time during aerobic biodegradation of *n*-pentane and *n*-hexane in microcosms.

2.4.2 Discussion

Hydrogen enrichment factors were found to be much larger than carbon enrichment factors, as known also from other studies (Mancini *et al.* 2003, Morasch *et al*. 2002, Hunkeler *et al.* 2001). In our study, the hydrogen enrichment factor for *n*-hexane degradation is 50 times larger than the carbon enrichment factor. This is mainly due to a larger relative mass difference in case of D/H compared to $^{13}C/^{12}C$. Deuterium is 100 % heavier that hydrogen, compared to 8 % mass difference between ^{13}C and ^{12}C. The larger H isotope effect compared to C is also known in the literature, expecting large H and small C enrichment factor with oxidation reactions (Cook, 1991).

2.5 Conclusions for microcosm experiments

Batch experiments carried out in the laboratory served to determine the enrichment factors occurring during biodegradation of numerous petroleum hydrocarbons in a sandy soil under unsaturated conditions. For *n*-alkanes, carbon enrichment factors decreased from propane (C_3) to *n*-decane (C_{10}), providing evidence that the magnitude of the enrichment factor is inversely proportional to the number of carbon atoms composing the saturated hydrocarbons. No measurable enrichment is expected for *n*-alkanes with chain lengths longer than C_{10} due to a large dilution of the ^{13}C in the molecule. The decrease in the isotope enrichment factor is

larger than expected based on the “dilution” effect suggesting that other factors such as rate limiting transport and enzyme binding steps play a role as well. Carbon enrichment factors for BTX were also measured and were systematically smaller than the *n*-alkane with equal number of carbons. The difference is related to diverse enzymatic mechanisms, as the direct H abstraction during oxidation of saturated hydrocarbons leads toward larger carbon isotope effect. A third compound family, saturated cyclic compound such as MCP and MCH, showed carbon enrichment factors with intermediary magnitude compared to the two other compound families with the same number of C atoms. This may implicate different enzyme activities.

Carbon enrichment factors for *n*-alkanes, toluene and *m*-xylene were found to be equivalent when individually tested or degraded in presence of other compounds. In contrast, benzene provided a smaller enrichment factor when individually tested. The two different results for benzene suggest a different active microflora in each microcosm which can be related to the presence of toluene known to be an enzyme inducer. These results for benzene obtained under aerobic conditions are of interest as the large majority of contaminated sites are multi-compound contaminations.

Finally, H enrichment factors were evaluated for *n*-pentane and *n*-hexane and provided much larger factors compared to C. Since only few compounds were tested, investigation on the hydrogen isotope fractionation on a larger choice of compounds should be carried out to provide additional enrichment factors.

Chapter 3

Diffusion effect on isotope fractionation

Abstract

The study focuses on the combined effect of VOC transport by diffusion and biodegradation on isotope ratios. Migration of VOCs under unsaturated conditions was simulated using a 1.1m long column filled with alluvial sand. This setup can be considered to represent VOC transport from a floating NAPL towards the atmosphere. A liquid mixture of 10 VOCs was emplaced in a void chamber at one end of the column and VOCs vapours were allowed to diffuse through the soil. Periodical measurements of concentrations and $\delta^{13}C$ were carried out in the source chamber and at different distances along the column. The $\delta^{13}C$ value in the column changed over distance especially for small molecules. Initially, shifts towards more negative values occurred. Subsequently, either a flat isotope ratio profile or a positive shift was observed. Measurements in the source chamber showed also an evolution in the $\delta^{13}C$ as the compound were depleting from the liquid source. Analytical simulations incorporating different diffusion coefficients for compounds with a different isotopic composition reproduced the observed isotope shifts well. The analytical simulations demonstrated that the large positive shift observed in the column for some compounds at later time was related to the change in the isotope signature in the source chamber and not to biodegradation. These findings underline the significance of the diffusion isotope effect and the importance of source monitoring when assessing biodegradation in the unsaturated zone using isotope analysis.

Bouchard D, Höhener P, Hunkeler D. **Carbon isotope fractionation during natural attenuation petroleum hydrocarbons in unsaturated zone: column experiment.**

To be submitted to the **Journal of Contaminant Hydrology**

3.1 Introduction and aims

While the previous chapter investigated the effect of biodegradation in absence of transport, this chapter focussed on the combined effect of transport by diffusion and biodegradation on isotope ratios of VOC using a column study. The study has several aims: (1) to investigate whether the transport by diffusion is accompanied by significant isotope fractionation (2) to evaluate how the isotope ratio of the VOC source evolves and (3) to evaluate whether the isotopes can still be used to assess biodegradation despite a possible diffusion isotope effect and varying source isotope ratio. The column can be considered to represent transport of VOCs from a floating NAPL pool source across the unsaturated zone to the atmosphere. A mixture of VOCs typically found in gasoline was emplaced at one end of the column. Concentrations and isotope ratios were monitored at the source and along the column for 14 days. The highly controlled experimental setup makes it possible to monitor the isotope changes at the source in detail and to evaluate the effect of the source/column interaction on the isotope evolution. Analytical modelling using reactive transport model based on Fick's law was used to gain more detailed insight into the factors that control the $\delta^{13}C$ values of the VOCs. The calculations made it possible to evaluate the hypothesis of a diffusion isotope effect and to dissociate the diffusion isotope effect from the biodegradation effect.

3.1.1 Isotope effect during volatilisation

Few studies were conducted on the evolution of the $\delta^{13}C$ during successive volatilisation of VOCs from a liquid source. Most studies focussed on isotope effects during volatilisation of a pure organic liquid. An equilibrium isotope effect was first shown to occur between organic liquids and the corresponding saturated vapour phases by Baertschi *et al.* (1953). The enrichment of heavy isotopes in the gas phase was explained by a higher vapour pressure for heavy compounds (Narten & Kuhn, 1961). This inverse isotope effect was later indirectly confirmed by (Bartell & Roskos, 1966) when demonstrating a greater surface tension (intermolecular attraction) for lighter compounds. The smaller volume and the heavier mass confers larger motion energy for ^{13}C-molecules in the liquid phase, and along with lower intermolecular cohesive forces, the volatility of heavy isotope is therefore superior (Van Hook, 1966; Van Hook, 1967; Van Hook, 1985; Wolfsberg, 1963). Other studies also demonstrated a small enrichment of ^{13}C in the headspace above the liquid phase contained in closed vessels for hydrocarbons petroleum (Balabane & Létolle, 1985; Harrington *et al.*,

1999; Slater *et al*., 1999), and a larger effect for chlorinated solvents (Hunkeler & Aravena, 2000; Slater *et al.*, 1999). When the vessel containing the liquid compound is open to the atmosphere, continuous evaporation of the compounds occurs until the source runs dry. Results obtained by Huang *et al.* (1999) and Poulson & Drever (1999) showed as well preferential volatilisation of heavy molecules as progressive depletion of ^{13}C in the air phase were monitored. Therefore, based on the results of all these experiments, the remaining liquid NAPL and hence the vapour phase should get depleted in heavy compounds as the source gets progressively exhausted over time.

3.2 Material and methods

3.2.1 Fuel compound mixture

A liquid mixture of 10 volatile organic compounds commonly found in gasoline was prepared. The weight proportion of each compound is listed in Table 3.1. The theoretical vapour concentration in the headspace calculated with Raoul's law is given as well assuming ideal behaviour. The percentages of the less volatile compounds were higher than in typical gasoline in order to increase the lifetime of the source. All organic compounds were obtained from Fluka (Buchs, Switzerland) in their purest form.

3.2.2 Alluvial sand

The selected alluvial sand was previously used to evaluate the biodegradation of volatile gasoline compounds (Höhener *et al.*, 2003; Pasteris *et al*., 2002). The physico-chemical characteristics of the sand are described in these studies. The sand was sieved at 4 mm and no other microbial cultures were added to the indigenous population. The total porosity of the sand packed in the column was estimated as 0.41, the organic carbon content (f_{oc}) was 0.2 % (Pasteris *et al.*, 2002) and the water content, calculated by gravimetric mass lost after drying at 105°C of sand samples was 3.3%. The tortuosity (τ) was estimated to be 0.613 using the empirical approximation of (Millington & Quirk, 1961):

$$\tau \approx \theta_a^{2.33} / \theta_t^2 \qquad (3.1)$$

where θ_t *and* θ_a is the total and the soil air porosity, respectively.

Table 3.1

Composition of the fuel mixture with initial concentration in the headspace (according to Raoul's law), molecular diffusion coefficient and the calculated fraction of compound in the soil air (f_a) at room temperature (23.5°C).

Compound	**Weight in mixture (%)**	**Initial air phase conc. (g/m^3)**	**D_m[1] (m^2/d)**	**f_a[2] (%)**
n-Pentane	4.56	129.24	0.7211	0.838
n-Hexane	9.62	77.45	0.6268	0.737
n-Octane	10.25	7.92	0.5275	0.395
n-Decane	18.62	1.74	0.4630	0.595
Benzene	2.55	13.52	0.7981	0.243
Toluene	4.11	6.11	0.7271	0.119
m-Xylene	5.67	2.52	0.5892	0.061
Isooctane (2,2,4 trimethyl-pentane)	17.65	42.12	0.5275	0.840
Methyl-cyclohexane	12.62	29.99	0.5863	0.719
1,2,4-Trimethyl-benzene	14.36	1.7	0.6080	0.005

[1] from Lugg (1968), [2] with equation 1.11

3.2.3 Column experiment

The experimental setup and the dimensions of the cylindrical column are illustrated in Figure 3.1. The column consists of a steel cylinder with a length of 1.20 m and an internal diameter of 8.1 cm that can be tightly closed at both ends with steel caps and Teflon O-rings. The column was filled with the moist sand described above and firmly compacted providing a 1.06 m long homogeneous system. The column was left for 2 weeks in horizontal position in order to acclimatize the microbial community to the new setting and to room temperature. The clean-cut edges of the compacted moist sand remained stable without any need of support separating the sand from the caps, and creating a void chamber of 7 cm depth at both ends. An open vessel containing 10 ml of the mixture (Table 3.1) was emplaced at one end of the column and the chamber was then immediately closed with the steel caps. The exit chamber at the opposite end of the column was constantly purged with humidified air at a rate of about 5 ml/minute to evacuate VOCs out of the chamber into a bag with activated coal. Vapour

samples were obtained from the column using gas-tight syringes (Hamilton Company, Geneva, Switzerland) and steel needles (26s/2"/2 L) stung through samplings ports which consisted of 4.8 mm holes closed with GC septa (Injection rubber plugs, Shimadzu, Kyoto, Japan). The sampling in the column was conducted with a high frequency for the first three days followed by a lower frequency until 14 days. During the high frequency sampling, only the sampling ports every 20 cm along the column were used due to the limited number of sample that could be processed. Later, spatial resolution increased to 5 cm for *n*-octane, toluene and *m*-xylene. The room temperature was recorded by continued measurements with a reading every 30 minutes and remained stable at 23.5 ±0.5°C during the whole experiment.

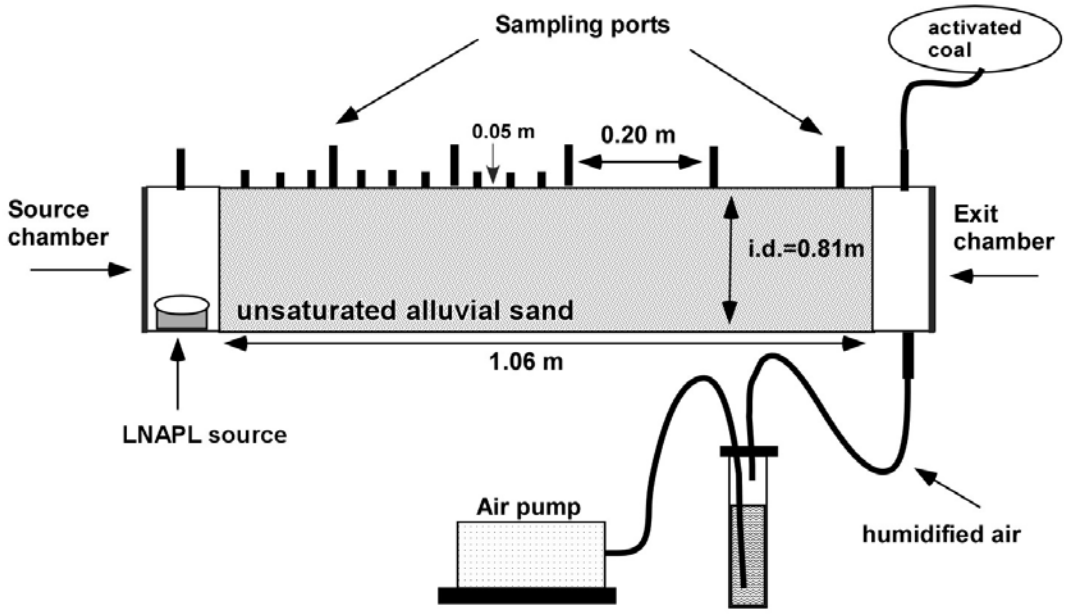

Figure 3.1: Experimental setup and dimensions of the column

3.2.4 Analytical solution for 1-D finite domain

Diffusion described by Fick's law is the dominant process for 1-dimensional VOC transport and biodegradation is assumed to be first-order with respect to the VOC vapour concentration as described by equation 1.14. The different phases of VOC evolution in the source and column (i.e. a transient state soon after source emplacement, a steady state later on and a second transient state due to source depletion) complicate the solution of equation 1.14. In order to be able to accommodate the different boundary conditions at the source, the transfer

function model approach as described by Jury & Roth (1990) is used. The model approach combines the transfer function term with a specific boundary condition term to describe the response in a given domain to any type of boundary condition. In a first step, the transfer function, which corresponds to the response to a time-Dirac input $\delta(t)$ is transformed in the Laplace space to obtain:

$$\hat{g}(x,p) = \exp^{-\sqrt{\frac{k+p}{D_s}}x} = Lp\left\{\frac{x}{2\sqrt{\pi D_s}\,t^{3/2}}\exp^{-\frac{x^2}{4D_s t}-kt}\right\} \tag{3.2}$$

where x is the distance from the source (m), p is the complex Laplace variable (d^{-1}), k is the apparent biodegradation rate applied to the gaseous phase (d^{-1}), Lp denotes the Laplace transform operator, t is the time (d) and D_s is the sorption-affected diffusion coefficient of the compound (m^2d^{-1}).

The time-dependent boundary condition *C(0,t)* can be expressed in the time domain and then be converted into a Laplace space. The concentration resulting from any time-dependent input is obtained by applying the principle of superposition, which can be expressed as the convolution integral of equation 3.2 with the boundary condition function *C(0,t)*. In the Laplace space, the convolution product reads:

$$\hat{C}(x,p) = \hat{C}(0,p).\hat{g}(x,p) = Lp\left\{\int_0^t C(0,u)\,g(x,t-u)\,du\right\} \tag{3.3}$$

For a constant source, $C(0,t)=C_0$ (initial concentration) and assuming no contaminant elsewhere in the domain at time t=0, the boundary condition in the Laplace space corresponding to the initial transient-state response followed by steady-state conditions is:

$$\hat{C}(0,p) = Lp\{C_0\} = \frac{C_0}{p} \tag{3.4}$$

For a constant source during the time span ω and followed by source depletion, the boundary conditions in Laplace space can be written as:

$$\hat{C}(0,p) = Lp\left\{C_0\left[H(\omega-t)+H(t-\omega)\exp^{-\beta(t-\omega)}\right]\right\} = \frac{C_0}{p(p+\beta)}\left[p+\beta\left(1-\exp^{-p\omega}\right)\right] \tag{3.5}$$

where H is the Heaviside step function and β is the source decay rate (d^{-1}). As ω indicates the moment when the source starts decaying, the initial transient-state and steady-state conditions are imposed for $t < \omega$ (for t sufficiently long) and a final transient-state condition with source depletion for $t > \omega$. Exponential depletion of a compound in the source is assumed and expressed in the form of $C_a=C_0\exp^{-\beta t}$. A Fortran program was used for the numerical inversion of the Laplace transformed functions in the time domain, following the algorithm of (Crump, 1976) and coupled with the quotient-difference algorithm to accelerate the convergence of the Fourier series (De Hoog *et al.*, 1982).

3.2.5 Biodegradation quantification at steady state

Biodegradation is assumed to proceed only in the water phase and obey first order kinetics. Some justifications for these assumptions can be found in a previous studies using the same column (Höhener *et al.*, 2003). A simple solution to equation 1.16 can directly be derived when steady-state condition is assumed in the system. The solution is provided by Wilson (1997) and was used to estimate the biodegradation rates of VOCs volatilizing from a constant source and migrating under steady-state conditions. For the boundary conditions:

$$C_a = C_0 \quad at \quad z = 0 \tag{3.6 a}$$

$$C_a = 0 \quad at \quad z = L \tag{3.6 b}$$

The following solution is obtained:

$$C_a(x) = C_0 \frac{\sin h\left[\sqrt{\frac{k}{D_e}}(L-x)\right]}{\sin h\left[\sqrt{\frac{k}{D_e}}L\right]} \tag{3.6 c}$$

where L (m) is the length of the column filled with sand. The coefficient k was determined by fitting the solution to the measured concentrations in the column using the solver module included in the Excel software (Microsoft).

3.2.6 Simulation of isotope data

The presence of the ^{13}C isotope in a molecule is the key point in this simulation approach. The modelling of the spatial and temporal variation in $\delta^{13}C$ is based on two major assumptions:

- ^{13}C-molecules degrade slower than ^{12}C-molecules
- ^{13}C-molecules diffuse slower than ^{12}C-molecules

The approach with 2 subspecies was used in this study to take into account those two effects in the model. The selected approach makes abstraction of reactive positions and thus indicated here for the aromatic compounds (see section 1.5.3). Thereby, the division of all compounds to be modelled was performed as shown in Figure 1.1. Evolution of each subspecies was then independently simulated as there would be two different compounds. The simulated quantities of two subspecies are then combined to calculate the isotope ratio.

3.2.6-A Initial concentration

Concentrations of each compound in the headspace calculated using Raoult's law and measurements of initial $\delta^{13}C$ values were used to determine initial concentrations of each subspecies. The initial isotope ratio $^{13}C/^{12}C$ (R_{atom}) must be first converted into molecule ratio ^{13}C-molecule/^{12}Cmolecule ($R_{molecule}$) using:

$$R_{molecule} = \frac{R_{atom}}{\left(\frac{1-\left(n-1\left(R_{atom}\right)\right)}{n}\right)} \tag{3.7}$$

where n is the number of C in the molecule. Then, the initial concentration (C_0) is distributed to subspecies ($^{l}C_0$ and $^{h}C_0$) according to $R_{molecule}$ obtained from equation 3.7 (Table 3.2).

3.2.6-B Diffusion coefficients

Due to the supplementary weight, molecules containing one ^{13}C are expected to diffuse slower and hence isotope-specific diffusion coefficients were calculated. The molecular diffusion coefficient obtained from the literature was attributed to the dominant light subspecies (^{l}D). The molecular diffusion coefficient for molecule with ^{13}C was derived from ^{l}D (Craig, 1953; Jost, 1960) according to equation 15 (Cerling *et al.*, 1991) and was attributed to the heavy subspecies (^{h}D):

$$\frac{{}^{l}D}{{}^{h}D} = \sqrt{\frac{{}^{h}M_w({}^{l}M_w + M_a)}{{}^{l}M_w({}^{h}M_w + M_a)}} \tag{3.8}$$

where ${}^{l}M_w$ and ${}^{h}M_w$ are the atomic masses of subspecies I, subspecies with one ^{13}C. M_a is the average mass of nitrogen, oxygen and hydrocarbons in the air, calculated using the initial hydrocarbon concentration at the source. Molecular diffusion coefficients used for the modelling simulations are listed for each contaminant in Table 3.2.

3.2.6-C Biodegradation rates

The biodegradation rate calculated based on measured concentrations was attributed to ^{12}C-molecules (${}^{l}k$). The smaller biodegradation rate for ^{13}C-molecules (${}^{h}k$) was determined using:

$$\alpha = {}^{h}k_{2sp} / {}^{l}k \tag{3.9}$$

Where α is the isotope fractionation factor for the compound of interest taken from the microcosm study.

3.2.6-D Source depletion

As volatilisation of VOCs from the source progresses, depletion of some compounds is expected to occur. A fickian-based equation can be used to link the change in mass of a compound in the source with mass loss across the column. If one assumes simultaneous equilibrium with linear exchange between gas and liquid phase in the source chamber and a linear concentration profile in the column as expected for steady state conditions in absence of biodegradation, the equation expressing the change in mass is:

$$\frac{\partial w_i}{\partial t} = -\frac{AD_m\theta_a\tau C_{a,i}}{L} \tag{3.10}$$

where w_i is the quantity of the compound i and A is the cross section area. Using Raoult's law to determine the partial pressure of a compound in the headspace above a mixture, equation 3.10 becomes:

$$\left(V_g + \frac{m_{tot}}{C_{sat}}\right)\frac{\partial C_{a,i}}{\partial t} = -\frac{AD_m\theta_a\tau C_{a,i}}{L} \tag{3.11}$$

where V_g is the gas phase volume of the source, m_{tot} the total amount of compounds in the source and C_{sat} the vapour pressure expressed as concentration. V_g corresponds to the contribution of compounds in the gas phase to the total mass in the source and can be neglected because it is much smaller than the amount of compound present in the organic liquid. For compounds present in a small amount (w_i) in the liquid mixture, m_{tot} can be assumed to remain constant over time. Finally, the solution to equation 3.11 with a boundary condition imposing initial vapour concentration $C_{0,i}$ simply reads:

$$C_{a,i}(t) = C_{0,i} \exp(-\beta t) \tag{3.12}$$

where β (d^{-1}) is the compound depletion rate described by:

$$\beta = \frac{AD_m \theta_a \tau}{\left(m_{tot} / C_{sat}\right) L} \tag{3.13}$$

The term compound depletion rate refers to the rate at which the compound is disappearing from the organic liquid. An equation that described the evolution of $^{13}C/^{12}C$ of the compound *i* can be obtained by dividing equation 3.12 for ^{13}C by an analogous equation of ^{12}C followed by rearrangement:

$$\frac{{}^{h}C_{a,i}}{{}^{l}C_{a,i}} = \frac{{}^{h}C_{0,i}}{{}^{l}C_{0,i}} \exp^{\left({}^{l}\beta - {}^{h}\beta\right)} \tag{3.14}$$

The form of equation 3.14 is analogous to the Rayleigh equation (1.7). Therefore, isotope fractionation during depletion of a compound is expected to follow a Rayleigh trend and a linear relationship with a slope corresponding to the isotopic enrichment factor is expected if the natural logarithm of the concentration is plotted against the $\delta^{13}C$. The isotope factor is expected to correspond to:

$$\alpha = \frac{{}^{h}\beta}{{}^{l}\beta} \tag{3.15}$$

Using equation 3.13 and the ideal gas law to relate saturation concentrations to vapour pressure (*P*), the ratio between the compound depletion rate for light and heavy molecules corresponds to:

$$\alpha = \frac{{}^{h}\beta}{{}^{l}\beta} = \frac{{}^{h}D_m \cdot {}^{h}C_{sat}}{{}^{l}D_m \cdot {}^{l}C_{sat}} = \frac{{}^{h}D_m \cdot {}^{h}P}{{}^{l}D_m \cdot {}^{l}P} \tag{3.16}$$

The ratio between the vapour pressures corresponding to the equilibrium isotope effect is much closer to 1 than the ratio between the diffusion coefficients and hence the former can usually be set to 1 leading to the following approximation for the isotope fractionation factor:

$$\alpha = \frac{{}^{h}\beta}{{}^{l}\beta} = \frac{{}^{h}D_m}{{}^{l}D_m} \tag{3.17}$$

The diffusion coefficient of the ^{13}C-molecule can be calculated from the diffusion coefficient of the ^{12}C molecule using equation 3.8. Equation 3.17 makes it possible to calculate the compound depletion rate for the ^{13}C-molecule if the rate of the ^{12}C-molecule is known.

Table 3.2

initial concentration (C_0) and $^{13}C/^{12}C$ ratio (δ), enrichment factor (ε), sorption-affected diffusion coefficients (D_s), biodegradation (k) and source decay (β) rates for selected compounds to be modelled (at 23.5 °C).

	$^{l}C_0$ (g/m^3)	**$^{h}C_0$ (g/m^3)**	**$\delta^{13}C$ (‰)**	**ε [1] (‰)**	**$^{l}D_s$ (m^{2}d^{-1})**	**$^{h}D_s$ (m^{2}d^{-1})**	**^{l}k [2] (d^{-1})**	**^{h}k (d^{-1})**	**$^{l}\beta$ (d^{-1})**	**$^{h}\beta$ (d^{-1})**
n-Pentane	122.2681	6.9719	-29.41	-3.8	0.3670	0.3662	0	0	0.1905[3]	0.1901
n-Hexane	72.4368	5.0132	-29.51	-2.2	0.2791	0.2787	0.34	0.3393	0.0812[3]	0.08107
n-Octane	7.2373	0.6827	-30.68	-1.0	0.1239	0.1238	3.25	3.2468	na	na
Benzene	12.6425	0.8775	-26.81	-2.1	0.1087	0.1085	0.36	0.3592	0.0807[3]	0.08055
Isooctane	38.4627	3.6473	-23.53	na	0.2691	0.2688	0	0	na	na
Toluene	5.648	0.462	-28.25	-0.8	0.0498	0.0497	0.74	0.7394	na	na
MCH	27.7158	2.2742	-25.38	-1.1	0.2543	0.2539	0.11	0.1099	na	na

[1] from Table 2.1 (varied within range of uncertainty)

[2] Value for *n*-pentane from Höhener *et al*. (2003)

[3] Using ω=0 for *n*-pentane and 96h for *n*-hexane and benzene

na: not available/ not applicable

3.3 Results

3.3.1 Evolution of concentration profiles

After source emplacement, the concentration profiles of all VOCs evolved in the column as illustrated in Figure 3.3. In general, larger concentrations of all compounds were measured close to the source and diminished with distance. *n*-Pentane and *n*-hexane were the first compounds to reach the end of the column (within 12 hours). In contrast, *n*-octane and *m*-xylene were never detected further away than 0.8 m and 0.6 m, respectively. No data for *n*-decane were obtained as the vapour pressure of the compound was too low to lead to significant gas phase concentrations. Values for 1,2,4-TMB are not reported since concentrations were too close to detection limit and fluctuated. The concentration profiles measured later than 96h for methyl-cyclohexane (MCH), isooctane and *n*-octane, and later than 145h for toluene remained stable until the end of the experiment. The concentrations profiles for *n*-pentane were observed to decrease with time after more than to 72h until almost complete depletion, while for *n*-hexane and benzene, a decrease in concentration was noted after more than 145h.

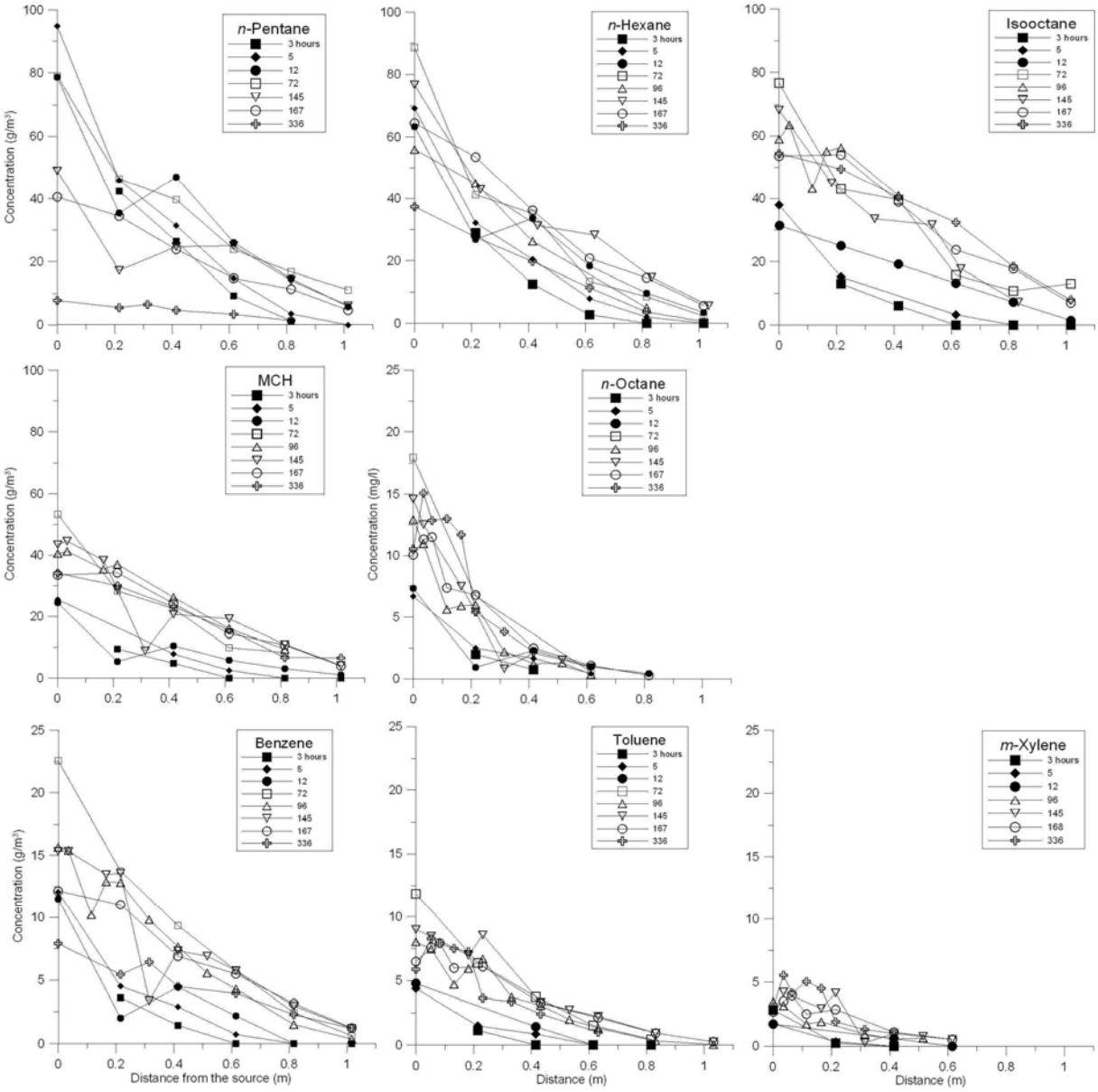

Figure 3.3: Concentration profile evolution for VOCs in the column at selected times.

Expected concentrations for each compound at the farthest sampling point (x=1.015 m) were simulated to evaluate the required time to reach steady state concentration profiles. A constant source for all compounds was assumed (Figure 3.4). *n*-Pentane was the first to reach the steady state at t=55h and toluene, the latest at t=140h. Hence it is indeed plausible that a steady state was reached for most of the compounds within the experimental period.

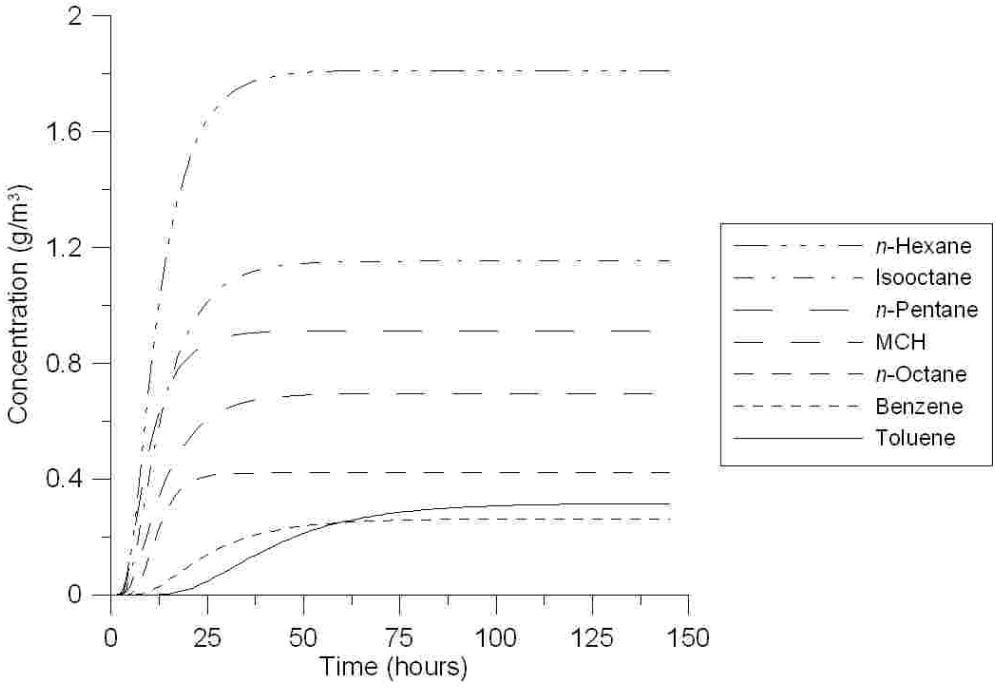

Figure 3.4: Concentration evolution at distance x=1 m in the column from source emplacement until t=140 hours for seven VOCs. Note that concentration of *n*-octane was multiplied by 100 in order to have similar range of concentrations.

3.3.2 Evolution of $\delta^{13}C$ profiles

Measurements of the $\delta^{13}C$ in the column are presented for *n*-pentane, *n*-hexane, benzene, MCH isooctane and *m*-xylene in Figure 3.5 and for *n*-octane and toluene in Figure 3.6. The isotope evolution varied in space and time and the extent of variation was compound dependent. Globally, lighter molecules exhibited larger isotopic variations than heavier molecules. Early after the source emplacement, the measurements show negative shifts with increasing distance in respect to the source signal. The maximal isotope shift (measured at t=5h) was as follows: 4.8‰ for *n*-pentane, 3.8‰ for *n*-hexane, 2.8‰ for benzene, 2.3‰ for toluene, 2.1‰ for *n*-octane, 1.7‰ for MCH and 1.4 ‰ for isooctane. With time, the shifts were continuously becoming smaller until, at time t=26h or 58h, the isotope ratio of all compounds had mostly levelled out with distance at the value measured in the source chamber. Finally, different $\delta^{13}C$ profiles were observed during source depletion. The isotope ratios of MCH and isooctane (>72h) remained unchanged close to the initial isotope ratio of the source chamber, while *n*-pentane (>72h) and benzene (>96h) also showed flat isotope ratio profile, but with globally more positive $\delta^{13}C$ values. The isotope ratios measured for *n*-

hexane at t=72h and 96h (figure 3.5) tended to shift to positive values with respect to the source chamber and the same tendency is later observed for *n*-octane whereas negative shifts were still observed for toluene (Figure 3.6). A general movement toward more positive values of the profile is noted for *n*-hexane from t=168h, with the exception that it still shows to some extent a positive shift with distance compared to *n*-pentane and benzene.

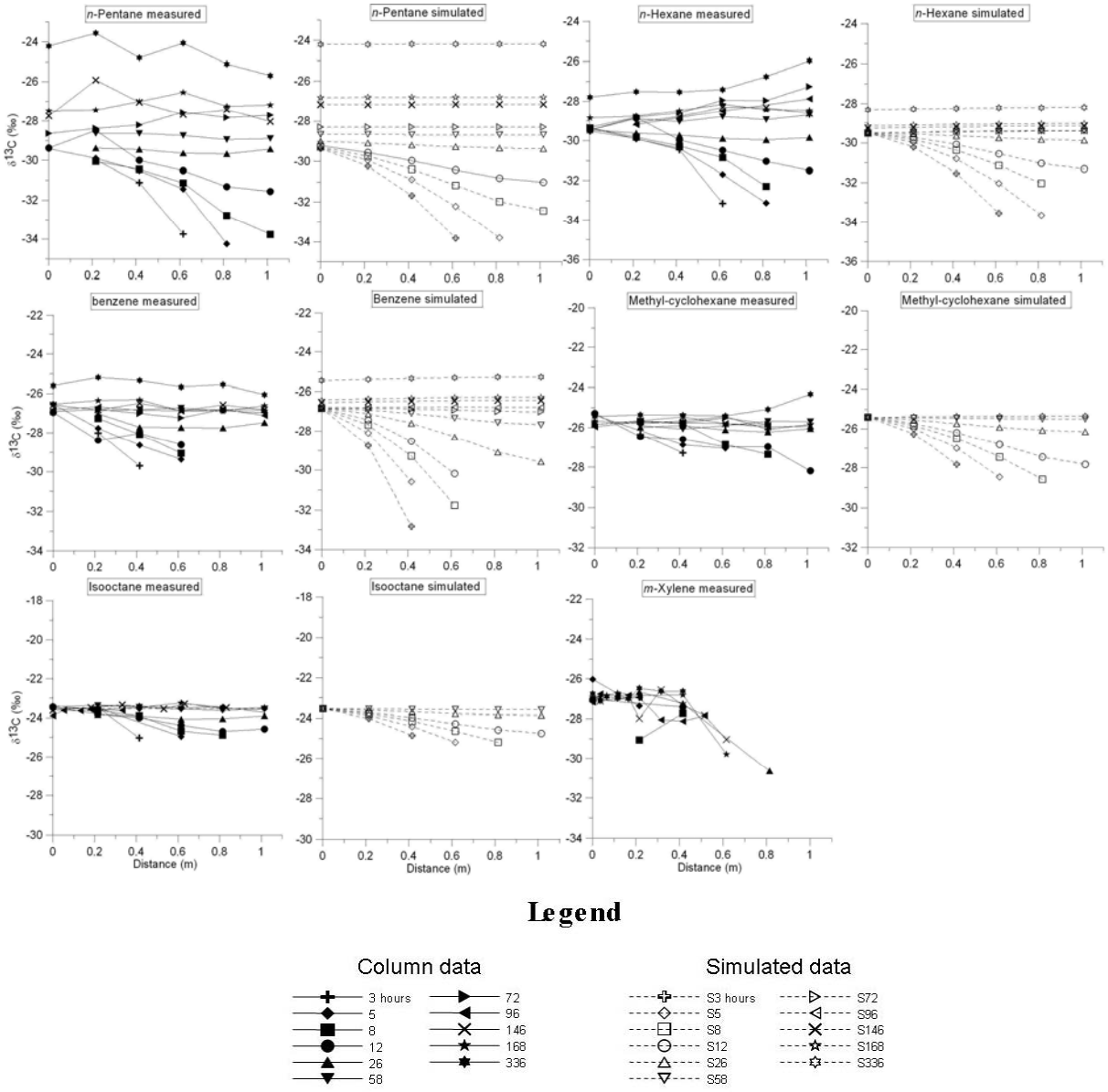

Figure 3.5: Measured (filled symbols) and simulated (open symbols) $\delta^{13}C$ values in the column at selected distances and periodicities. No simulation was performed for *m*-xylene.

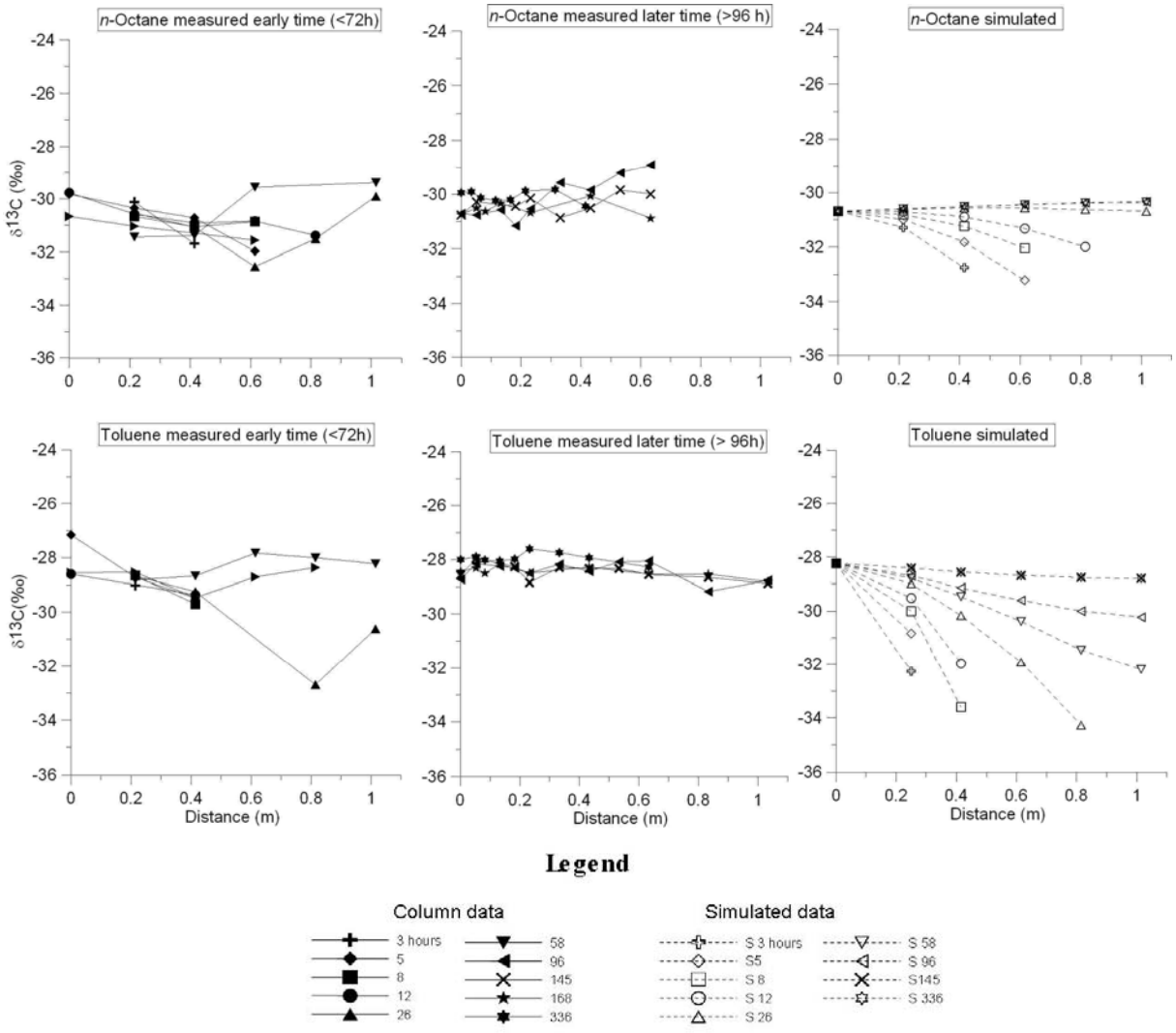

Figure 3.6: Measured (filled symbols) and simulated (open symbols) $\delta^{13}C$ values in the column at selected distances and periodicities. After more than 145h, the simulated isotope profile remained constant.

3.3.3 Evolution of source concentration and $\delta^{13}C$

The vapour concentration and $\delta^{13}C$ values monitored in the source chamber during 14 days are illustrated in Figure 3.7. All concentrations showed a decrease in the first 12 hours after source emplacement. By day 3, the concentration went back to the initial value, except for *n*-pentane which stayed about 40% lower. Later, three compounds clearly showed gradual concentration decreases indicating that they became depleted in the source. The strongest depletion was observed for *n*-pentane starting from the initial time, followed by *n*-hexane and benzene at day 6. Isooctane and MCH showed a tendency to decrease from day 6 to day 11, but increased again later.

The isotope ratios measured for most of the compounds (Figure 3.7) showed an initial rapid response in form of a positive shift in the first 12 hours after source emplacement and then fell back to initial values at the latest at day 3. The $\delta^{13}C$ of isooctane remained stable during the whole period. The $\delta^{13}C$ of MCH and *m*-xylene remained stable until day 8 and then showed a very slight tendency towards more positive values. The $\delta^{13}C$ for *n*-octane and toluene remained stable during 11 days and then a rapid positive shift was observed. Nonetheless, in neither case these isotopic tendencies were associated with concentration changes in the source chamber. The isotope ratio of *n*-pentane was constantly increasing until the end of the experiment, while *n*-hexane and benzene were constant during an initial period and started to increase at later times as the concentration decreased in the source chamber. *n*-Pentane showed a shift of +5.28‰ with 10% of compound remaining after 14 days, whereas *n*-hexane and benzene showed a shift of +1.72‰ and +1.21‰ respectively, with 50% of compound remaining. Using a Rayleigh-type plot (Figure 3.8), the positive isotope shift occurring in the source chamber is linearly related with the natural logarithm of the concentration decrease from which a diffusion-isotope enrichment factor can be estimated as outline in 3.2.6-D. The enrichment factors for *n*-pentane, *n*-hexane and benzene are -2.14‰, -1.73‰ and -1.55‰, respectively.

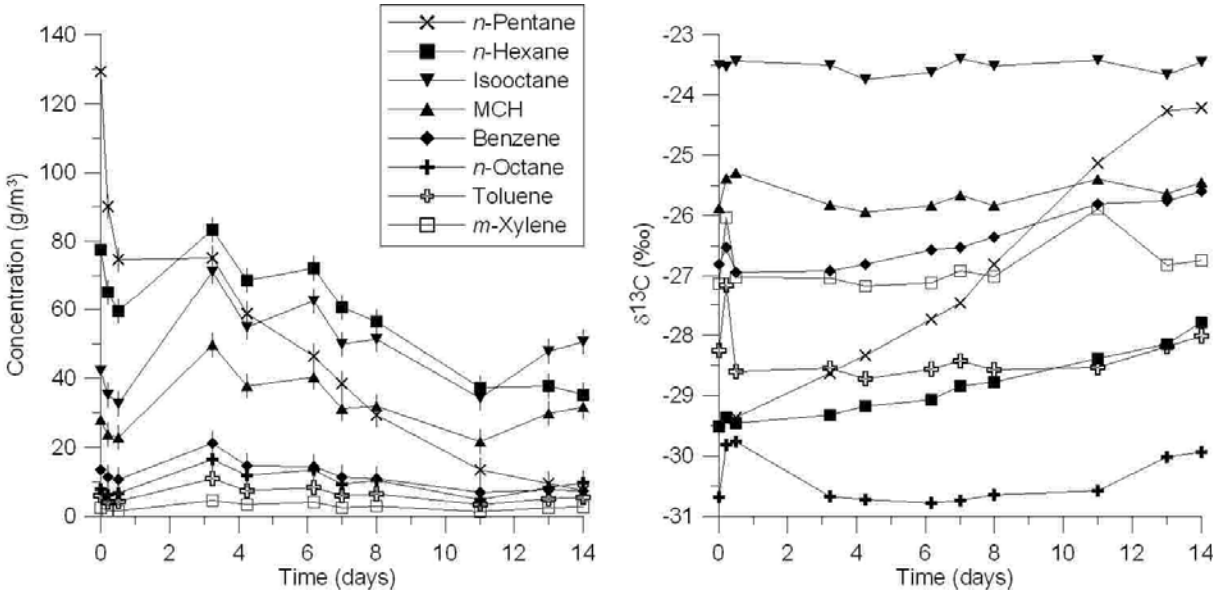

Figure 3.7: Evolution of VOCs concentration and the $\delta^{13}C$ in the source chamber during 14 days.

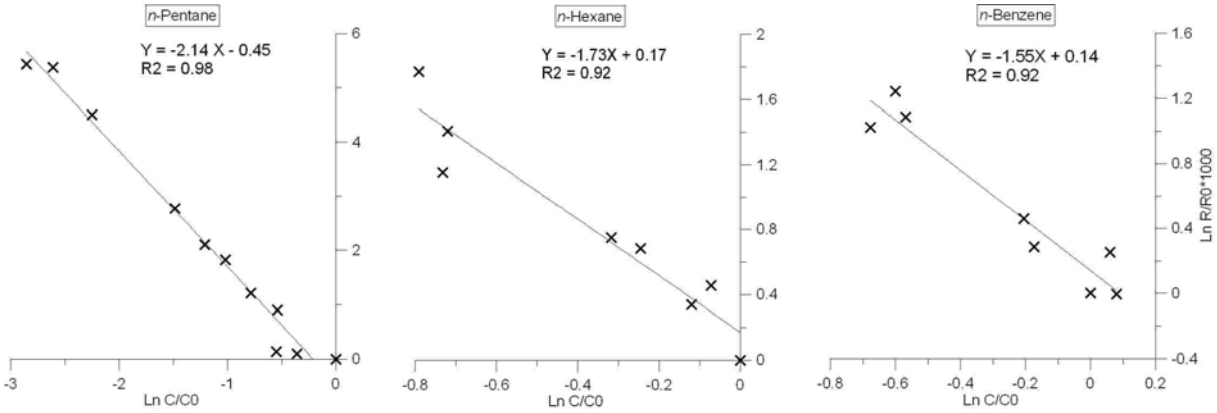

Figure 3.8: Relative isotope ratio (R/R_0) as a function of the concentration decrease (C/C_0) on a natural logarithm basis measured in the source chamber over a period of 14 days. Data measured at t=5h, 12h and 77h were omitted for *n*-hexane and benzene as the source was still constant.

3.3.4 Biodegradation

Biodegradation rates were estimated by fitting equation 3.6c to selected concentration profiles (Table 3.3). The sampling time t=145h was selected as the moment when a near steady-state was approximately reached, as indicated by stable concentration profiles (Figure 3.3), by the predicted concentrations at the farthest sampling point (Figure 3.4) and by the evolution of concentration and isotope ratios in the source chamber (Figure 3.7). However, due to the early depletion of *n*-pentane in the source, a steady-state was not reached for this compound and therefore, no biodegradation rate was calculated. However, a previous study (Höhener *et al.*, 2003) indicated that biodegradation of this compound does not occur in the sand. For *n*-hexane and benzene, the biodegradation rate was calculated at t=96h because isotope ratios in the source chamber indicated first signs of compound depletion at t=145h.

Table 3.3

Biodegradation rates for selected VOCs estimated from steady-state vapour profiles[1]. The values are compared to two other studies where the same alluvial sand was used.

	This study Eq. 3.6c	**Höhener *et al.* (2003)**	**Pasteris *et al.* (2002)**
n-Pentane	nm	<0.01	<0.01
n-Hexane	0.34	0.26	0.4
n-Octane	3.25	5.0	6.7 ± 1.7
Benzene	0.36	na	na
Toluene	0.74	1.31	3.2
Isooctane	0.09	0.09	0.12 ± 0.03
MCH	0.11	0.16	0.8 ± 0.4

[1] After 145 hours except for *n*-hexane and benzene: after 96 hours

nm: not measurable since steady-state condition not fulfilled

na: not applicable

3.4 Discussion

3.4.1 Evolution of concentration and $\delta^{13}C$ in source

The measured concentrations indicated depletion of *n*-pentane in the liquid source shortly after its emplacement, while the concentration of other compounds increases (Figure 3.7). These trends can be explained by increasing mole fractions for the other compound due to the depletion of *n*-pentane by volatilization. The changes in isotope composition as a function of the concentration decrease (Figure 3.8) were expected according to equation 3.14 and were due to the diffusion isotope effect. The linear relationship between isotope ratios and the ln of concentration measurements confirms that the isotope fractionation due to the diffusion isotope effect obeys to the Rayleigh's law. The slopes obtained with linear regression (Figure 3.7) for *n*-pentane, *n*-hexane and benzene (-2.14‰, -1.73‰ and -1.55‰, respectively) correspond well with the theoretically value calculated with equation 3.15, which are -2.18‰, -1.62‰, and -1.91‰, respectively. The good agreement for *n*-pentane is consistent with the absence of biodegradation. The small deviations for benzene, and to a lesser extent for *n*-

hexane, may be due to the relatively small concentration change that occurred during the period of measurement leading to larger uncertainty of the calculated isotope enrichment factor. Alternatively, biodegradation may have slightly altered the isotope enrichment factor. However, at this stage, it is not known how strongly biodegradation influences the isotope enrichment factor. A good agreement between measured (-4.2‰) and calculated (-4.4‰) diffusion isotope effect was previously observed by for CO_2 in the unsaturated zone (Cerling *et al.*, 1991). The large isotope enrichment factor for CO_2 compared to VOCs can be explained by its smaller mass. The remarkably good reproduction of isotope trend by the Rayleigh equation indicates that it may be used to quantify the extent of contaminant volatilization in a porous medium where diffusion controls the volatilization rate.

Several compounds (methyl-cyclohexane, *n*-octane, benzene, toluene and *m*-xylene) showed a short term ^{13}C increase at t=5 and for some also at 12h. This increase could be due to the strong concentration gradients in the column at the beginning of the experiment, which lead temporarily to a depletion of the gas phase of the source chamber associated with a diffusion isotope effect. This hypothesis is consistent with drop in the gas phase concentration observed simultaneously for these compounds. For other compounds, the effect may have occurred before the first measurement.

The isotope evolution were simulated using the equation 3.3 and are illustrated on Figure 3.5. For distance=0, the calculated results represent measurements in the source chamber. The global β (in equation 3.5) calculated with the decreasing concentrations (assuming exponential decrease) was attributed to ^{12}C-molecules ($^{l}\beta$) whereas β for ^{13}C-molecules ($^{h}\beta$) was derived with equation 3.17 (Table 3.2). No biodegradation of the compound was assumed to occur in the source chamber. Initialization of the source decay (ω) (in equation 3.5) was selected based on concentration measurements in the source chamber and was set to t=0 for *n*-pentane and to t=96h for both *n*-hexane and benzene. At t=336h, simulated $\delta^{13}C$ values at the source are -24.38‰, -28.31‰ and -25.46‰ for *n*-pentane, *n*-hexane and benzene, respectively which corresponds well to the measured data (-24.22‰, -27.79‰ and -25.6‰, respectively).

The measurements and simulations demonstrate that the evolution of the source isotope ratio of depleting compounds is dominated by different diffusion fluxes across the column for molecules with a different isotopic composition, rather than by an equilibrium isotope effect during the volatilisation step. Hence, at field sites, depleting compounds are expected to

become enriched in ^{13}C and not depleted in ^{13}C as predicated in previous studies based on the equilibrium isotope effect. Indeed, a ^{13}C enrichment trend was observed at a controlled field experiment as will be discussed in the next chapter.

3.4.2 Evolution of concentration profiles

Concentration profiles of each VOC were evolving in the column at different velocities during the first 12 hours after the source emplacement. The high concentrations and the rapid concentration variations for *n*-pentane, *n*-hexane and isooctane in the column can be explained by their high vapour pressure and high initial concentration in the source. For less volatile compounds, the concentrations varied to a lesser extend. *n*-Pentane and *n*-hexane more quickly reached the end of the column than benzene and toluene. These latter compounds have similar diffusion coefficient in the air as *n*-pentane and *n*-hexane (Table 3.1), but partition more strongly into the aqueous phase and hence their migration is retarded. Similar tendency due to hydrophobicity were also observed by Christophersen *et al,* (2005) during a field experiment. Migration of *n*-octane and *m*-xylene was restrained to 0.8 m and 0.6 m, respectively, likely due to microbial degradation. The biodegradation rates measured in this study were similar to those evaluated with the same sand by Höhener *et al.* (2003) and Pasteris *et al.* (2002) (Table 3.2). However, although concentration profiles suggested steady-state conditions after 145 hours, the full potential of biodegradation was probably not yet reached considering that cell growth may occur (Höhener *et al*., 2003).

3.4.3 Diffusion effect on $\delta^{13}C$ profile

During early time, decreasing $\delta^{13}C$ values with increasing distance from the source can be observed (negative shift). Large negative shifts caused by diffusion were also observed by (Zhang & Krooss, 2001) during initial transient-state diffusion of methane through water-saturated sedimentary rocks and gradually decreased when approaching the steady state. The depletion of ^{13}C with distance is due to a faster diffusion of compounds with ^{12}C only. The presence of a supplemental neutron in the carbon nucleus diminishes the velocity of the molecule as indicated by equation 3.8. This tendency was observed for all compounds, but to a different extent. The supplemental weight of a heavy carbon is more relevant in small molecules, and the difference between the two isotope-specific diffusion coefficients (^{12}C-molecule vs ^{13}C-molecule) is thus more pronounced. As expected, the largest negative shift was observed for *n*-pentane and the smallest shifts were observed for isooctane and *n*-octane.

A negative shift was seen until ^{13}C-molecules have compensated the retard due to a slower diffusion velocity.

The simulated isotope ratios provided a good match with the measured data (Figure 3.5 and 3.6). The isotope ratios measured at early times are well reproduced by the model using isotope-specific diffusion coefficients, confirming the strong influence of diffusion in the initial phase. The progressive transfer from sorption-affected diffusion (at transient-state condition) to effective diffusion (at steady-state condition) may affect the accuracy of the simulated isotope ratios as it can not be taken into account in the modelling. This change affects particularly compounds with higher hydrophobicity such as aromatic compounds and may explain the reduced fit of simulated data for benzene. A better fit with the measured data can be obtained if the diffusion coefficients are slightly modified from default values, by either adjusting the tortuosity and/or the water content within the incertitude error. It should be noted that calculations for isooctane were performed until t=58h as the fractionation factor is unknown and biodegradation is not expected to be relevant at early time. Data for *m*-xylene were scarce due to the low concentration of the compound and were thus not modelled.

3.4.4 Degradation effect on $\delta^{13}C$ profile

Evolution of the isotope signature at the source has obviously a repercussion on the isotope ratio thought out the column. Therefore, evaluation of biodegradation in column must be performed in relation with the state of the source. For more clarity, data interpretation for compounds with relatively constant concentrations and constant isotope ratios at the source will be treated first and separately for the others.

When the source $\delta^{13}C$ signal remains unchanged and no biodegradation occurs in the column, the $\delta^{13}C$ profile is expected to converge to a constant value (flat profile) after the initial diffusion effect has disappeared (further detailed in chapter 5). In contrast, when biodegradation occurs, the $\delta^{13}C$ values are expected to shift in positive direction with distance. The reason is the slightly faster degradation of ^{12}C-molecules leading to an accumulation of ^{13}C-molecules with distance. Indeed, the isotope ratios measured at later time for *n*-octane (Figure 3.6) showed small but consistent gradual positive shift more or less greater than what the modelling predicts. In contrast, toluene showed negative shifts even at steady-state (t>145h). Although unusual, these shifts are expected based on the model. As toluene is degraded, the concentration gradient forces the light toluene to travel faster, and

due to a small enrichment factor, the shift can not become positive. In this case, the isotope ratio is still dominated by the diffusion effect. However, the positive or negative change in $\delta^{13}C$ values in the profile for both *n*-octane and toluene are small.

In contrast to the previous compounds, the isotope pattern for *n*-pentane, *n*-hexane and benzene showed a global increase of the whole isotopic profile which was stronger than the change with distance. Theoretically, the steady state was reached for the benzene and *n*-hexane prior to 96h (Figure 3.4), and therefore it is possible to evaluate biodegradation based on the isotope data. A positive shift with distance can be seen for *n*-hexane suggesting biodegradation. The shift is larger than expected by the model. During the final measurement, a shift towards more positive values is observed through out the profile which is related to source decay rather than biodegradation as it occurred only after *n*-hexane started to deplete. For *n*-pentane, the large shifts to more positive values are not at all related to biodegradation since they correspond relatively well to the values simulated without taking into account biodegradation.

In this study, the experimental features such as the short length of the column, the source depletion and low biodegradation rates were not optimal to identify isotope fractionation due to biodegradation. To confirm positive measured isotope shifts due to biodegradation, a longer steady-state period is needed in order to duplicate profile measurements and a column long enough to provide $\delta^{13}C$ shifts greater than 1‰ as required to statistically distinguish two $\delta^{13}C$ measurements (Slater, 2003).

3.4.5 Field implication of isotope fractionation at the source

For contaminations in the unsaturated zones, isotope monitoring may also become a powerful tool to indicate depletion of compounds in the source more accurately than conventional concentration measurements. Isotope ratios at the source were much more regular than concentration data (Figure 3.6) and hence may be a more sensitive tool to identify depletion of a compound. The contrast between the two types of data may even larger in field situation where concentrations are influenced by numerous factors (e.g. varying temperature, barometric pressure). In addition, the prediction of vapour concentrations adjacent to a multicomponent NAPL based on Raoult's law becomes a laborious task with increasing number of compounds in the source, which impedes clear distinction of concentration depletion (Broholm *et al.*, 2005; Gioia *et al.*, 1998; Liang & Udell, 1999; Schaefer *et al.*,

1998). For instance, the positive trends seen for toluene and *n*-octane at later time (Figure 3.6) are perhaps indicating an eventual depletion of the compound not observed yet by concentration measurements. The independency of the isotope analysis is an advantage as it will provide robust measurements to clearly assess depletion of a compound. As the biodegradation effect on the isotope ratio is stage associated with the eventual source depletion effect, the assessment remains on a qualitative base.

3.5. Conclusions for the column experiment

The aim of this study was to investigate the effect of diffusion on carbon isotope fractionation, isotope evolution during volatilisation of the source and whether isotope data of gaseous volatile compounds can be used to obtain clear evidence for biodegradation in a simple one-dimensional setting. The column study successfully demonstrated a diffusion isotope effect which leads to significant isotope fractionation at early stage in the VOC vapours away from the source and at later stage at the source itself. The effect was larger for small molecules as the additional weight brought by the heavy isotope is more significant in the total weight of the molecule. The use of Fick's law to describe concentration distribution of ^{12}C-compounds and ^{13}C-compounds was shown to be appropriate in order to reproduce the isotope evolution. Measurements in the source chamber showed positive evolution of the $\delta^{13}C$ in the vapour phase as the compound is getting depleted from the liquid mixture. The isotopic evolution follows the Rayleigh equation whereas the fractionation factor is proportional to the different diffusion coefficients of the two isotopes. The new isotope signature in the source chamber is thus affecting the $\delta^{13}C$ measured in the whole system, and the analytical simulations effectively related the positive $\delta^{13}C$ values measured into the column to the source evolution instead of biodegradation. Therefore, findings on this isotope fractionation in the source chamber are fundamental knowledge and underline the imperative necessity of source monitoring. Finally, an enrichment in $\delta^{13}C$ we observed for *n*-hexane and *n*-octane due to biodegradation. However, because of the small variation of the $\delta^{13}C$ values with distance, a conclusion of presence of biodegradation can not be drawn and a longer soil system is therefore recommended.

Chapter 4

Controlled field experiment

Abstract

A field experiment was conducted in Denmark in order to evaluate the biodegradation of 13 volatile organic compounds (VOCs) that were buried in the form of an artificial fuel source in the unsaturated zone. Compound specific isotope analysis showed distinct phases in $^{13}C/^{12}C$ ratio variation over space and time which can originate either from preferential microbial degradation of ^{12}C-compounds over ^{13}C-compounds or from isotope fractionation during the migration of the compounds. Different diffusion coefficients according to different isotopic masses would be responsible for a physical isotope fractionation. A reactive 2D-radial transport model was used to reproduce the isotopic shifts of four VOCs in the unsaturated zone measured over space and time during the field experiment. Input parameters were the carbon isotope fractionation factor, the calculated mass-specific diffusion coefficients, and biodegradation rate data previously evaluated from model calibration to measured field concentration data. The model simulations showed that transport dominates the isotope fractionation during the initial days of VOC vapour migration, whereas biodegradation dominates the fractionation in later time. The model simulation helped to evaluate whether physical aspect like diffusion can influence the evolution of $^{13}C/^{12}C$ ratio over space and also demonstrated the feasibility of using carbon isotope fractionation to assess biodegradation of contaminants in the unsaturated zone.

Bouchard D, Hunkeler D, Gaganis P, Aravena R, Höhener P and Kjeldsen P; **Diffusion and biodegradation effect on $\delta^{13}C$ measurements during migration of petroleum hydrocarbon vapours in the unsaturated zone: field experiment and modelling simulations**

To be submitted to **Environmental Science & Technology**

4.1 Introduction and aims

The aim of this study is to evaluate if CSIA can also be used to demonstrate biodegradation in the unsaturated zone and to evaluate the factors that control the isotope ratios of VOCs. For this purpose, temporal and spatial variations of carbon isotope ratios of a number of VOCs and CO_2 were measured during a controlled field experiment at the Varloese airbase, Denmark. The experimental setup consisted in burying a multicomponent hydrocarbon source in the unsaturated zone of a highly controlled field site, in Denmark. In the unsaturated zone, isotope ratios can potentially also be affected by diffusion in addition to biodegradation, as indicated by studies on isotope ratios of CO_2 (Cerling *et al.*, 1991) and CH_4 (Galimov, 1967; Pernaton *et al.*, 1996; Reitsema *et al.*, 1981; Zhang & Krooss, 2001) and by the previous chapter. To gain more detailed insight into the factors controlling the isotope shifts, a numerical model was used that incorporates isotope fractionation and it was attempted to reproduce the isotope variations observed at the field scale.

4.2 Materials and methods

4.2.1 Field experiment

A controlled field experiment was carried out at the Værløse Airbase, in Denmark, as part of the GRACOS project, to simulate a light NAPL spill in the unsaturated zone (GRACOS project: Groundwater risk assessment at contaminated sites, 5th EC framework programme, http://www.uni-tuebingen.de/gracos/). The artificial point source contamination was created by mixing 13 petroleum hydrocarbons and burying this mixture to a depth between of 0.8 m and 1.3 m in the unsaturated zone of a sandy aquifer. A dense network of sampling devices was installed in both saturated and non saturated zones to study the behaviour of the VOCs in the system. Soil gas concentrations were monitored in great detail in the unsaturated zone and the sampling methodology used is described in Christophersen *et al.*, (2005). Concentration and carbon isotope analyses described in this manuscript were sampled within a restrained section of the experimental area (Figure 4.1). Selected sampling points were located at 1 m depth and varied laterally up to 5 m away from the center of the source, and the sampling frequency was established according to model predictions previously run. Gaseous organic compounds stored in glass bottles and closed with Mininert® valves were extracted using a solid phase microextraction (SPME) as described in Hunkeler & Aravena (2000) and stable carbon isotope analyses were performed at the University of Waterloo, Canada, using a

Hewlett-Packard gas chromatograph (GC) connected via a combustion interface to a Micromass Isochrom isotope-ratio mass spectrometer (MS) (Micromass, Manchester, U.K.). Analytical uncertainty for isotope measurements was 0.14‰.

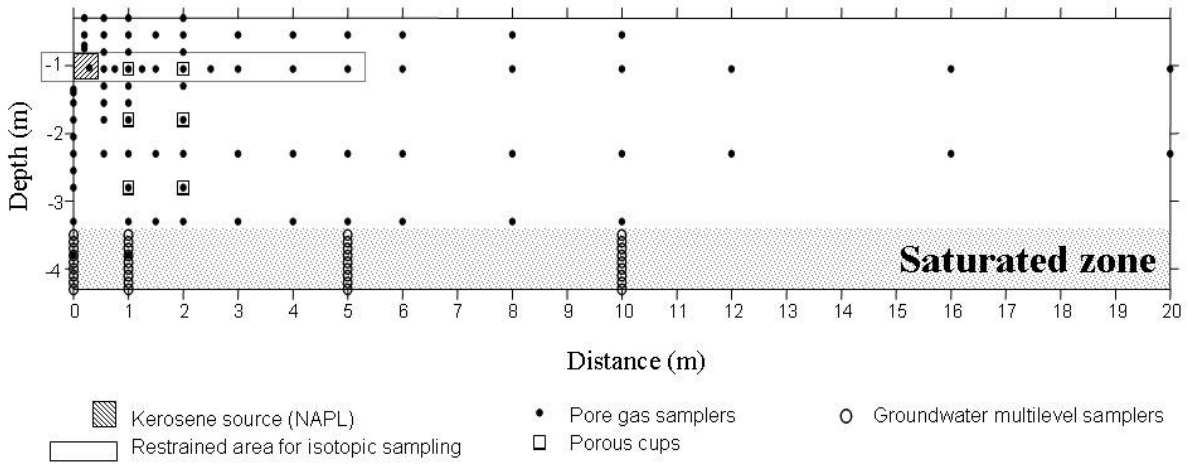

Figure 4.1: Cross-section of the field sampling network at the Værløse Airbase experimental site with location of pore gas samplers and porous cups. The restrained area for the isotopic measurements is delineated by a rectangle. Modified from Kaufmann *et al*. (2004)

4.2.2 Model simulation

The MOFAT code is a two-dimensional finite element program for multiphase flow and multicomponent transport/reaction in the subsurface. The model takes into account transport in the gaseous and liquid phase, equilibrium partitioning between gas, water and organic phase and first order biodegradation (Katyal *et al.*, 1991). Five components can be simulated at once in both saturated and unsaturated zones. The MOFAT code has previously been used to simulate VOC transport in the field experiment carried out at the Værløse Airbase (Gaganis *et al*, 2004) and succeeded to quantify the biodegradation rates of six selected VOCs occurring under natural attenuation conditions.

The modelling of the isotope ratio evolution over space and time was performed based on the same assumptions developed earlier. The division allowed each subspecies to be treated separately in the model with their specific behaviours as it would be for distinct contaminants and all other compounds from the fuel mixture were regrouped as pseudo species with effective physico-chemical parameters (Gaganis *et al.*, 2002; Karapanagioti *et al.*, 2003; Karapanagioti *et al.*, 2004). Then, for selected periodicities and distances corresponding to the

sampling days of the field experiment, the remaining number of moles of ^{13}C estimated with the model is divided by the number of moles ^{12}C to provide the resulting isotopic ratio. *n*-Hexane and *n*-octane were modelled under both approaches in order to confirm the similarity whereas toluene and methyl-cyclopentane (MCP) were modelled with the approach of 2 subspecies. Biodegradation rates, diffusion coefficient and the initial mass have to be quantified for each subspecies.

4.2.2-A Initial masses

In order to carry out the calculations, not only the degradation rates for the different subspecies have to be known but also the initial quantity of each subspecies in the contaminant source. The quantity of ^{12}C and ^{13}C atoms for a compound in the source, m_{12} and m_{13}, respectively, can be calculated as follows from the total quantity of carbon (w_0):

$$m_{12} = \frac{w_0}{(13 * R_0) + 12} \tag{5.1}$$

$$m_{13} = \frac{w_0}{\left(\frac{12}{R_0}\right) + 13} \tag{5.2}$$

where R_0 is the initial isotope ratio of the compound. For the 2 subspecies approach, the initial number of mole of subspecies I ($m_{0,I}$) and subspecies II ($m_{0,II}$) is then given by:

$$m_{0,I} = \frac{m_{12} - (m_{13}(n-1))}{n} \tag{5.3}$$

$$m_{0,II} = m_{13} \tag{5.4}$$

Subspecies I contains all ^{12}C minus the ^{12}C required in the constitution of subspecies II. The number of subspecies II corresponds directly to the number of ^{13}C atoms. For the 3 subspecies approach, $m_{0,I}$ remains unchanged while $m_{0,II}$ is divided into $m_{0,IIa}$ and $m_{0,IIb}$ according to:

$$m_{0,IIa} = m_{13} * (n-b)/n \tag{5.5}$$

$$m_{0,IIb} = m_{13} * (b/n) \tag{5.6}$$

Initial quantities of subspecies are listed in table 4.1.

4.2.2-B Biodegradation rates

The biodegradation rates attributed to subspecies I and IIa was the overall rate rate applied to the water phase previously estimated by numerical modelling (Gaganis *et al*, 2004). To establish the lower biodegradation rate of subspecies II, equation 1.17 was used. To establish the lower biodegradation rate of subspecies IIb, the equation 1.19 was used. The fractionation factors α for *n*-hexane, *n*-octane, MCH and toluene were taken from section 2.3. Table 4.1 lists the apparent biodegradation rates applied for the gaseous phase (related by the equation 1.13).

Table 4.1

Values for isotope fractionation factor, apparent biodegradation rate applied for the gaseous phase, diffusion coefficient and initial quantity of VOCs used for the numerical simulations.

		***n*-Hexane 2 species**	***n*-Hexane 3 species**	***n*-Octane 2 species**	***n*-Octane 3 species**	**Toluene**	**MCP**
	units						
α [1]		0.9982	0.9946	0.9993	0.9972	0.9991	0.9986
$k_{app,L}$ [2]	d^{-1}	0.065	0.065	1.06	1.06	0.47	0.18
$k_{app,II}$	d^{-1}	0.0649		1.0593		0.4695	0.1797
$k_{app,IIa}$	d^{-1}		0.065		1.06		
$k_{app,IIb}$	d^{-1}		0.0646		1.0571		
D_L [3]	m^2/d	0.6324	0.6324	0.5322	0.5322	0.7335	0.672
D_H	m^2/d	0.6315	0.6315	0.5317	0.5317	0.7325	0.671
$m_{0,I}$ [4]	moles of VOC	5.92	5.92	4.3	4.3	2.21	4.83
$m_{0,II}$	moles of VOC	0.41		0.4		0.18	0.33
$m_{0,IIa}$	moles of VOC		0.27		0.3		
$m_{0,IIb}$	moles of VOC		0.14		0.1		

[1] From table 2.1 (within uncertainty values) [2] From Höhener *et al*. (2006), [3] From Lugg (1968), [4] from Broholm *et al*. (2005).

4.2.2-C Diffusion coefficients

Molecular diffusion coefficients to different subspecies was done as described in section 3.2.6-B. Molecular diffusion coefficients were adjusted in the model by taking into account the tortuosity and the partitioning of the compound (with air, water and solid phases) for diffusion through a porous media (Gaganis *et al.*, 2004; Werner *et al*., 2004). Diffusion coefficients are listed in table 4.1

4.3 Field results and discussion

4.3.1 VOC concentration values

The temporal and spatial variations of VOC concentrations at 1 m below ground are illustrated in Figure 4.2 for selected compounds. In generally, the concentrations were high in the source vicinity and decreased with distance. The compounds generally migrated outwards quickly. For *n*-hexane, 3-methylpentane (3MP) and methyl-cyclopentane (MCP), the highest concentrations were observed after 6 days followed by a rapid decrease of the concentrations until day 114 when concentrations dropped below the detection limit. The high initial concentrations, rapid concentration variations and rapid depletion of these compounds can be explained by their high vapour pressure. For less volatile compounds, the concentrations varied less rapidly and the compounds persisted longer. For a more detailed concentration profile and the evolution on each VOC at the field site, the reader is referred to Christophersen *et al*. (2005) and to Broholm *et al*. (2005) for the source evolution. Based on VOC concentrations data, it is difficult to distinguish compound loss due to biodegradation from loss due to the degassing to the atmosphere.

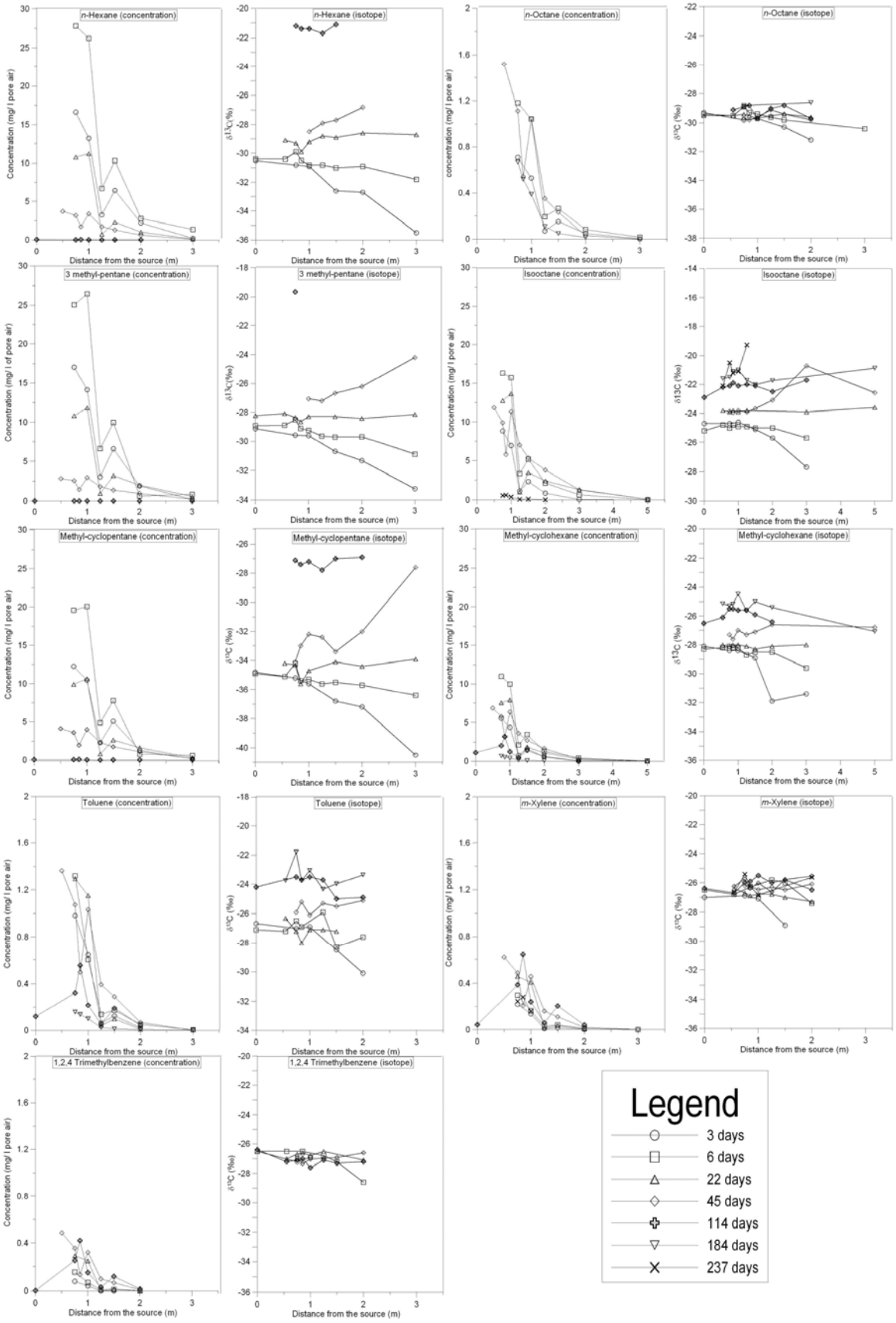

Figure 4.2: Concentration and $\delta^{13}C$ evolution in the unsaturated zone according to space and time for 9 VOCs. Measurements were made at constant depth (1m) and at diverse lateral distances and periodicities.

4.3.2 VOC $\delta^{13}C$ values

The $\delta^{13}C$ values of VOC are presented in Figure 4.3. Initially, a shift towards more negative $\delta^{13}C$ values with distance was observed for all compounds. The shifts varied depending on the compounds with shifts of -1.9‰ for *m*-xylene and *n*-octane to -5.7‰ for MCP at day 3 (Table 4.2). The $\delta^{13}C$ values then levelled out, followed by an increase towards more positive $\delta^{13}C$ values, starting at day 22 or 45. The increase in $\delta^{13}C$ was initially the more pronounced the further away the sampling points were from the source and the isotope profile resembled to the typical evolution observed in the saturated zone when biodegradation occurs. However, on day 114 more positive values were also observed for points closer to the source, leading again to a levelled out isotope profile for most compounds. The magnitude of the shift depended again on the compound. At day 45, the maximal shift varied between -0.5‰ for *n*-octane to 3.7‰ for *n*-hexane, at day 114 between 0.1‰ for 1,2,4-TMB and 9.5‰ for 3-MP. The majority of profiles provided shift greater than 1‰, the minimum difference required to distinct statistically two measured data on the field with 95% of confidence (Slater, 2003), thus confirms significant isotope effects.

The initial shift to more negative $\delta^{13}C$ values with distance is likely due to the faster diffusion of molecules containing only ^{12}C compared to molecules containing one ^{13}C. The largest negative shifts are observed for VOCs with low molecular weight (*n*-hexane, 3-MP and MCP) as the presence of a ^{13}C atom creates larger velocity differences (Table 4.2). A diffusion effect should be seen until ^{13}C-molecules have compensated the retard caused by their slower velocity. Isotope fractionation due to diffusion was previously observed at the field scale (Cerling *et al.*, 1991) for CO_2 or postulated based on theoretical investigations (Craig, 1953; Jost, 1960). Similarly isotope fractionation during diffusion of methane was also reported by several other studies (Galimov, 1967; Pernaton *et al.*, 1996; Stahl *et al.*, 1981; Zhang & Krooss, 2001).

The shift towards more positive values in later stage of the experiment (days 22 and 45), reflecting an accumulation of ^{13}C-molecules, strongly indicates biodegradation. Generally larger shifts are observed for compounds with a larger isotope enrichment factor (Table 4.2). However, preferential loss of ^{12}C-molecules to the atmosphere may contribute as well to the increase in $\delta^{13}C$. The more positive $\delta^{13}C$ values very close to the source in the final phase correspond well with the similar trend observed in the source chamber of the column experiment. The source is preferentially getting depleted of light compounds, which causes

positive shift. However, the rate of biodegradation is as well expected to affect the magnitude of the shift. The relative contribution of diffusion and biodegradation to the isotope evolution will be investigated in more detail below using a numerical model.

Table 4.2: Negative and positive isotopic shifts over time, variation in velocity due to the presence of a ^{13}C atom in the molecule, and enrichment factors for different VOCs.

	$\delta^{13}C$ shift at 2 m and day 3 (‰)	**$\delta^{13}C$ shift at 2 m and day 45 (‰)**	**$\delta^{13}C$ shift at day 114 (‰)**	**(D_L/D_H-1) *1000 (‰)**	**Enrichment factor (‰)**	**Source half life[1] (days)**
n-Hexane	-5.0	3.7	9.3	1.5	-2.2 ±0.4	14.2
3-MP	-4.1	2.9	9.5	1.5	-1.1 ±0.1	11.0
MCP	-5.7	2.8	7.9	1.5	-1.5 ±0.1	13.7
MCH	-3.8	1.5	2.6	1.2	-1.1 ±0.1	38.9
Toluene	-3.4	1.6	3.2	1.3	-0.7 ±0.1	66.6
Isooctane	-3.0	1.6	3.0	0.9	nd	36.9
n-Octane	-1.9	-0.5	0.5	0.9	-0.7 ±0.2	104.7
m-Xylene	-1.9	0.9	1.5	1.0	-0.8 ±0.1	161.7
1,2,4 TMB	-2.1	-0.1	0.1	0.8	nd	313.3

[1] from Broholm *et al.* (2005). nd: not determined

4.3.3 Concentration and $\delta^{13}C$ of CO_2

CO_2 concentrations initially ranged from 0.2% to 0.8% and slightly increased to range between 0.4% and 0.8% at day 22 and between 1.2% and 2% at day 87. The temporal and spatial evolution of the $\delta^{13}C$ of CO_2 is presented in Figure 4.3. Between day 3 and 22, the $\delta^{13}C$ shifted by about -3‰ and then stabilized until day 114. The $\delta^{13}C$ values were generally more negative close to the source than further away. The shift towards more negative $\delta^{13}C$ confirms that biodegradation of VOCs occurred. Biodegradation of the VOC is expected to add CO_2 with a $\delta^{13}C < -28.2$‰, the average $\delta^{13}C$ of the most degradable 9 VOCs (excluding benzene, decane, dodecane and cyclopentane).

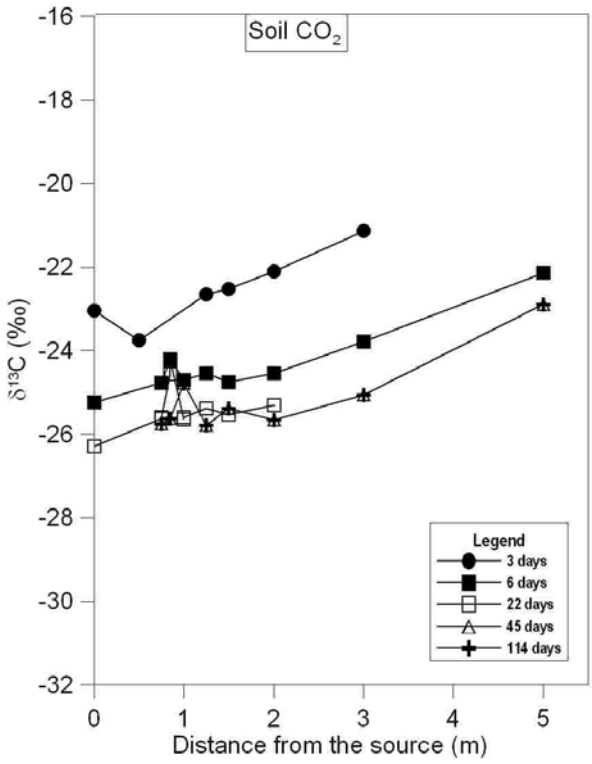

Figure 4.3: $\delta^{13}C$ evolution of the soil CO_2 in space and time after source burial.

4.4 Numerical modelling results and discussion

Numerical modelling was used to gain more insight into the contribution of diffusion and biodegradation to observed isotope evolution. Three different scenarios were simulated: only biodegradation fractionates, only diffusion fractionates, or both processes fractionate. *n*-Hexane and *n*-octane were modelled with the 2 and 3 subspecies approach, toluene and methyl-cyclopentane using only the 2 subspecies approach. Except for the subdivision of the compounds in different subspecies, the same modelling approach and parameters as described in Gaganis *et al.* (2004) was used. The parameters related to different subspecies are summarized in Table 4.1. As will be discussed in more detail below, the 2 and 3 subspecies approach gave similar results. Therefore, in Figure 4.4 only the results obtained by one calculation method are presented for *n*-hexane and *n*-octane.

4.4.1 Isotope fractionation by biodegradation

Figure 4.4a illustrates the expected $\delta^{13}C$ values of *n*-hexane if only biodegradation was associated with isotope fractionation. The *n*-hexane becomes increasingly enriched in ^{13}C with distance from the source due to preferential degradation of molecules with lighter isotopes with a shift in $\delta^{13}C$ of up to +15‰. With increasing time, the whole isotope profile tends to shift to a more positive $\delta^{13}C$ value. As the source strength decreases and fewer molecules with the initial isotope signature are delivered to the gas phase, biodegradation becomes more effective in enriching the *n*-hexane in ^{13}C. At day 22 and 45, there is a relatively good agreement between the general shape of the simulated (Figure 4.4a) and measured (Figure 4.2) isotope profiles. However, the calculations failed to reproduce trends observed during early (shift to more negative values) and later periods (shift to more positive values close to the source) indicating that during these two phases other processes strongly influence isotope ratios as well.

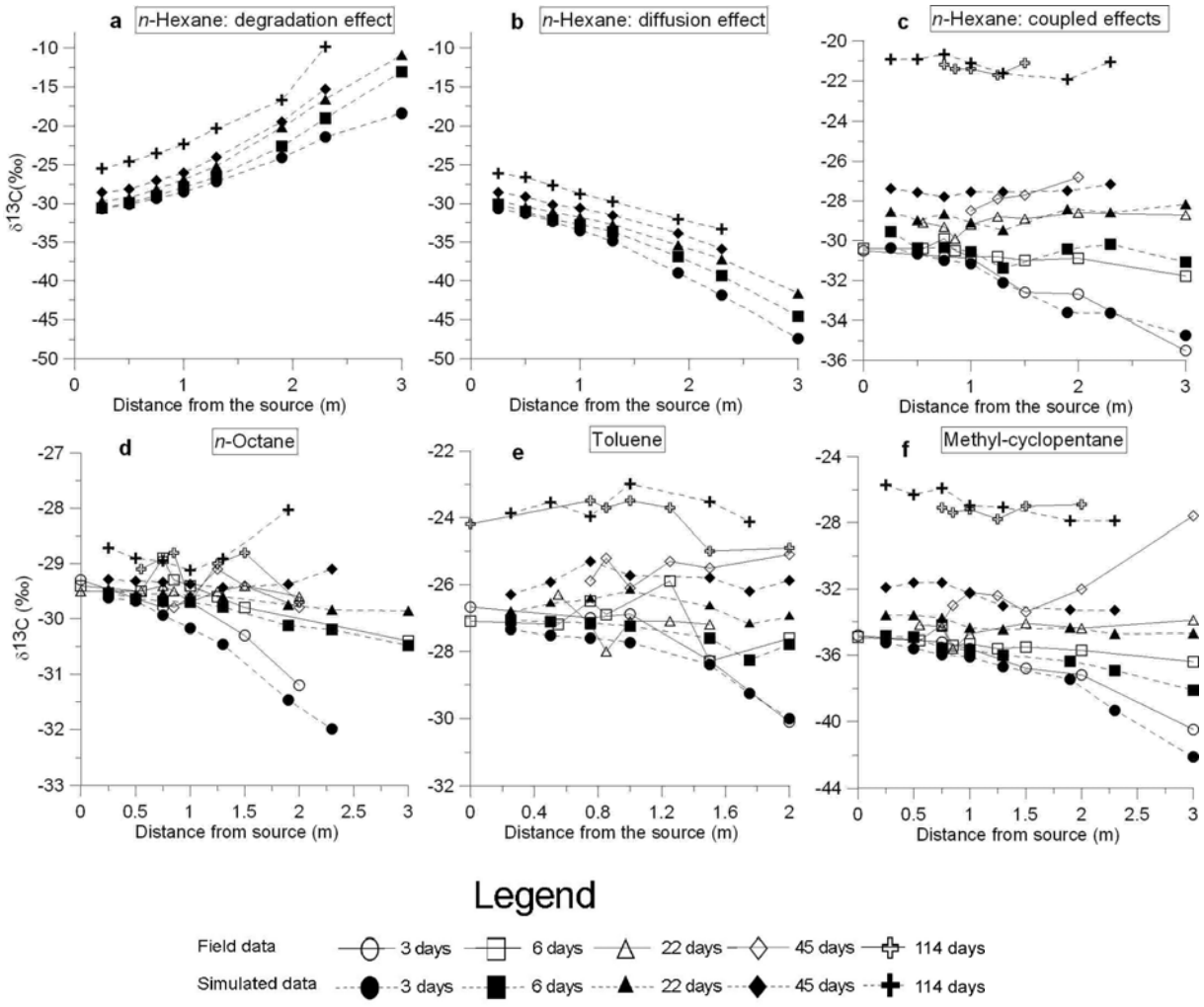

Figure 4.4: Numerically simulated values of $\delta^{13}C$ (black symbols) over space and time when only degradation contributes to the isotope fractionation of *n*-hexane, when only diffusion contributes to the isotope fractionation of *n*-hexane and when both processes are coupled for *n*-hexane (3 subspecies) and for *n*-octane, toluene and MCP (2 subspecies). White symbols represent field data.

4.4.2 Isotope fractionation by diffusion

Figure 4.4b illustrates the modelled $\delta^{13}C$ values of *n*-hexane under the assumption that only diffusion fractionates. Unlike for biodegradation, the $\delta^{13}C$ values become more negative with distance because heavier molecules diffuse slower than the lighter ones. Similarly as for biodegradation, the whole profile shifts to more positive values with time, which is again likely due to the decay of the source. There is a good agreement between simulated (Figure 4.4b) and measured (Figure 4.2) isotope profiles for day 3 and 6 indicating that diffusion controls the carbon isotope ratios during the early stage of the experiment.

4.4.3 Isotope fractionation by biodegradation and diffusion

Figure 4.4 shows the modelling results assuming that both biodegradation and diffusion fractionate for *n*-hexane (c), as well for *n*-octane (d), toluene (e) and MCP (f). Isotope measurements from the field experiment are also presented in the same figure. Biodegradation rate coefficients and isotope enrichment factors were manually varied within their range of uncertainty until the best fit between modelled and measured results was obtained. In general, the model reproduced the measured data well. The average divergence between field measurements and predicted values of $\delta^{13}C$ for *n*-hexane and toluene was 0.55 ‰ and 0.53 ‰ (regardless of positive or negative divergence), respectively (Table 4.3). The model successfully reproduced the different phases observed. In particular, it also reproduced the elevated $\delta^{13}C$ profile observed in the final stage (on day 114). The results demonstrate that both diffusion and biodegradation affect the isotope ratio, but their influence varies during the experiment. The initial stage (day 3 and 6) was governed by diffusion. Afterwards, the contribution of biodegradation became more significant (day 22 and 45) than diffusion. Finally, during the final phase, both biodegradation and diffusion contributed to a significant enrichment of ^{13}C close to the source for *n*-hexane, toluene and MCP. The isotope-diffusion effect during depletion of the compound at the source seen during the column experiment is confirmed by the field experiment. In contrast, the amount of *n*-octane in the source was still

sufficient to keep the ratio relatively stable. It has to be underlined that the enrichment factors used for this study were not evaluated with soil from the experimental site (glacial melt water sand) but with another unrelated soil sediment (alluvial sand). It was found that enrichment factors for toluene and *n*-octane were directly providing the best fit whereas enrichment factors below the range of uncertainty for *n*-hexane and MCP would have provided a better fit. Evaluating the enrichment factor with soil from the contaminated site would certainly improve the match of the predictions to the field data, but nevertheless, enrichment factors from the literature was shown to be reliable.

Table 4.3

Differences in $\delta^{13}C$ between field data and predictions from the model with the approach of 2 subspecies over space and time for *n*-hexane and toluene.

		$\Delta\delta^{13}C$ (‰) ($\delta^{13}C$ field data - $\delta^{13}C$ predicted)				
	Distance (m)	3 days	6 days	22 days	45 days	114 days
	0.55		-0.21	-0.19		
	0.75	0.24	0.70	-0.30		-0.32
***n*-Hexane**	1	0.78	-0.38	-0.17	-0.67	-0.73
	1.3		-0.24	0.40	-0.58	-0.68
	2	1.22	-0.49	-0.15	0.67	
	Distance (m)	3 days	6 days	22 days	45 days	114 days
	0.55		-0.07	0.27		
	0.75	0.60	0.65	-0.76	-0.60	0.46
Toluene	1	0.84		-0.91	-0.38	-0.51
	1.5	0.11	-0.70	-0.53	0.30	-1.48
	2	0.01	0.19		0.78	

4.4.4 Evaluation of the two approaches

The similarity between the two approaches was tested on both *n*-alkanes and the $\delta^{13}C$ values predicted with either two or three subspecies (with coupled effects) provided negligible discrepancy (Table 4.4). The average divergence between the two approaches on the $\delta^{13}C$ predicted is 0.28‰ (regardless of positive or negative divergence) for *n*-hexane and 0.09‰ for *n*-octane out of 38 and 40 predictions respectively, which is under typical analytical uncertainty of 0.2 to 0.5‰. Among all these predictions, only one prediction diverges more than 1‰. Therefore, the approximating approach with 2 subspecies can be used to assess

biodegradation of common contaminants for whom biodegradation pathways are not yet fully identified (such as alicyclic compounds). The approximating approach was slightly more accurate in predicting $\delta^{13}C$ values for *n*-octane compared to *n*-hexane and the reason can be attributed to a lower accumulation of subspecies IIb for *n*-octane due to a smaller enrichment factor. Smaller the enrichment factor, smaller the gap between subspecies IIa and IIb over time. Thus, the use of the approach with 2 subspecies has restrictions in order to keep valid the similarity between the two approaches and the limits must be beforehand clearly identified prior to field data analysis. The limits likely depend on several possible combinations of the joint effect of the enrichment factor, increasing degree of biodegradation and the distance from the source. These limits are investigated in the next chapter.

Table 4.4

Introduced discrepancy for predicted $\delta^{13}C$ over space and time when *n*-hexane and *n*-octane are divided into two and three subspecies.

			***n*-Hexane $\Delta\delta^{13}C$ (‰)**		
			($\delta^{13}C$ 3sp - $\delta^{13}C$ 2sp)		
Distance (m)	3 days	6 days	22 days	45 days	114 days
0.25	-0.11	0.18	-0.06	-0.08	-0.34
0.5	0.11	-0.18	-0.07	0.02	-0.42
0.75	0.04	0.25	0.33	0.15	0.22
1	0.52	-0.13	-0.07	0.29	-0.44
1.3	-0.52	-0.83	-0.27	-0.23	-0.61
1.9	0.30	-0.02	0.05	-0.02	-0.74
2.3	0.91	0.44	0.04	0.10	-0.29
3	-1.12	-0.01	0.18		
			***n*-Octane $\Delta\delta^{13}C$ (‰)**		
			($\delta^{13}C$ 3sp - $\delta^{13}C$ 2sp)		
Distance (m)	3 days	6 days	22 days	45 days	114 days
0.25	0.00	-0.01	0.03	0.00	0.01
0.5	-0.15	0.13	0.15	-0.01	0.01
0.75	0.00	0.13	0.07	-0.05	-0.22
1	0.03	-0.16	0.07	-0.03	-0.09
1.3	0.04	-0.15	0.02	0.03	0.00
1.9	-0.27	-0.41	-0.12	-0.01	-0.01
2.3	-0.17	-0.37	0.00	-0.04	0.00
3	0.01	-0.22	0.05	0.00	0.00

4.5 Analytical modelling results and discussion

Similarly to the column experiment, analytical simulations were performed to reproduce the carbon isotope ratios for *n*-hexane and MCP measured in the field. The simulation approach was similar as for the column study, except that the underlying transport equation is for a spherical source. The solution will be detailed in the next chapter. The source depletion rates were taken from Broholm *et a.l* (2005) and attributed to the subspecies with ^{12}C only. The source depletion rate for the subspecies with ^{13}C was calculated using equation 3.15. The simulations intent to demonstrate that the main isotope trends observed in the field can also be reproduced with a simpler analytical model. In addition to carbon, simulations for hydrogen isotope ratios were performed as well to evaluate the effect of the large isotope fractionation for biodegradation compared to diffusion. The hydrogen enrichment factor from the microcosm study was used (Table 2.1) and division of subspecies was made according to section 1.5.6.

4.5.1 Carbon isotope fractionation

Figure 4.5 shows the simulation results for *n*-hexane and MCP assuming that both biodegradation and diffusion are responsible for the isotope fractionation in the porous media. The analytical simulations (Figure 4.5) reproduced the field data (Figure 4.2) well, but more importantly reproduced consistently the different phases in the $\delta^{13}C$ evolution.

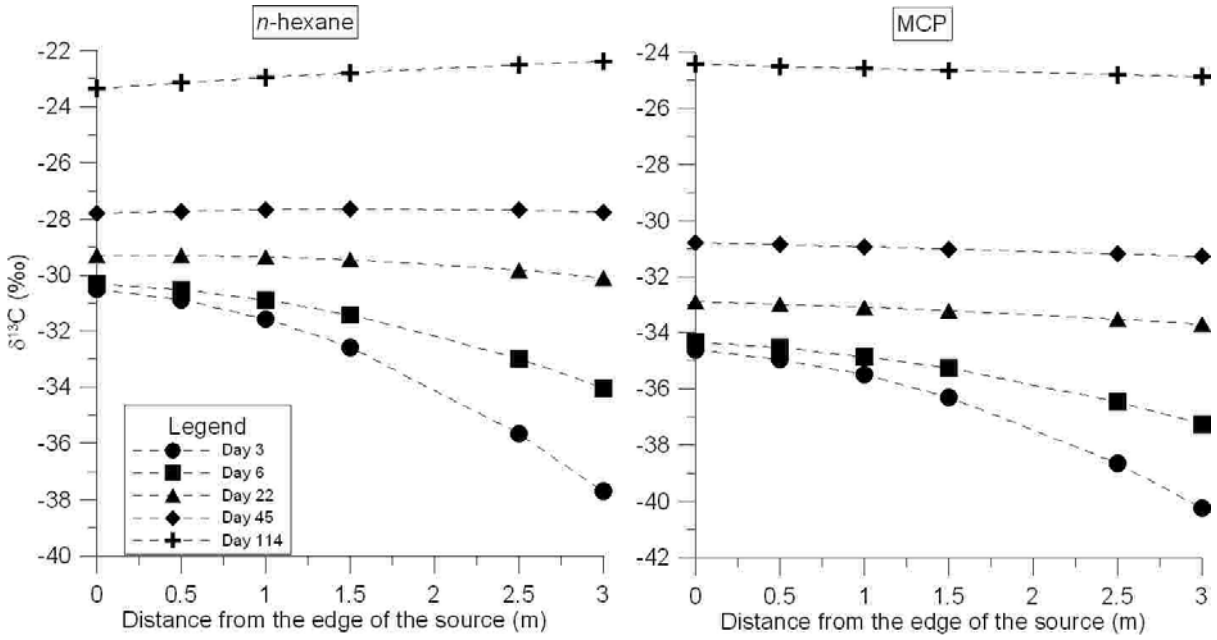

Figure 4.5: Analytically predicted values of $\delta^{13}C$ for *n*-hexane and MCP over time and distance when biodegradation and diffusion control the isotope fractionation, with a depleting source.

4.5.2 Hydrogen isotope fractionation

The results from the H isotope simulations are illustrated in Figure 4.6 for *n*-hexane assuming that both biodegradation and diffusion are responsible for the isotope fractionation. In contrast to carbon, positive shifts are expected at early time due to a large hydrogen enrichment factor. Consequently, the strong effect of biodegradation dominated over the effect of diffusion, making the latter irrelevant.

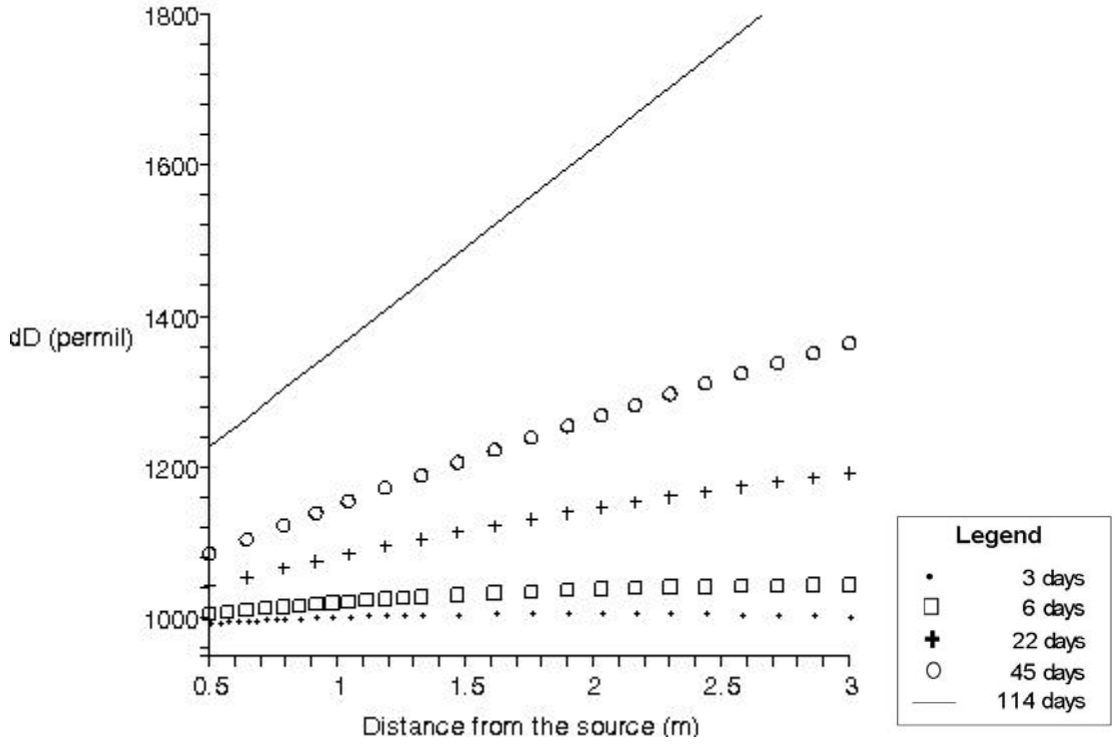

Figure 4.6: Analytically predicted values of δD for *n*-hexane over time and distance when biodegradation and diffusion control the isotope fractionation, with a depleting source.

4.6 Conclusions for field experiment

Measurements of isotopic ratios were realised during a highly controlled field experiment carried out in an artificially contaminated unsaturated zone (GRACOS project). These measurements showed significant variation in $\delta^{13}C$ for several VOCs over space and time. Variations in the isotopic ratios measured in the field were expected to be controlled by the biodegradation process (as seen by microcosm experiments), by the diffusion effect and by the depletion of the compound at the source (as seen by the column experiment). Including biodegradation and diffusion processes, the results of the field experiment were simulated using a modified numerical code (MOFAT). Modelling results showed that it was possible to reproduce the evolution of the carbon isotopic ratio of *n*-hexane, *n*-octane, and toluene and methyl-cyclopentane in the unsaturated zone by making use of the enrichment factor and an isotope-specific diffusion coefficient. The positive shifts commonly expected by biodegradation were only encountered after in an initial diffusion dominated phase and before source depletion occurred. By reproducing the $\delta^{13}C$ variations using an independently

determined biodegradation rate, the isotopic modelling directly confirmed the biodegradation rate and showed evidence of biodegradation within only a few meters from the source. The numerical modelling furthermore demonstrated the reliability of the division of the compounds into two subspecies to track variations of $\delta^{13}C$. Consequently, any common contaminant independently of their biodegradation mechanism can be simulated using this approach. Due to the higher isotope fractionation of hydrogen compared to carbon, simulation performed with hydrogen showed great potential to trace biodegradation in the unsaturated zone.

Reproduction of field data was also realized by making use of an analytical solution of the diffusion equation in radial coordinate. Although numerical modelling is more accurately reproducing the field data, the analytical solution can be used to gain insight into the isotope evolution in the unsaturated zone as it was shown to reproduce the main features of the field experiment. Therefore, the analytical approach will be used in the following chapter to further explore the expected isotope evolution for different source scenarios.

Chapter 5

Analytical simulation of isotope fractionation in the unsaturated zone

Abstract

A theoretical investigation on $\delta^{13}C$ distribution of volatile organic compounds (VOCs) in a surrounding area of a point source contamination in the unsaturated zone is presented. The investigation is based on analytical solutions which predict spatiotemporal $\delta^{13}C$ profiles affected by diffusive transport of VOCs, biodegradation and source depletion. The chosen modelling approach was previously shown to reproduce well isotope trends observed in a column and field experiment. This investigation improves the understanding needed for assessing natural attenuation of VOC in the unsaturated zone with isotope analysis, from the spill moment to source exhaustion. The mass transport was assumed to be governed by Fick's law for diffusion and the equation for reactive transport of VOCs in the soil gas phase was solved for different source geometries (plane, spherical and cylindrical) and for different boundary conditions. The calculated concentrations for molecules with light and heavy isotopes were used to derive $\delta^{13}C$ values for *n*-hexane over space and time under two major assumptions: molecules including one ^{13}C degrade at a slower rate and diffuse at a slower velocity compared to molecules composed of only ^{12}C atoms. Results showed a significant diffusion isotope effect during initial dispersion of VOC in the media and also during the depletion of the compound in the source. During VOC migration under steady state conditions, the $\delta^{13}C$ values were shown to be linearly related with the VOC flux variations, making qualitative biodegradation assessment possible.

Bouchard D, Höhener P, Cornaton F and Hunkeler D. **Investigation on stable carbon isotope ($\delta^{13}C$) variations of volatile organic compounds in the unsaturated zone for different contamination scenarios. Analytical simulations**

5.1 Introduction and aims

In the unsaturated zone, the diffusion of VOCs can be described adequately by Fick's law for diffusion of dilute organic vapours (Baehr & Bruell, 1990) and this diffusion model was applied to a column (chapter 3) and a field experiment (chapter 4) to understand the mechanisms responsible for isotope fractionation. These studies provided evidence for carbon isotope fractionation due to a diffusion isotope effect and due to biodegradation. Molecules including a ^{13}C were found to diffuse slower than molecules with only ^{12}C atom, which caused a significant isotope fractionation. The previous model simulations demonstrated that the chosen modelling approach incorporating isotope fractionation during diffusion adequately reproduces the observed concentration and isotope data. Based on isotope ratio measurements in the source over time, the studies also put in evidence a diffusion-related enrichment of ^{13}C-molecules in the source. The magnitude of the positive shift at the source, only encountered as the compound is depleting, increases over time proportionally to the diffusion coefficient ratio $^{h}D/^{l}D$.

The aim of this study is to investigate how isotope ratios are expected to evolve for different contaminant source configurations and thus extends the knowledge gained by the field experiment for a point source to other situations. The calculations provide a basis to evaluate under which conditions isotope ratio can serve as an indicator for biodegradation. In addition, the study evaluates if isotope ratios can also be used to quantify biodegradation, similarly as in the saturated zone, in addition to be a qualitative indicator. Several analytical simulations were performed for two spill scenarios, a spherical source and a floating NAPL pool. Each of them were simulated for three successive states including an initial transient phase, a steady-state phase and a source depletion phase to evaluate how the diffusion and biodegradation isotope effect interact. The simulations were completed with two other scenarios, a cylindrical source representing vertical NAPL migration across the unsaturated zone and a cylindrical source combined with a floating NAPL pool. For these two scenarios, only steady-state simulations were carried out due to the complexity of mathematical solutions for transient state.

5.2 Simulated scenarios and mathematical formulation

Analytical simulations were based on the reactive transport equation 1.14. The contaminant vapours are assumed to diffuse through a homogeneous and isotropic porous medium at a

temperature of 15°C. At first the analytical solutions for the different source scenarios are given and then it is explained how isotope fractionation was incorporated.

5.2.1 Spherical source of NAPL

In this scenario, VOCs are released from a spherical source located in the unsaturated zone and undergo biodegradation as they migrate through the unsaturated zone (Figure 5-1A). Evolution of the soil vapour contamination in the surrounding of such a source was previously investigated at the field scale by Christophersen *et al.* (2005) and Conant *et al.* (1996). The equation 1.14 in radial coordinates reads:

$$\frac{\partial C_a}{\partial t} = D\left[\left(\frac{\partial^2 C}{\partial r^2}\right) + \frac{2}{r}\left(\frac{\partial C_a}{\partial r}\right)\right] - kC_a \qquad (5.1)$$

where r is the radial distance from the centre of the sphere. D stands for either D_s or D_e, depending on the state condition, and k must be therefore adequately adjusted (see equations 1.14 to 1.16). The transfer function model approach (Jury & Roth, 1990) is once more used (as in section 3.2.4) to obtain a solution of equation 5-1 in a semi-infinite domain. The transfer function is first solved in the Laplace space for the boundary conditions:

$$C_a(r = r_0, t) = \delta(t) \qquad (5.2\text{ a})$$

$$C_a(r = \infty, t) = 0 \qquad (5.2\text{ b})$$

to obtain:

$$\hat{g}(r, p) = \frac{r_0}{r} e^{-\sqrt{\frac{k+p}{D_s}}(r - r_0)} \qquad (5.2\text{ c})$$

where p is the complex Laplace variable (T^{-1}) and r_0 is the radius of the sphere. In the Laplace space, the convolution product reads:

$$\hat{C}(r, p) = \hat{C}(0, p).\hat{g}(r, p) = Lp\left\{\int_0^t C(0, u)\, g(r, t-u)\, du\right\} \qquad (5.3)$$

Assuming a spherical source of initial concentration C_0 with a radius r_0, an initial concentration of 0 everywhere else and the boundary condition:

$$C_a(r_0,t) = C_0 e^{-\beta t} \tag{5.4 a}$$

the convolution solution of equation 5-1 in the time-domain is:

$$C_a(r,t) = \frac{C_0 e^{-\beta t} r_0}{2r}\left[e^{-\sqrt{\frac{(k-\beta)}{D_s}}(r-r_0)} erfc\left(\frac{(r-r_0)-2\sqrt{D_s(k-\beta)}\,t}{2\sqrt{D_s t}}\right) + e^{\sqrt{\frac{(k-\beta)}{D_s}}(r-r_0)} erfc\left(\frac{(r-r_0)+2\sqrt{D_s(k-\beta)}\,t}{2\sqrt{D_s t}}\right)\right] \tag{5.4 b}$$

In case where the source is constant (β=0) and $t=\infty$ (steady state condition) in equation 5.4 b, the solution simply becomes:

$$C_a(r) = \frac{C_0 r_0}{r} e^{-\sqrt{\frac{k}{D_e}}(r-r_0)} \tag{5.5}$$

In a system with steady-state diffusion and biodegradation, the mass flux in a given direction decreases with distance and can be calculated by differentiating equation 5.5 with respect to *r*. The mass flux is thus given by:

$$F(r) = -D\frac{\partial C}{\partial r} = C_0\sqrt{D_e k}\,\frac{r_0}{r}\left(1+\sqrt{\frac{D_e}{kr^2}}\right) e^{\left(-\sqrt{\frac{k}{D_e}}(r-r_0)\right)} \tag{5.6}$$

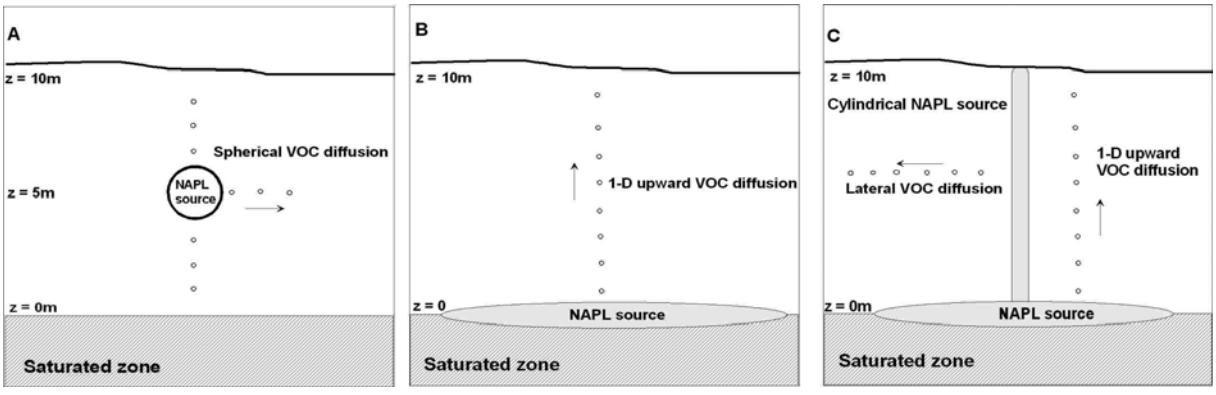

Figure 5.1: Illustration of three different spill scenarios: (a) a spherical source in a semi-finite domain, (b) a floating NAPL pool on the water table in a finite domain, (c) a cylindrical source with underlying NAPL pool of finite extension. Boundary conditions for each scenario are described in the text.

5.2.2 Floating light NAPL pool on groundwater

The second scenario deals with a large horizontal pool of light NAPL which has accumulated on the water table. The VOCs released from the contaminant source are diffusing upwards through the unsaturated zone where biodegradation takes place and, if biodegradation is incomplete, are lost to the atmosphere (Figure 5-1B). This common spill scenario for light NAPL was studied by several researchers investigating the fate of VOCs in the unsaturated zone under field conditions (Franzmann *et al.*, 1999; Hers *et al.*, 2000; Lahvis *et al.*, 1999; Ostendorf & Kampbell, 1991; Smith *et al*., 1996). The transfer function model approach used for the calculations is described in section 3.2.4. In the case of a floating pool with the boundary conditions expressed by equations 3.6 a-b, the equation to calculate the mass flux is given by Wilson (1997):

$$F(z) = -D\frac{\partial C}{\partial z} = \frac{(kD_e)^{1/2} C_0 \cos h\left[(k/D_e)^{1/2}(L-z)\right]}{\sin h\left[(k/D_e)^{1/2} L\right]} \qquad (5.7)$$

The solution approaches $C_0(1-x/L)$ when $k/D_e \to 0$.

5.2.3 Cylindrical source of NAPL

The scenario consists in a NAPL migrating downward in the unsaturated zone and roughly establishing a cylindrical form spill. This scenario can be considered to represent an industrial pipeline or an underground storage tank from which the NAPL is leaking. A constant source is assumed all along the length of the cylinder, from the soil surface to the water table (Figure 5.1C). The boundary conditions are as follows:

$$C_a(r_0, z) = C_0 \qquad (5.8a)$$

$$C_a(r, L) = 0 \qquad (5.8b)$$

$$\frac{\partial C_a(r,0)}{\partial z} = 0 \qquad (5.8c)$$

$$C_a(\infty, r) = 0 \qquad (5.8d)$$

where r and z are the horizontal and vertical coordinates respectively, L is the length of the cylinder of a radius r_0 fully penetrating the unsaturated zone (thus equal to the thickness of the unsaturated zone). Taking into account different diffusivities in vertical and horizontal direction and the boundary conditions given above, the 1-D solution at steady state condition is provided by Wilson (1997):

$$C(r,z) = \frac{4C_0}{\pi} \sum_{n=1}^{\infty} \frac{(-1)^{n-1} \mathrm{K}_0 \left[\left(\gamma_n + \frac{k}{D_e} \right)^{1/2} r \right]}{(2n-1) \mathrm{K}_0 \left[\left(\gamma_n + \frac{k}{D_e} \right)^{1/2} r_0 \right]} \cos \left[\frac{(2n-1)\pi z}{2L} \right] \tag{5.9}$$

where K_0 is the modified Bessell function of second kind and zero order, and γ_n is the eigenvalue corresponding to:

$$\gamma_n = \left[\frac{(2n-1)\pi}{2L} \right]^2 \tag{5.10}$$

5.2.4 Cylindrical source with underlying pool of light NAPL

The last scenario is an extension of the previous one by simply adding an accumulation of NAPL on the water table under the vertical cylinder source. Both NAPL sources are considered to be constant in space and time (Figure 5.1C). The four prevailing boundary conditions are:

$$C_a(r,L) = 0 \tag{5.11a}$$

$$C_a(r_0,z) = C_0 \tag{5.11b}$$

$$C_a(r,0) = C_0 \tag{5.11c}$$

$$C_a(\infty,z) = C_0 \frac{\sinh\left[(k/D)^{1/2} (L-z) \right]}{\sinh\left[(k/D)^{1/2} L \right]} \tag{5.11d}$$

The solution that describes the concentration profile of the VOC at steady state is provided by Wilson (1997):

$$C_a(r,z) = C_0 \frac{\sin h\left[\left(\frac{k}{D_e}\right)^{1/2}(L-z)\right]}{\sin h\left[\left(\frac{k}{D_e}\right)^{1/2}L\right]} + \sum_{n=1}^{\infty} A_n \sin\frac{n\pi z}{L} \mathrm{K}_0\left\{\left[\left(\frac{n\pi}{L}\right)^2 + \frac{k}{D_e}\right]^{1/2} r\right\} \quad (5.12)$$

where:

$$A_n = \frac{2C_0}{\pi n}.\frac{\left[1-(-1)^n - \left(1+\frac{k}{D_e}\left(\frac{L}{n\pi}\right)^2\right)^{-1}\right]}{\mathrm{K}_0\left\{\left[r_0\left(\frac{n\pi}{L}\right)^2 + \frac{k}{D_e}\right]^{1/2}\right\}} \quad (5.13)$$

5.3 Modelling approach

5.3.1 Simulation of isotope data

The first simulation made use of the 2 and the 3 subspecies approach in order to investigate the limitation of the 2 subspecies approach. All other simulation only used the 3 subspecies approach. The selected compound was *n*-hexane and overall biodegradation rates for the scenario were 0.1 and 1 d^{-1}. The overall apparent biodegradation rates applied in the gaseous phase were directly attributed to subspecies I and IIa (equation 1.13). The smaller biodegradation rates affected by the presence of a heavy isotope were derived as described in the previous section (section 1.5), according to either 2 or 3 subspecies approach. An enrichment factor of -2.3 ‰ was used. The molecular diffusion coefficient of *n*-hexane is 0.5957 (m d^{-1}) and was attributed to the light subspecies. The diffusion coefficient of the heavy subspecies was calculated with equation 3.8. Further transformations are made on $^{l}D_m$ and $^{h}D_m$ to obtain either sorption-affected or effective diffusion coefficients as mentioned in section 1.5.1. Total porosity and water content values were taken from Werner *et al.* (2004) in

order to have typical field values. The f_a coefficient was calculated using equation 1.11 and the tortuosity coefficient was estimated by (Moldrup *et al.*, 2000):

$$\tau = \frac{\theta_a^{2.5}}{\theta_t^2} \tag{5.14}$$

The source decay rates observed for *n*-hexane in a field study (Broholm *et al.*, 2005) was attributed to ^{12}C-molecules ($^{l}\beta$). The decay rate of ^{13}C-molecules ($^{h}\beta$) was calculated with equation 3.17. The initial number of moles of the species was arbitrary set to 1 and the initial δ^{13}C value is -30‰. For the division into two subspecies, the initial amount (m_0) of each subspecies was calculated by:

$$m_{0,I} = \frac{m_0}{1 + R_{molecule}} \tag{5.15}$$

$$m_{0,II} = m_0 - m_{0,I} \tag{5.16}$$

In the case of division into three subspecies, $m_{0,I}$ remains identical while $m_{0,IIa}$ and $m_{0,IIb}$ were 4/6 and 2/6 of the value $m_{0,II}$, respectively (for *n*-hexane). All the parameters needed to perform the simulations are summarised in Table 5.1. The calculations were performed as explained in section 3.2.4 using a Fortran program, with number truncation after 16 decimals.

Table 5.1

Summary of model parameters, including calculated soil parameters and literature data

		Units
Henry's coefficient (15°C)	17.45	mol m^{-3}/mol m^{-3}
D_m (15°C)	0.5957	m^2 d^{-1}
f_{oc}	0.1	%
ρ	1.48	kg m^{-3}
K_d	5.57	mol kg^{-1}/ mol m^{-3}
f_a	0.4315	%
ε	-2.3	‰
θ_t	0.31	-
θ_a	0.25	-
τ	0.325	-

	Subspecies I	**Subspecies II**	**Subspecies IIa**	**Subspecies IIb**	**Units**
Biodegradation rate*	0.1 and 1	0.09977 and 0.9977	0.1 and 1	0.09931 and 0.9931	d^{-1}
Initial amount	0.9353	0.0647	0.0431	0.0216	mol
D_s	0.1036	0.1034	0.1034	0.1034	m^2 d^{-1}
D_e	0.0484	0.0483	0.0483	0.0483	m^2 d^{-1}
Depletion rate	0.049	-----	0.04892	0.04892	d^{-1}

*apparent rates applied to the gaseous phase

5.4 Results and discussion

5.4.1 Concentration evolution

When *n*-hexane starts to diffuse from the source (and no contamination is initially found in the domain), concentrations of the compound in the soil air expected at a fixed point away from the source will gradually increase, describing transient state conditions in the system. The transient state will be observed until the concentrations become stable, indicating steady state conditions. Of the two scenarios, i.e. spherical and floating pool source, the latter one

requires more time to reach steady state conditions throughout the 10 m system. When a steady state is reached at 10 m, any point closer to the source will be at steady state as well. Figure 5.2 illustrates the evolution of the relative concentration of *n*-hexane at an elevation of 9.9 m above a floating pool source. The steady state is reached after 175 days compared to roughly 100 days for the spherical source with a 5 m radial system (results not shown). During depletion of *n*-hexane, which was set to start to decay at day 300, a second transient phase occurs. The compound depletion is noted at the monitoring point only 18 days later when the concentration begins to decrease until total depletion of *n*-hexane in the domain. For the simulation, a biodegradation rate of 0.1 d^{-1} was used.

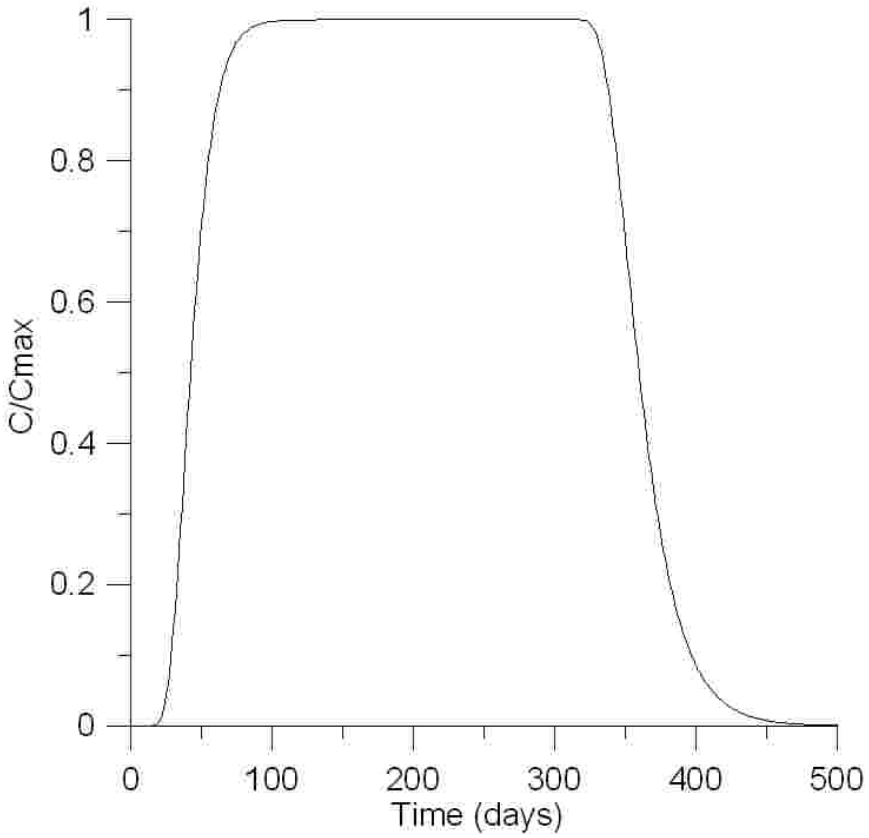

Figure 5.2: Evolution of the relative concentrations (C/C_{max}) of *n*-hexane at 9.9 m above a floating pool source in function of elapsed time with a constant source during 300 days and followed by a source decay of 0.049 d^{-1}, and biodegradation rate in the unsaturated porous medium of 0.1d^{-1}.

5.4.2 Equivalence of the two approaches

The differences introduced in the estimation of $\delta^{13}C$ by the approach with 2 subspecies versus the approach with 3 subspecies were evaluated using three different biodegradation rates (0.1, 0.5 and $1 d^{-1}$) coupled with four different ε (-1, -2, -3 and -5‰) and are presented in Table 5.2. The scenario of a floating pool at steady state conditions was used with an unsaturated zone thickness of 10 m and the values are discussed based on the commonly reported analytical error of 0.3‰. Using a fixed biodegradation rate of 0.1 d^{-1}, results revealed no significant differences between the two approaches up to 10 m away from the source for $|\varepsilon| < 3‰$ and up to 6 m for $|\varepsilon| < 5‰$ (table 5.2). Thus, with an enrichment factor usually less than 3‰ for molecules > 4C, any petroleum hydrocarbons degrading slower than 0.1 d^{-1} can be divided into two subspecies with negligible differences compared to the reference approach. For larger biodegradation rates of 0.5 d^{-1} and 1 d^{-1}, respectively, accurate results are still obtained within 6 m and 4 m, respectively (Table 5.2). When modelling is used for data interpretation using the approach with 2 subspecies under either saturated or unsaturated conditions, the enrichment factor and an estimated biodegradation rate found in literature can be used to delineate the maximum reliable distance for site specific conditions.

Discrepancies reported in Table 5.2 are always positive; meaning that 2 subspecies approach underpredicts the isotope ratios (as shown also by Figure 1.2). As explained before, the difference is due to a progressive accumulation of subspecies IIb over time compared to subspecies IIa as the latter is degraded at a higher rate. With substantial amount of subspecies having the ^{13}C at the reactive site, the overall biodegradation of molecules with ^{13}C slows down and therefore creates more enrichment. The 2 subspecies approach does not take into account the two different rates as the subspecies II are degrading at an averaged rate and the value predicted are thus underestimated. The approximation of equation 1.19 holds until the proportion of subspecies IIa and IIb in the remaining substrate has significantly deviated over time from the original proportion. The discrepancy between 2 and 3 subspecies approach increases with increasing biodegradation rate, increasing isotope enrichment factor (as for hydrogen) and increasing extent of biodegradation.

Table 5.2

Differences for predicted $\delta^{13}C$ when species is divided into 2 and 3 subspecies, respectively. Example with different biodegradation rate coefficients and different enrichment factors for *n*-hexane, using the floating NAPL pool scenario at steady state conditions.

	$\Delta\delta^{13}C$ (‰) ($\delta^{13}C$ 3sp - $\delta^{13}C$ 2sp)								
	k=0.1 (d^{-1})			k=0.5 (d^{-1})			k=1 (d^{-1})		
z	ε =-1	ε =-3	ε =-5	ε =-1	ε =-2	ε =-3	ε =-1	ε =-2	ε =-3
2	0.0	0.0	0.0	0.0	0.0	0.0	0.0	0.0	0.1
4	0.0	0.0	0.1	0.1	0.1	0.2	0.1	0.2	0.5
5	0.0	0.0	0.2	0.1	0.2	0.3	0.1	0.4	0.8
6	0.0	0.1	0.2	0.1	0.2	0.5	0.2	0.5	1.1
8	0.1	0.2	0.5	0.2	0.4	1.0	0.3	0.9	2.1
10	0.1	0.2	0.7	0.3	0.7	1.5	0.5	1.4	3.2

5.4.3 $\delta^{13}C$ evolution during initial transient state

The expected isotope evolution of *n*-hexane at transient state over space and time is illustrated in Figure 5.3 for a spherical source and a floating pool source denoted as 1-D model. When biodegradation and diffusion control the isotope fractionation (Figures 5.3 A,C), large negative shifts are noted initially (day 3 to 20) which gradually evolve in positive direction throughout the transient state. It can be noted on the same figures that, for a fixed distance and time, larger shifts are observed for the 1-D model than for the spherical model. The radial dispersion of VOCs implies steeper concentration gradients which increases the isotope fractionation due to the diffusion effect. In contrast, when only biodegradation controls isotope fractionation, the isotope ratios observed in the migrating vapours are never and nowhere more negative than the source signature (Figures 5.3 B,D). On day 160, close to steady state, the magnitude of the shifts is larger when the fractionation due to diffusion is omitted. The simulations coupling diffusion and biodegradation effect are consistent with the measurements in a column corresponding to the 1D-model (chapter 3) and with the measurements at the Værløse site with a buried spherical source (chapter 4) in the early stage of VOC migration. During the initial phase, the diffusion effect largely dominates the biodegradation effect and causes a negative shift with distance. The isotope fractionation is

due to a slower diffusion velocity of molecules containing a ^{13}C. Later, positive shifts are due to a biodegradation effect, but since the diffusion effect counterbalances the effect of biodegradation, smaller shifts are observed when both processes fractionate simultaneously.

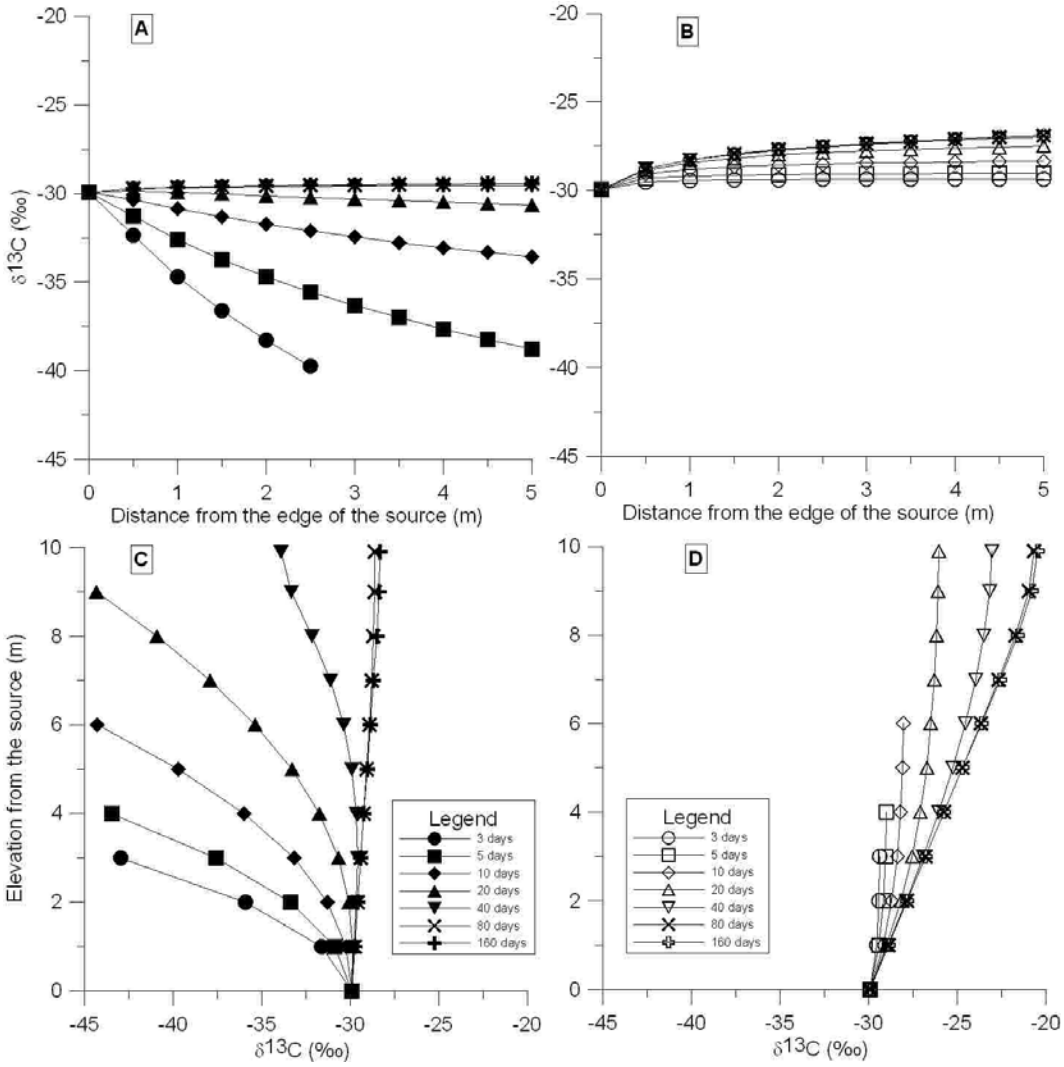

Figure 5.3: Effect of diffusion and biodegradation (A and C) and of biodegradation only (B and D) on the $\delta^{13}C$ of *n*-hexane migrating through the unsaturated zone for a spherical constant source (A and B) and for a floating LNAPL pool (C and D) at transient state conditions with $k=0.1d^{-1}$ and $\varepsilon=-2.3‰$. For the spherical source simulations, data are reported for a fixed vertical depth equivalent to the depth of the source.

5.4.4 $\delta^{13}C$ evolution during steady state

Figure 5.4 shows the calculated isotope ratios for *n*-hexane under steady state conditions for a spherical (A) and a floating pool source (B), for three different biodegradation rates. Once again, for the same distance and time, shifts observed for 1-D diffusion are larger than for radial diffusion. The results indicate an effect of biodegradation on the isotope ratios, but also demonstrate once more the importance of the diffusion isotope effect. In absence of biodegradation (k=0), the simulations show no shift with distance (or depth), even when the two isotope-specific diffusion coefficients are used. For the scenarios with biodegradation, inclusion of the diffusion isotope effect reduces the magnitude of the isotope shift with distance. The reduction is the larger, the higher the degradation rate is. When biodegradation occurs, larger concentration gradients are created. This leads to faster diffusion and hence the diffusion effect more strongly counteracts the biodegradation effect. This also explains the larger shifts observed for the floating pool source compared to the spherical source, since radial diffusion of VOCs in the latter case creates steeper concentration gradients across comparable distances. Finally, as shown for a small enrichment factor ε (-1‰) coupled with a small biodegradation rate of 0.1 d^{-1} (cross signs), the biodegradation is unable to dominate over the diffusion effect and the shift remains negative. This tendency was previously observed for toluene in the column experiment, although the shift was small.

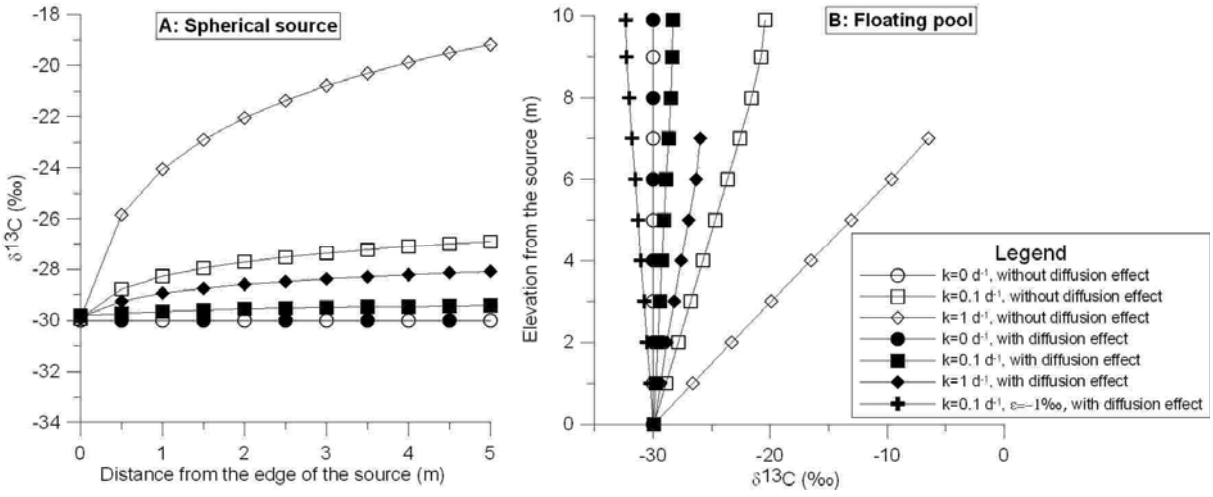

Figure 5.4: Effect of diffusion and biodegradation (bold symbols) and biodegradation only (open symbols) on the evolution of $\delta^{13}C$ of *n*-hexane emanating from a spherical source (A) or from a floating pool source (B), at steady state with ε=-2.3‰.

Similar simulations can also be performed in a case where VOCs are out gassing from contaminated groundwater instead of a floating pool. However, potential mass transfer limitation between groundwater and soil gas have to be taken into account. For groundwater with dissolved contaminant, the vertical mixing within the saturated zone significantly limits the volatilization flux (Parker, 2003). Due to the small volatilization flux, upward diffusion can deplete the contaminant pool in the gas phase above the water table, which is expected to be associated with isotope fractionation. Hence an offset in $\delta^{13}C$ in the positive direction may occur between groundwater and gas phase above it.

The effect of diffusion is also likely to occur for the third and the fourth scenarios, i.e. cylindrical source and cylindrical source with an underlying floating pool source. The scenarios were also simulated in order to evaluate the effect of biodegradation with and without the diffusion effect on the $\delta^{13}C$ under steady state conditions (Figure 5.7). The predicted isotope ratios are displayed in form of an isobar contour plot with the source as a central point. The shape of the isotope isobars are identical to the VOC concentration isobars predicted by Wilson (1997) and clearly indicate the presence or absence of an underlying floating pool of LNAPL. Without the underlying pool source, the $\delta^{13}C$ values increase with increasing lateral distance and remain unchanged vertically. For both scenarios, the diffusion added to biodegradation effect show once more negative isotope ratios compared to results without the diffusion effect. In absence of biodegradation, and based on results above (Figure 5.4), the $\delta^{13}C$ value will remain unaffected in both lateral and vertical directions.

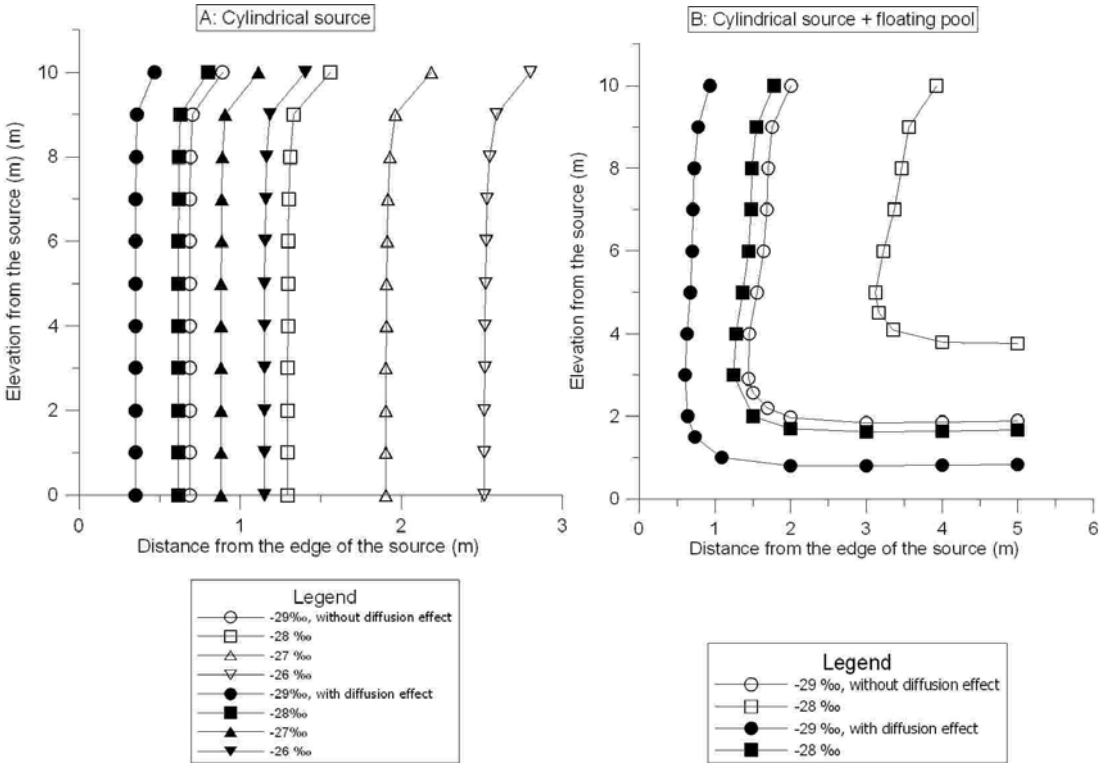

Figure 5.7: Isotopic isobars for a fully penetrating vertical cylindrical source (A) and the same cylindrical source with an underlying floating pool (B) at steady state conditions with biodegradation rate set to 1 and 0.1 d^{-1},respectively. Effect of diffusion and biodegradation (bold symbols) and biodegradation only (open symbols) on the evolution of $\delta^{13}C$ of *n*-hexane.

5.4.5 Assessment of biodegradation under steady state conditions

Analogous to the Rayleigh plot (see microcosm experiments, section 2.3), the ln of the mass flux can be plotted versus the carbon isotope ratios and, if a Rayleigh-type behaviour occurred, the slope should correspond to the isotope enrichment factor. Indeed, a linear trend can be observed for either a spherical or an underlying pool source with biodegradation rate set to 0.1 and 1 d^{-1}, respectively (Figure 5.6). However, the slope (Table 5.3) is significantly smaller than isotopic enrichment factor for biodegradation of *n*-hexane (-2.3‰) used in the simulations. The smaller isotope enrichment factor can be explained by the fact that the faster diffusion of ^{12}C-molecules partially compensates the preferential removal of ^{12}C-molecules by biodegradation. It is interesting to note that the net isotope enrichment factors are close to the sum of the biodegradation isotope enrichment factor (-2.3‰) and the diffusion isotope enrichment factor (+1.62‰), which is -0.68‰ although no theoretical mathematical expression for the “effective” isotope enrichment factor was developed yet. The observed

isotope enrichment factor varies somewhat between the scenarios and for different biodegradation rates. The smallest of the four slopes from the table 5.3 is observed for the lower biodegradation rate (0.1 d^{-1}) with the spherical source, source geometry that constantly described larger diffusion isotope effect in reason of steeper concentration gradients (Figures 5.3 and 5.4). It is appropriate to recall here findings illustrated on figure 5.4A (with concentration), showing no isotope fractionation due to diffusion when no biodegradation occurs in the system at steady state, which would give here a slope of 0.

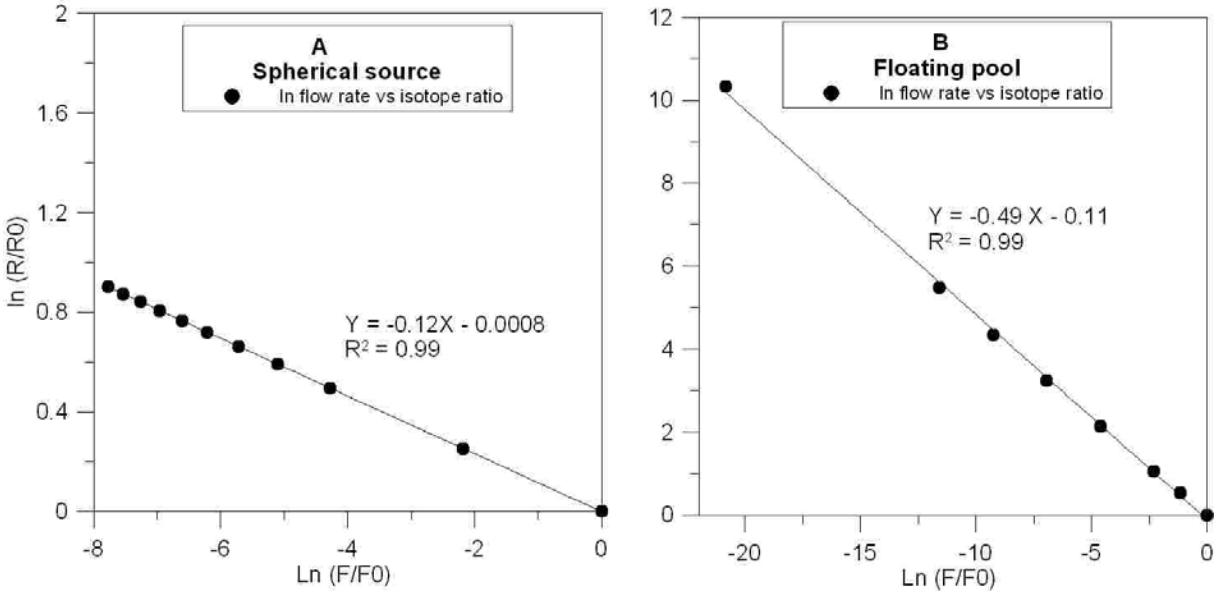

Figure 5.6: Carbon isotope ratio as function of the relative flux in a case of a spherical source (A) with k=0.1 d^{-1} and a floating NAPL pool (B) at steady state conditions with k=1 d^{-1}. The slope yields the net isotope enrichment factor that accounts for fractionation by diffusion and biodegradation.

The magnitude of the slope is regulated by the joint effect of biodegradation and diffusion. The shift in isotope ratio due to biodegradation is constant, independently of the rate. However, the shift in isotope ratio due to diffusion is dependent of the biodegradation rate and expected to increase as the biodegradation rate increases. The remaining fraction of contaminant not reacted cannot be straightforward calculated using the Rayleigh equation. The magnitude of the diffusion effect must be first quantified in relationship with the specific biodegradation rate. A linear trend between the mass flux and the isotope ratio was also observed for hydrogen. Even if the diffusion effect on the isotope ratio is negligible in the case of H, the net enrichment factor is again smaller than the actual enrichment factor, but in a

much less extend compared to C. This small but systematic deviation of the net enrichment factor compared to the original value is likely due to different time travel distributions as mathematically demonstrated by Abe & Hunkeler (2006).

Table 5.3
Net enrichment factors obtained by the relationship "ln(R/R0) vs ln(F/F_0)" for the spherical source and the floating pool scenarios.

	Net enrichment factors (‰)		
	0 d^{-1}	**0.1 d^{-1}**	**1 d^{-1}**
Spherical source	0	-0.12	-0.27
Floating pool	0	-0.45	-0.49

An alternative approach to quantify biodegradation is by fitting calculated isotope ratios to measured values as function of distance from the source under steady state conditions using the biodegradation as a variable parameter. A significant isotope shift with distance is essential to provide a reliable assessment and therefore, the magnitude of the shift must be at least 1‰ given the common analytical uncertainty range of 0.1-0.3‰ (Slater, 2003).

5.4.6 $\delta^{13}C$ evolution during final transient state due to source depletion

As it was shown in chapter 3 and 4, a positive isotope shift is expected to occur in the source as the compound is depleting. Figure 5.8 shows the predicted isotope evolution when the system has reached the transient state due to compound depletion from the source for a spherical source (A) and a floating pool source scenario (B) at a biodegradation rate of 0.1 d^{-1}. Without isotope fractionation caused by the diffusion effect, the source signature remains constant until the end and $\delta^{13}C$ values at distance only slightly change towards more positive values with time. In contrast when diffusion is fractionating as well, a shift of the source and the whole profile towards more positive values is observed as it is governed by the evolving

source signature. A curved isotope profile is observed at day 350 as the source isotope ratio begins to increase but values further away have not yet fully adjusted.

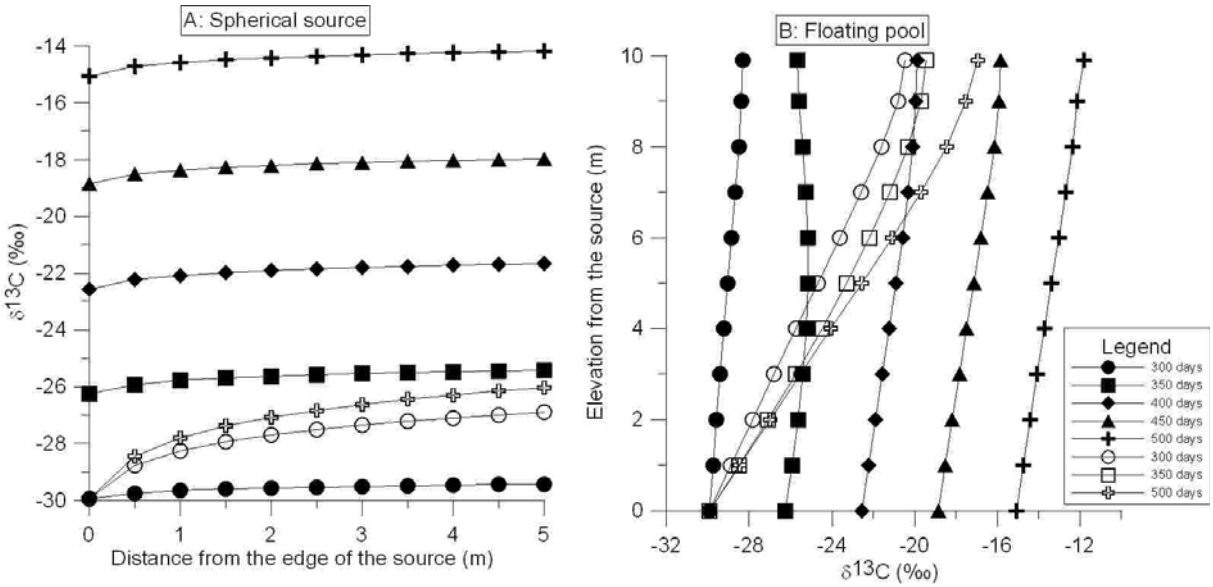

Figure 5.8: Coupled diffusion and biodegradation effects (black dots) and biodegradation effect only (white dots) on the evolution of $\delta^{13}C$ of *n*-hexane emanating from a spherical source (A) and a floating LNAPL pool source on the water table (B). A biodegradation rate of 0.1 d^{-1} and source depletion rate of 0.049 d^{-1} was used. Data for the spherical source are provided for a fixed depth equivalent to the depth of the source.

In these simulations, the isotope fractionation at the source due to diffusion was set to remain constants. However, this might not be the case in the field as biodegradation of the compound in the system increases the concentration gradient which, in turn, increases volatilisation of the source (Baehr, 1987; McCarthy & Johnson, 1993; Ostendorf & Kampbell, 1991). This effect on the isotope ratio at the source has no been investigated in details.

5.5 Conclusions for analytical simulations

In this chapter, isotope ratios for different source scenarios were simulated using an approach that successfully reproduced isotope ratios measured in a column and field study. Based on the modelling results, some conclusions can be drawn regarding the potential of using isotope data to demonstrate biodegradation in the unsaturated zone. Application of CSIA in the unsaturated zone is more demanding since a significant diffusion isotope effect occurs, which is not expected in the saturated zone. The diffusion isotope effect was shown to affect the

$\delta^{13}C$ values from the spill moment until the exhaustion of the source and is particularly pronounced during the initial period after source emplacement and during depletion of compounds from the source.

While diffusion affects isotope ratios throughout the lifetime of a contaminant source, it is still possible to draw some conclusions regarding biodegradation during the steady state period. A lack of biodegradation in a system can easily be identified since uniform $\delta^{13}C$ values with distance are expected although ^{13}C-molecules migrate slower than ^{12}C-molecules. Furthermore, the change in $\delta^{13}C$ and δD is linearly related to the VOC flux variations. However, the Rayleigh equation can not be directly applied to calculate the remaining flux of the migrating VOCs. The net isotope enrichment factor changes depending on the biodegradation and the source geometry. Finally, the shift towards more positive isotope ratios of the whole profile due to the source depletion can be seen as an indicator of the final stage in the $\delta^{13}C$ evolution and that the corresponding compound is depleting from the source.

Chapter 6

Summary and general conclusions

The principal goal of this study was to investigate whether compound specific isotope analysis can be used to assess biodegradation of volatile organic compounds in the unsaturated zone. To achieve this goal, the study was conducted in three major parts which consisted of batch, column and field experiments in order to identify processes that control isotope fractionation in the unsaturated zone. The conclusions are formulated firstly by the insights on the processes controlling the isotope fractionation in the unsaturated zone put in evidence by this work, then by an outline of the new conceptual model developed to incorporate isotope fractionation into reactive transport of VOCs through the unsaturated zone, and finally, by the application of the findings to assess biodegradation of VOCs in the unsaturated zone.

6.1 Biodegradation effect on isotope fractionation

The first objective was to quantify isotope fractionation factors during biodegradation of common volatile organic compounds under oxic conditions with unsaturated sediments. The laboratory microcosm experiments were performed for several VOCs frequently found at petroleum hydrocarbon contaminated sites. Because biodegradation of compounds mainly occurs in the water phase, the question whether isotope fractionation is likely to be observed in the air phase can be asked. The microcosm experiments answered this question. Isotope fractionation was measured for each compound tested, such as aromatic, aliphatic and alicyclic hydrocarbons. Furthermore, the carbon isotope enrichment factors were in a similar range as in studies under saturated conditions. Therefore, an instantaneous compound exchange between the gas and the liquid phase can be assumed.

Biodegradation of a series of *n*-alkanes provided evidence that the carbon isotope enrichment factor is inversely related to the number of carbon atoms composing the molecule due to a "dilution" of the isotope effect by ^{13}C present at non-reactive positions. *n*-Decane was the longest chain for which detectable isotope fractionation occurred. The *n*-alkane study also indicated that transport limitations across the cell membrane reduce the magnitude of isotope

fractionation for larger compounds. Therefore, the use of CSIA for carbon in VOCs would be limited to compound with 10 C at the most for petroleum hydrocarbons (C-H bonds).

Investigations were also carried out regarding fractionation of H during biodegradation of *n*-pentane and *n*-hexane. The isotope enrichment factors were much larger for H compared to C. For this reason, H isotopes may be a more sensitive tool to demonstrate biodegradation compared to C. Therefore, investigation on H enrichment factors for common contaminants biodegraded under oxic conditions is of interest, but unfortunately was limited in this study due to analytical reasons.

The two experiments that included transport processes in 1-D (column) and 3-D (field) also provided evidence for a ^{13}C enrichment related to biodegradation. However, in the column studies the shifts were quite small due to the small length of the column. In contrast, the field experiment showed significant positive shifts of the isotope ratios for most of the compounds monitored. Positive shifts were observed during an intermediate phase of the experiments and the duration of the phase was variable. The modelling studies confirmed that during an intermediate phase, shifts in $\delta^{13}C$ that are clearly due to biodegradation should be detected.

6.2 Diffusion effect on isotope fractionation

Another objective of the thesis was to evaluate the effect of diffusion on the $\delta^{13}C$ values of VOC during their migration through a porous medium. The laboratory column experiment unequivocally demonstrated the occurrence of a diffusion isotope effect, especially for small molecules. Substantial negative $\delta^{13}C$ were apparent during the initial phase of the experiment.

These observations in laboratory experiment were confirmed by the field experiment as large negative shifts were also monitored during the initial phase. The use of Fick's law to describe concentration distribution of ^{12}C-compounds and ^{13}C-compounds was shown to be adequate to reproduce the isotope evolution caused by the diffusion isotope effect.

6.3 Source effect on isotope fractionation

Another important process regulating the isotope ratios was identified during the column experiment and later confirmed by the field experiment. The $\delta^{13}C$ in the source chamber of the column experiment remained stable as long as concentration in the air phase of the source remained relatively stable. Then, as the compound was depleting from the liquid source,

gradual $\delta^{13}C$ shifts in positive direction were observed. Hence, the shift was in opposite direction compared to what was predicted in other studies based on the inverse isotope effect during the organic liquid-vapour phase transfer under equilibrium conditions. This suggests that diffusion across the column controlled the source isotope ratio rather than the volatilization step. To evaluate this hypothesis in more detail, a separate analytical model was derived that links the $\delta^{13}C$ values in the source to the isotope-dependant diffusion mass flux across the column and predicted that the isotope fractionation factor should correspond to ratio of diffusion coefficients for molecules with a different isotope composition, $^{h}D/^{l}D$. Using the data for *n*-pentane, a good agreement between measured and expected isotope fractionation factor was indeed observed confirming the dominant effect of diffusion.

Although the fractionation is linked to diffusion, it is more appropriate to denote it as source effect since it is observed only during depletion of the compound in the liquid source in contrast to the diffusion isotope effect which is permanently influencing the $\delta^{13}C$ value in zones around the source. A significant enrichment of ^{13}C was observed in the column study as well as during the field experiment. The phenomenon was observed for both, compounds that undergo biodegradation (e.g. toluene, *n*-octane, MCH) and compounds for which biodegradation is very low or absent (e.g. *n*-pentane, isooctane, 3-methylpentane). These findings underline the importance of monitoring the source isotope ratios, in order to separate shifts in positive direction due to biodegradation from shifts due to source depletion. The evolving isotope signature at the source has a clear repercussion on the $\delta^{13}C$ values measured in the soil profile.

6.4 Modelling of $\delta^{13}C$ in the unsaturated zone

An analytical model that simulates $\delta^{13}C$ distribution of volatile organic compounds (VOCs) in a surrounding area of a source contamination in the unsaturated zone was developed. The model is based on Fick's law for diffusion and adjusted for reactive transport of VOCs through unsaturated soils. The key feature of the model is the heavy isotope and the subdivision of the species is made according to the presence of a ^{13}C atom in the molecule. Each subspecies is then individually treated in the model as would be different contaminants under two major assumptions: molecules including one ^{13}C degrade at a slower rate and diffuse at a slower velocity compared to molecules composed of only ^{12}C atoms. Therefore, the model requires knowledge of isotopic enrichment factors for the compounds and the

diffusion coefficient of the two isotopes differs proportional to their difference in weight. Processes such as dissolution and sorption which imply no bond breaking activity were omitted in the model as they were known to create negligible magnitude of fractionation. Remaining quantities of subspecies can then be combined at any time and desired distance from the source to derive the isotope ratio.

6.5 Assessment of biodegradation by CSIA

The large variations in $\delta^{13}C$ values measured for several VOCs in the field reveal the potential application of the CSIA method in the unsaturated zone. However, caution must be taken as variations in $\delta^{13}C$ were not only due to biodegradation but also due to a diffusion isotope effect. The necessity to couple the biodegradation effect with both the diffusion and source depletion effects complicate the interpretation of the evolving $\delta^{13}C$ profile. The latter two effects causing an isotope fractionation are not likely to occur in the saturated zone. Therefore, assessment of biodegradation by means of CSIA is less straightforward in the unsaturated zone than in the saturated zone and thus remains a more demanding task.

The isotope ratio can be reproduced by numerical model if isotope fractionation during both biodegradation and diffusion processes are taken into account. The model simulations confirmed that isotope ratios for VOCs can be assessed in the unsaturated zone and that Fick's law commonly used to predict concentration distribution is appropriate to link the concentration evolution with the altered isotope ratio. In practical application, it may not be feasible to apply a numerical model on contaminated sites, and especially when the initial concentration and the age of the spill are unknown.

Nevertheless, it is possible to assess biodegradation without numerical modelling during the intermediary phase, after the strong initial diffusion effect and prior to source depletion. For sources containing a large amount of compounds, this intermediary phase should last for a relatively long period while the initial transient phase is even difficult to sample because it lasts only some days as indicated by the field experiment. Thus it is likely that this intermediate phase is captured during several independent sampling campaigns. During this phase, isotope ratios were shown by the numerical modelling to be dominated by biodegradation. In addition, analytical simulations linearly related the isotope shift ($\delta^{13}C$ and δD) to the ln of the mass flux for steady-state conditions. This simple correlation provides the opportunity to calculate the remaining fraction of the compound. However, a quantitative

expression for the isotope enrichment factor when both biodegradation and diffusion affect isotope ratios is still lacking. Until it is available, the non negligible diffusion effect restrains the assessment to qualitative interpretation when no numerical modelling is performed. Finally, for the same phase and still under steady-state regime, stable $\delta^{13}C$ values with distance indicate a lack of biodegradation in the system.

When the compound of interest is depleting from the source, the gradually changing isotope ratio at the source impedes simple assessment of biodegradation without numerical modelling. However, this shift opens the possibility to clearly identify depletion of a compound in the source based on isotope data. Because the isotope evolution in this case follows a Rayleigh trend, it should even be possible to quantify the fraction of compound remaining in the source.

Isotope fractionation due to biodegradation can only be observed for compounds with substantial isotope enrichment factors, typically small molecules in the case of C. As an alternative, H isotopes could represent an option for large molecules as the enrichment factors are known to be of much larger magnitude. It is important to note that the presence of a D in a molecule has the same effect on diffusion coefficients as a ^{13}C, but a much larger effect on the biodegradation rate. Hence, when using H isotopes, isotope fractionation due to diffusion is likely negligible. Thus, assessment of biodegradation using D/H ratio may be simpler as only isotope fractionation due to biodegradation needs to be taken into account. However, the analytical method is more demanding and the required mass higher.

6.6 Application of CSIA in the unsaturated zone

Monitoring programs that include isotope analysis in addition concentration analysis would undoubtedly increase the level of information gained with the same network of sampling points and the same sampling frequency. For instance, the accuracy of the biodegradation rate evaluated with concentration data can be tested by predicting the isotope ratios using the obtained biodegradation rate and comparing them with measured values. Such a complementary evaluation greatly enhances the assessment of in situ biodegradation and strengthens the quantitative evaluation of biodegradation rates. As isotope ratio measurements are independent of VOC concentrations, isotope analyses make it possible to identify processes such biodegradation and source depletion even if concentrations fluctuate due to various factors. Moreover, using simple analytical simulations for systems under steady state, isotopes analysis can be used to elaborate isotope isobars plots for different biodegradation

rates which can be compared with measured isotope ratios to estimate or verify the biodegradation rate. Last but not least, the observation of a gradually changing isotope signature in the source is a good indicator for a depleting source. The $\delta^{13}C$ data may be used for determining the mass loss by diffusion-controlled volatilisation of sources in the unsaturated zone as the changes in $\delta^{13}C$ due to diffusion was found to obey to the Rayleigh distillation. This is potentially a useful tool for monitoring the natural attenuation of source zones.

6.7 Further development

For the application of CSIA, the enrichment factor remains a crucial parameter that needs to be reliable. More data are available how robust isotope enrichment factors are between different sites and how they are linked to the often diverse microbial populations.

In addition, the alternative offered by H isotopes should be explored in more detail. As mentioned, the large enrichment factor for biodegradation combined with a similar diffusion isotope effect as for carbon is an attractive feature of hydrogen isotopes. However, assessment using the approach with 2 subspecies can only be qualitative as it was shown to significantly deviate from the accurate 3 subspecies approach over time. Accordingly, further work should be addressed to establish an efficient way to divide the species under two subspecies or to derive a quantitative expression applied on the δD over time as a correcting term in order to use the 2 subspecies approach in a quantitative purpose.

Finally, the demonstrated linear relationship between the relative change in flux of VOC and the $\delta^{13}C$ variations is an important aspect that can substantially increase the benefits of using of CSIA in the unsaturated zone. This linearity allows the isotope data to be quantitatively assessed. Further mathematical development should be attempted to evaluate the interaction between the diffusion and biodegradation effect and derive a relationship for the resulting net enrichment factor. With this relationship, the application of the Rayleigh equation will be possible in order to assess the extent of biodegradation as it is currently being used in the saturated zone, however, only under steady state conditions. The results of these mathematical developments will consequently also clarify the effect of biodegradation on the isotope ratio of a depleting compound at the source, which in turn, will allow a quantitative assessment of the remaining compound even for degrading compounds.

References

Abe, Y. and Hunkeler, D., 2006. Does the Rayleigh equation apply to evaluate field isotope data in contaminant hydrogeology? Environmental Science and Technology, 40 (5): 1588-1596.

Abriola, L.M. and Pinder, G.F., 1985a. A multiphase approach to the modeling of porous media contamination by organic compounds, 1. Equation development. Water Resources Research, 21(1): 11-18.

Abriola, L.M. and Pinder, G.F., 1985b. A multiphase approach to the modeling of porous media contamination by organic compounds, 2. Numerical simulation. Water Resources Research, 21(1): 19-26.

Aggarwal, P.K. and Hinchee, R.E., 1991. Monitoring in situ biodegradation of hydrocarbons by using stable carbon isotopes. Environmental Science and Technology, 25: 1178-1180.

Alvarez, P.J.J. and Vogel, T.M., 1995. Degradation of BTEX and their aerobic metabolites by indigenous aquifer microorganisms under nitrate reducing conditions. Water Science and Techology, 31: 15-28.

Anderson, R.S., Huang, L., Iannone, R., Thompson, A.E. and Rudolph, J., 2004. Carbon kinetic isotope effect in the gas phase reactions of light alkanes and ethene with the OH radical at 296 K. Journal of Physical Chemistry A., 108: 11537-11544.

Arvin, E., Jensen, B.K. and Gundersen, A.T., 1989. Substrate interaction during aerobic degradation of benzene. Applied and Environmental Microbiology, 55: 3221-3225.

Atlas, R.M. 1981. Microbial degradation of petroleum hydrocarbons: an environmental perspective. Microbiological Reviews, 45: 180-209.

Baehr, A.L., 1987. Selective transport of hydrocarbons in the unsaturated zone due to aqueous and vapor phase partitioning. Water Resources Research, 23: 1926-1938.

Baehr, A. L. and Corapcioglu, M.Y., 1987. A compositional multiphase model for groundwater contamination by petroleum products. 2. Numerical solution. Water Resources Research, 23 :201-213.

Baehr, A.L. and Bruell, C.J., 1990. Application of the Stefan-Maxwell equations to determine limitations of Fick's law when modeling organic vapor transport in sand columns. Water Resources Research, 26: 1155-1163.

Baehr, A.L., Stackelberg, P.E. and Baker, R.L., 1999. Evaluation of the atmosphere as a source of volatile organic compounds in shallow groundwater. Water Resource Research, 35(1): 127-136.

Baertschi, P., Kuhn, W. and Kuhn, H., 1953. Fractionation of Isotopes by Distillation of some Organic Substances. Nature, 171: 1018-1020.

Bailey, N.J.L., Krouse, H.H., Evans, C.R. and Rogers, M.A., 1973. Alteration of crude oil by waters and bacterial-evidence from geological and isotope studies. Bulletin of the American Association of Petroleum Geologists, 57: 1276-1290.

Balabane, M. and Létolle, R., 1985. Inverse overall isotope fractionation effect through distillation of some aromatic molecules (anethole, benzene and toluene). Chemical Geology, 52: 391-396.

Bartell, L.S. and Roskos, R.R., 1966. Isotope effects on molar volume and surface tension: simple theoretical model and experimental data for hydrocarbons. Journal of Chemical Physics, 44(2): 457-463.

Beneteau, K.M., Aravena, R. and Frape, S.K., 1999. Isotopic characterisation of chlorinated solvents - laboratory and field results. Organic Geochemistry, 30: 739-753.

Berthe-Corti, L. and Fetzner, S., 2002. Bacterial metabolism of n-alkanes and ammonia under oxic, suboxic and anoxic conditions. Acta Biotechnologica, 22(3-4): 299-336.

Broholm, M.M., Christophersen, M., Maier, U., Stenby, E.H., Höhener, P. and Kjeldsen, P. 2005. Compositional Evolution of the Emplaced Fuel Source in the Vadose Zone Field Experiment at Airbase Værlse, Denmark. Environmental Science and Technology, 39(21): 8251-8263.

Cerling, T.E., Solomon, D.K., Quade, J. and Bowman, J.R., 1991. On the isotopic composition of carbon in soil carbon dioxide. Geochimica et Cosmochimica Acta, 55: 3403-3405.

Chang, M.K., Voice, T.C. and Criddle, C.S., 1993. Kinetics of competitive inhibition and cometabolism in the biodegradation of benzene, toluene, and p-xylene by two Pseudomonas isolates. Biotechnology and Bioengineering, 41: 1057-1065.

Christophersen, M., Broholm, M.M., Mosbæk, H., Karapanagioti, H.K., Burganos, V.N. and Kjeldsen, P.2005. Transport of hydrocarbons from an emplaced fuel source experiment in the vadose zone at Airbase Værløse, Denmark. Journal of Contaminant Hydrology, 81: 1-33.

Chu, K.H., Mahendra, S., Song, D.L., Conrad, M.E. and Alvarez-Cohen, L., 2004. Stable carbon isotope fractionation during aerobic biodegradation of chlorinated ethenes. Environmental Science and Technology, 38: 3126-3130.

Clark, I.D. and Fritz, P., 1997. Environmental isotopes in hydrogeology. Lewis Publishers, Boca Raton, Florida, USA, 328 pp.

Coleman, D.D., Risatti, J.B. and Schoell, M., 1981. Fractionation of carbon and hydrogen isotopes by methane-oxidizing bacteria. Geochimica et Cosmochimica Acta, 45: 1033-1037.

Conant, B.H., Gillham, R.W. and Mendoza, C.A., 1996. Vapor transport of trichloroethylene in the unsaturated zone: Field and numerical modeling investigations. Water Resources Research, 32(1): 9-22.

Conrad, M.E. and DePaolo, D.J., 2004. Carbon isotopic evidence for biodegradation of organic contaminants in the shallow vadoze zone of the radioactive waste management complex. Vadose Zone Journal, 3: 143-153.

Cook, P.F., 1991. Enzyme mechanism from isotope effects. CRC Press, Boca Raton.

Costanza-Robinson, M.S. and Brusseau, M.L., 2002. Gas phase advection and dispersion in unsaturated porous media. Water Resources Research, 38(4): 71-79.

Craig, H., 1953. The geochemistry of stable carbon isotopes. Geochimica et Cosmochimica Acta, 3: 53-92.

Craig, H., 1968. Isotope separation by carrier diffusion. Science, 159(3810): 93-96.

Crump, K.S., 1976. Numerical inversion of Laplace Transforms using Fourier Series Approximation. J. Ass. Comp. Mech., 23(1): 89-96.

Dakhel, N., Pasteris, G., Werner, D. and Höhener, P., 2003. Small-Volume Releases of Gasoline in the Vadose Zone: Impact of the Additives MTBE and Ethanol on Groundwater Quality. Environmental Science and Technology, 37(10): 2127-2133.

Davis, G.B., Rayner, J.L., Fisher, S.J. and Patterson, B.M., 2000. Soil profile layering and seasonal effects on the fate and biodegradation of gasoline vapours in a sandy vadose zone. In: Contaminated Site Remediation: from Source Zones to Ecosystems., Johnston C.D. (Ed), Centre for Groundwater Studies, Perth Australia, pp. 391-398.

De Hoog, F.R., Knight, J.H. and Stokes, A.N., 1982. An improved method for numerical inversion of Laplace transforms. SIAM J. Sci. Stat. Comput, 3: 357-366.

El Tayar, N., Van de Waterbeemd, H., Gryllaki, M., Testa, B. and Trager, W.F., 1984. The lipophilicity of deuterium atoms. A comparaison of shake-flask and HPLC methods. International Journal of Pharmaceutics, 19: 271-281.

Elsner, M., Zwank, L., Hunkeler, D. and Schwarzenbach, R.P., 2005. A new concept to link observed stable isotope fractionation to degradation pathways of organic groundwater contaminants. Environmental Science and Technology, 39: 6896-6916.

Falta, R.W., Javandel, I., Pruess, K. and Witherspoon, P.A., 1989. Density driven flow of gas in the unsaturated zone due to the evaporation of volatile organic components. Water Resources Research, 25: 2159-2169.

Feng, J., Barcelona, M.J., Krishnamurthy, R.V. and Atekwana, E.A., 2000. Stable carbon isotope geochemistry of a shallow sand aquifer contaminated with fuel hydrocarbons. Applied Geochemistry, 15: 157-169.

Franzmann, P.D., Zappia, L.R., Power, T.R., Davis, G.B. and Patterson, B.M., 1999. Microbial mineralisation of benzene and caracterisation of microbial biomass in soil above hydrocarbon-contaminated groundwater. FEMS Microbiology Ecology, 30: 67-76.

Gaganis, P., Karapanagioti, H.K. and Burganos, V.N., 2002. Modelling multicomponent NAPL transport in the unsaturated zone with the constituant averaging technique. Advances in Water Resources, 25: 723-732.

Gaganis, P., Kjeldsen. P. and Burganos, V.N., 2004. Modeling natural attenuation of multicomponent fuel mixtures in the vadoze zone: use of field data and evaluation of biodegradation effects. Vadose Zone Journal, 3: 1262-1275.

Galimov, E.M., 1967. A ^{13}C isotope enrichment effect in methane carbon in the course of its infiltration through rocks. Geochem. Internat., 4: 1180-1181.

Galimov, E.M., 1985. The biological fractionation of isotopes. Academic Presse, London.

George, S.C., Boreham, C.J., Minifie, S.A. and Teerman, S.C., 2002. The effect of minor to moderate biodegradation on C5 to C9 hydrocarbons in crude oils. Organic Geochemistry, 33: 1293-1317.

Gioia, F., Murena, F. and Santoro, A., 1998. Transient evaporation of multicomponent liquid mixtures of organic volatiles through a covering porous layer. J. Hazard. Mater., 59: 131-144.

Griebler, C., Safinowski, M., Vieth, A., Richnow, H.H. and Meckenstock, R.U., 2004. Combined application of stable carbon isotope analysis and specific metabolites determination for assessing in situ degradation of aromatic hydrocarbons in a tar oil-contaminated aquifer. Environmental Science and Technology, 38: 617-631.

Gülensoy, N. and Alvarez, P.J.J., 1999. Diversity and correlation of specific aromatic hydrocarbon biodegradation capabilities. Biodegradation, 10: 331-340.

Hall, J.A., Kalin, R.M., Larkin, M.J., Allen, C.C.R. and Harper, D.B., 1999. Variation in stable carbon isotope fractionation during aerobic degradation of phenol and benzoate by contaminant degrading bacteria. Organic Geochemistry, 30: 801-811.

Harrington, R.R., Poulson, S.R., Drever, J.I., Colberg, P.J.S. and Kelly, E.F., 1999. Carbon isotope systematics of monoaromatic hydrocarbons: vaporization and adsorption experiments. Organic Geochemistry, 30: 765-775.

Hers, I., Atwater, J., Li, L. and Zapf-Gilje, R., 2000. Evaluation of vadose zone biodegradation of BTX vapours. Journal of Contaminant Hydrology, 46(3-4): 233-264.

Hinchee, R.E., Wilson, J.T. and Downey, D.C., 1995. Intrinsic bioremediation. Battelle Press., Columbus, OH., 266 pp.

Hirschorn, S. K., Dinglasan, M. J., Elsner, M., Mancini, S. A., Lacrampe-Couloume, G., Edwards, E. A. and Sherwood Lollar, B., 2004. Pathway Dependent Isotopic Fractionation during Aerobic Biodegradation of 1,2-Dichloroethane. Environmental Science and Technology, 38: 4775-4781.

Hoering, T. and Moore, H., 1958. The isotopic composition of the nitrogen in natural gases and associated crude oils. Geochimica et Cosmochimica Acta, 13: 225-232.

Hoff, J.T., Mackey, D., Gillham, R. and Shiu, W.Y., 1993. Partitioning of organic chemicals at the air-water interface in environmental systems. Environmental Science and Technology, 27: 2174-2180.

Höhener, P., Dakhel, N., Christophersen, M., Broholm, M.M. and Kjeldsen, P., 2006. Biodegradation of hydrocarbons vapors: Comparison of laboratory studies and field investigations in the vadose zone at the emplaced fuel source experiment, Airbase Værløse, Denmark. Journal of Contaminant Hydrology(88): 337-358.

Höhener, P., Duwig, C., Pasteris, G., Kaufmann, K., Dakhel, N., and Harms, H., 2003. Biodegradation of petroleum hydrocarbon vapors: laboratory studies on rates and kinetics in unsaturated alluvial sand. Journal of Contaminant Hydrology, 66: 93-115.

Huang, L., Sturchio, N.C., Abrajano, T.A.jr., Heraty, L.J. and Holt, B.D., 1999. Carbon and chlorine isotope fractionation of chlorinated aliphatic hydrocarbons by evaporation. Organic Geochemistry, 30: 777-785.

Hunkeler, D., Anderson, N., Aravena, R., Bernasconi, S.M. and Butler, B.J., 2001. Hydrogen and carbon isotope fractionation during aerobic biodegradation of benzene. Environmental Science and Technology, 35(17): 3462-3467.

Hunkeler, D. and Aravena, R., 2000. Determination of stable carbon isotope ratios of chlorinated methanes, ethanes and ethenes in aqueous samples. Environmental Science and Technology, 34: 2839-2844.

Hunkeler, D., Aravena, R., Berry-Spark, K. and Cox, E., 2005. Assessment of Degradation Pathways in an Aquifer with Mixed Chlorinated Hydrocarbon Contamination Using Stable Isotope Analysis. Environmental Science and Technology, 39: 5975-5981.

Hunkeler, D., Aravena, R. and Butler, B.J., 1999. Monitoring microbial dechlorination of tetrachloroethene (PCE) in groundwater using compound-specific stable carbon Isotope ratios: Microcosm and field studies. Environmental Science and Technology, 33: 2733-2738.

Hunkeler, D., Meckenstock, R.U. and Richnow, H.H., 2002. Quantification of isotope fractionation in experiments with deuterium-labeled substrate. Applied and Environmental Microbiology, 68: 5202-5207.

IUPAC, 1991. Isotopic compositions of the elements. Pure and Applied Chemistry, 63: 991-1002.

Jackson, A. and Pardue, J., 1999. Quantifying the mineralization of contaminants using stable carbon isotope ratios. Organic Geochemistry, 30: 787-792.

Jin, Y., Streck, T. and Jury, W.A., 1994. Transport and biodegradation of toluene in unsaturated soil. Journal of Contaminant Hydrology, 17(2): 111-127.

Jost, W., 1960. Diffusion in Solids, Liquids and Gases, 3d ed. Academic Press, New-York.

Jury, W.A. and Roth, K., 1990. Transfer functions and solute movement through soil: Theory and applications, Birkhauser, Boston, 289 pp.

Jury, W.A., Spencer, W.F. and Farmer, W.J., 1983. Behavior assessment model for trace organics in soil: I. Model description. Journal of Environmental Quality, 12: 558-563.

Jury, W.A., Spencer, W.F. and Farmer, W.J., 1984. Behavior assessment model for trace organics in soil: IV. Review of experimental evidence. Journal of Environmental Quality, 33:1637-1644.

Karapanagioti, H.K., Gaganis, P. and Burganos, V.N., 2003. Modeling attenuation of volatile organic mixtures in the unsaturated zone: codes and usage. Environmental Modelling and Software, 18(3-4): 329-337.

Karapanagioti, H.K., Gaganis, P., Burganos, V.N. and Höhener, P., 2004. Reactive transport of volatile organic compound mixtures in the unsaturated zone: modelling and tuning with lysimeter data. Environmental Modelling and Software, 19: 435-450.

Katyal, A.K., Kaluarachchi, J.J., Parker, J.C., Cho, J.S. and Swaby, L.G., 1991. MOFAT: A two-dimensional finite element program for multiphase flow and multicomponent transport. EPA/600/2-91/020.

Kaufmann, K., Christophersen, M., Buttler, A., Harms, H. and Höhener, P., 2004. Microbial community response to petroleum hydrocarbon contamination in the unsaturated zone at the experimental field site Værløse, Denmark. FEMS Microbiology Ecology, 48(3): 387-399.

Keener, W. K., Watwood, M. E., Schaller, K. D., Walton, M. R., Partin, J. K., Smith, W. A. and Clingenpeel, S. R., 2001. Use of selective inhibitors and chromogenic substrates to differentiate bacteria based on toluene oxygenase activity. Journal of Microbiological Methods, 46(3): 171-185.

Kelley, C.A., Hammer, B.T. and Coffin, R.B., 1997. Concentrations and stable isotope values of values of BTEX in gasoline-contaminated groundwater. Environmental Science and Technology, 31: 2469-2472.

King, S.L., Quay, P.D. and Landsdown, J.M., 1989. The 13C/12C kinetic isotope effect for soil oxidation of methane at ambient atmospheric concentrations. Journal of Geophysical Research, 94: 18273-18277.

Kirtland, B.C., Aelion, C.M. and Stone, P.A., 2005. Assessing in situ mineralization of recalcitrant organic compounds in vadose zone sediments using delta 13C and 14C measurements. Journal of Contaminant Hydrology, 76: 1-18.

Kirtland, B.C., Aelion, C.M., Stone, P.A. and Hunkeler, D., 2003. Isotopic and geochemical assessment of biodegradation of chlorinated hydrocarbons. Environmental Science and Technology, 37: 4205-4212.

Kolhatkar, R., Kuder, T., Philip, P., Allen, J. and Wilson, J.T., 2002. Use of compound-specific stable carbon isotope analyses to demonstrate anaerobic biodegradation of MTBE in groundwater at a gasoline release site. Environmental Science and Technology, 36: 5139-5146.

Kopinke, F.D., Georgi, A., Voskamp, M. and Richnow, H.H., 2005. Carbon isotope fractionation of organic contaminants due to retardation on humic substances: Implications for natural attenuation studies in aquifers. Environmental Science and Technology, 39(16): 6052-6062.

Lahvis, M.A., Baehr, A.L. and Baker, R.J., 1999. Quantification of aerobic biodegradation and volatilization rates of gasoline hydrocarbones near the water table under natural attenuation conditions. Water Resources Research, 35(3): 753-765.

Lebedew, W.C., Owsjannikow, G.A., Mogilewskij, G.A. and Bogdanow, W.M., 1969. Fractionierung der Kohlenstoffisotope durch mikrobiologische Prozesse in der biochemischen Zone. Zeitschrift Angewandte Geologie., 15: 621-624.

Liang, H.C. and Udell, K.S., 1999. Experimental and theoretical investigation of vaporization of liquid hydrocarbon mixture in water-wetted porous media. Water Resources Research, 35: 635-649.

Lugg, G.A., 1968. Diffusion coefficients of some organic and other vapors in air. Analytical Chemistry, 40(7): 1072-1077.

Madsen, E.L., 1991. The degradation of organic compounds in situ is of critical importance for the biosphere. Environmental Science and Technology, 25(10): 1663-1673.

Mancini, S. A., Lacrampe-Couloume, G., Jonker, H., Van Breukelen, B. M., Groen, J., Volkering, F. and Sherwood Lollar, B., 2002. Hydrogen isotopic enrichment: An indicator of biodegradation at a petroleum hydrocarbon contaminated field site. Environmental Science and Technology, 36(11): 2464-2470.

Mansuy, L., Philp, R.P. and Allen, J., 1997. Source identification of oil spills based on isotopic composition of individual components in weathered oil samples. Environmental Science and Technology, 31: 3417-3425.

Mazeas, L., Budzinski, H. and Raymond, N., 2002. Absence of stable isotope fractionation of saturated and polycyclic aromatic hydrocarbons during aerobic bacterial biodegradation. Organic Geochemistry, 33: 1259-1272.

McCarthy, K.A. and Johnson, R.L., 1993. Transport of organic chemicals across the capillary fringe. Water Resources Research, 29: 1675-1683.

Meckenstock, R.U., Morasch, B., Griebler, C. and Richnow, H.H., 2004. Stable isotope fractionation analysis as a tool to monitor biodegradation in contaminated aquifers. Journal of Contaminant Hydrology, 75: 215-255.

Meckenstock, R.U., Morasch, B., Kastner, M., Vieth, A. and Richnow, H.H., 2002. Assessment of bacterial degradation of aromatic hydrocarbons in the environment by analysis of stable carbon isotope fractionation. Water, Air and Soil Pollution: Focus, 2(3): 141-152.

Melander, L. and Saunders, W.H., 1980. Reaction rates of isotopic molecules. John Wiley, New York, 331 pp.

Millington, R.J. and Quirk, J.P., 1961. Permeability of porous solids. Trans. Faraday Soc., 57: 1200-1207.

Milner, C.W., Rogers, M.A. and Evans, C.R., 1977. Petroleum transformations in reservoirs. Journal of Geochemical Exploration, 7: 101-153.

Moldrup, P., Olsen, T., Gamst, J., Schjonning, P., Yamaguchi, T. and Rolston, D.E., 2000. Predicting the gas diffusion coefficient in repacked soil: Water-induced linear reduction model. Soil Science Society of America Journal, 64: 1588-1594.

Morasch, B., Richnow, H.H., Schink, B. and Meckenstock, R.U., 2001. Stable hydrogen and carbon isotope fractionation during microbial toluene degradation: Mechanistic and environmental aspects. Applied and Environmental Microbiology, 67(10): 4842-4849.

Morasch, B., Richnow, H.H., Schink, B., Vieth, A. and Meckenstock, R.U., 2002. Carbon and hydrogen stable isotope fractionation during aerobic bacterial degradation of aromatic hydrocarbons. Applied and Environmental Microbiology, 68(10): 5191-5194.

Morrill, P.L., Lacrampe-Couloume, G., Slater, G.F., Sleep, B.E., Edwards, E.A., McMaster, M.L., Major, D.W. and Sherwood Lollar, B. 2005. Quantifying chlorinated ethene degradation during reductive dechlorination at Kelly AFB using stable carbon isotopes. Journal of Contaminant Hydrology, 76: 279-293.

Müller, P. and Wienholz, R.C., 1967. Bestimmung der natürlichen Variationen der Kohlenstoffisotope in Erdöl und Erdgaskomponenten und ihre Beziehung zur Genese. Zeitschrift Angewandte Geologie, 13: 456-461.

Mulligan, C.N. and Yong, R.N., 2004. Natural attenuation of contaminated soils. Environment International, 30: 587-601.

Narten, A. and Kuhn, W., 1961. Der 13C/12C-Isotopieeffekt in Tetrachlorkohlenstoff und in Benzol. Helv. Chim. Acta, 44: 1474.

Nijenhuis, I. et al., 2005. Stable isotope fractionation of tetrachloroethene during reductive dechlorination by Sulfurospirillum multivorans and Desulfitobacterium sp. strain PCE-S and abiotic reactions with cyanocobalamin. Applied and Environmental Microbiology, 71(7): 3413-3419.

NRC, 2000. Natural attenuation for Groundwater Remediation. National Academy Press, Washington DC, 274 pp.
O'Leary, M.H. and Yapp, C.J., 1978. Equilibrium carbon isotope effect on a decarboxylation reaction. Biochemical and Biophysical Research Communications, 80: 155-160.
Ostendorf D. W., Hinlein.E.S., Schoenberg T.H., 2000. Aerobic biodegradation kinetics and soil gas transport in unsaturated soil. in: D.L. Wise, D.J. Trantolo, E.J Cichon, H.I. Inyang and U. Stottmeister (Eds.), Bioremediation of contaminated soils., Marcel Dekker, New York: 607-632.
Ostendorf, D.W. and Kampbell, D.H., 1991. Biodegradation of hydrocarbon vapors in the unsaturated zone. Water Resources Research, 27(4): 453-462.
Paneth, P., 1994. Heavy isotope effects on enzymatic reactions. Journal of molecular structure, 321: 35-44.
Parker, J.C., 2003. Physical processes affecting natural depletion of volatile chemicals in soil and groundwater. Vadoze Zone Journal, 2: 222-230.
Pasteris, G., Werner, D., Kaufmann, K. and Höhener, P., 2002. Vapor phase transport and biodegradation of volatile fuel compounds in the unsaturated zone: a large scale lysimeter experiment. Environmental Science and Technology, 36(1): 30-39.
Pernaton, E., Prinzhofer, A. and Schneider, F., 1996. Reconsideration of methane signature as a criterion for the genesis of natural gas: influence of migration on isotopic signature. Rev. IFP, 51(5): 635-651.
Poulson, S.R. and Drever, J.I., 1999. Stable Isotope (C, Cl, and H) Fractionation during Vaporization of Trichloroethylene. Environmental Science and Technology, 33: 3689-3694.
Prinzhofer, A. and Pernaton, E., 1997. Isotopically light methane in natural gas: bacterial imprint of diffusive fractionation? Chemical Geology, 142: 193-200.
Reeburgh, W.S., Hirsch, A.I., Sansone, F.J., Popp, B.N. and Rust, T.M., 1997. Carbon kinetic isotope effect accompanying microbial oxidation of methane in boreal forest soils. Geochimica et Cosmochimica Acta, 61(22): 4761-4767.
Reitsema, R.H., Kaltenback, A.J. and Lindberg, F.A., 1981. Source and migration of light hydrocarbons indicated by carbon isotopic ratios. Bulletin of the American Association of Petroleum Geologists. 65: 1536-1542.
Richnow, H.H., Annweiler, E., Michaelis, W. and Meckenstock, R.U., 2003a. Microbial degradation of aromatic hydrocarbons in a contaminated aquifer monitored by carbon isotope fractionation. Journal of Contaminant Hydrology, 64: 59-72.
Richnow, H. H., Meckenstock, R. U., Ask Reitzel, L., Baun, A., Ledin, A. and Christensen, T. H., 2003b. In situ biodegradation determined by carbon isotope fractionation of aromatic hydrocarbons in an anaerobic landfill leachate plume (Vejen, Denmark). Journal of Contaminant Hydrology, 64(1-2): 59-72.
Riser-Roberts, E., 1998. Remediation of petroleum contaminated soils; biological, physical and chemical processess. Lewis Publishers, CRC Press., Boca Raton, London, New-York, Washington D.C.
Rittmann, B.E., 2004. Definition, objectives, and evaluation of natural attenuation. Biodegradation, 15: 349-357.
Scanlon, B.R., Nicot, J.P. and Massmann, J.M., 2000. Soil gas movement in unsaturated systems. In: M.E. Sumner (Editor), Handbook of soil sciences. CRC Press, Boca Raton, Florida, pp. A277-A319.
Schaefer, C.E., Unger, D.R. and Kosson, D.S., 1998. Partitioning of hydrophobic contaminants in the vadose zone in the presence of a nonaqueous phase. Water Resources Research, 35: 2529-2537.

Schmidt, T.C., Zwank, L., Elsner, M., Berg, M., Meckenstock, R U. and Haderlein, S.B., 2004. Compound-specific stable isotope analysis of organic contaminants in natural environments: a critical review of the state of the art, prospects, and future challenges. Anal Bioanal Chem, 378: 283-300.

Schüth, C., Taubald, H., Bolano, N. and Maciejczyk, K., 2003. Carbon and hydrogen isotope effects during sorption of organic contaminants on carbonaceous materials. Journal of Contaminant Hydrology, 64(2): 269-281.

Sherwood Lollar, B., Slater, G.F., Sleep, B., Witt, M., Klecka, G.M. and Spivack, J. 2001., Stable carbon isotope evidence for intrinsic bioremediation of tetrachloroethene and trichloroethene at Area 6, Dover Air Force Base. Environmental Science and Technology, 35: 261-269.

Silka, L.R., 1988. Simulation of vapor transport through the unsaturated zone - interpretation of soil-gas surveys. Groundwater Monit. Rev. 8:115-123.

Slater, G.F., 2003. Stable Isotope Forensics - When Isotopes Work. Environmental Forensics, 4: 13-23.

Slater, G.F., Ahad, J.M.E., Sherwood Lollar, B., Allen-King, R. and Sleep, B., 2000. Carbon isotope effects resulting from equilibrium sorption of dissolved VOCs. Analytical Chemistry, 72: 5669-5672.

Slater, G.F., Dempster, H.S., Sherwood Lollar, B. and Ahad, J., 1999. Headspace analysis: A new application for isotopic characterization of dissolved organic contaminants. Environmental Science and Technology, 33: 190-194.

Smith, J.A., Tisdale, A.K. and Cho, H.J., 1996. Quantification of natural vapor fluxes of trichloroethene in the unsaturated zone at Picatinny Arsenal, New Jersey. Environmental Science and Technology, 30: 2243-2250.

Sondermann, W.D. and Knorpp, B., 2004. Legal Aspects of Natural Attenuation in Germany. Biodegradation, 15(6): 467 - 473.

Song, D.L., Conrad, M.E., Sorenson, K.S. and Alvarez-Cohen, L., 2002. Stable carbon isotope fractionation during enhenced in situ bioremediation of trichloroethelene. Environmental Science and Technology, 36: 2262-2268.

Stahl, W., Faber, E., Carey, B.D. and Kirksey, D.L., 1981. Near-surface evidence of migration of natural gas from deep reservoirs and source rocks. Bulletin of the American Association of Petroleum Geologists. 65: 1543-1550.

Stahl, W.J., 1980. Compositional changes and $^{13}C/^{12}C$ fractionations during the degradation of hydrocarbons by bacteria. Geochimica et Cosmochimica Acta, 44: 1903-1907.

Stehmeier, L.G., Francis, M.M., Jack, T.R., Diegor, E., Winsor, L. and Abrajano, T.A. jr., 1999. Field and in vitro evidence for in situ bioremediation using compound-specific $^{13}C/^{12}C$ ratio monitoring. Organic Geochemistry, 30: 821-833.

Steinbach, A., Seifert, R., Annweiler, E. and Michaelis, W., 2004. Hydrogen and carbon isotope fractionation during anaerobic biodegradation of aromatic hydrocarbons- a field study. Environmental Science and Technology, 38: 609-616.

Sturchio, N.C., Clausen, J.L., Heraty, L.J., Huang, L., Holt, B.D. and Abrajano, T.A. jr. 1998. Chlorine isotope investigation of natural attenuation of trichloroethene in an aerobic aquifer. Environmental Science and Technology, 32: 3037-3042.

Suchomel, K.H., Kreamer, D.K. and Long, A., 1990. Production and transport of carbon dioxide in a contaminated vadose zone: A stable and radioactive carbon isotope study. Environmental Science and Technology, 24: 1824-1831.

Tomaszewski, J.E., Jerina, D.M. and Daly, J.W., 1975. Deuterium isotope effects during formation of phenols by hepatic monoxygenases. Evidence for an alternative to the arene oxide pathway. Biochemistry, 14: 2024-2031.

Tyler, S.C., Crill, P.M. and Brailsford, G.W., 1994. 13C/12C fractionation of methane during oxidation in a temperate forested soil. Geochimica et Cosmochimica Acta, 58(6): 1625-1633.

Van Hook, W.A., 1966. Vapor Pressures of the Deuterated Ethanes. Journal of Chemical Physics, 44(1): 234-251.

Van Hook, W.A., 1967. Isotope effects on vaporization from the adsorbed state. Methane system. Journal of Physical Chemistry, 71(10): 3270-3275.

Van Hook, W.A., 1985. Isotope effects in condensed phases, the benzene example. Influence of anharmonicity; harmonic and anharmonic potential surfaces and their isotope independence. Molar volume effects in isotopic benzenes. Journal of Chemical Physics, 83(8): 4107-4117.

Werner, D., Broholm, M. and Höhener, P., 2004. Simultaneous estimation of nonaqueous phase liquid (NAPL) saturation and diffusive fluxes of volatile organic compounds in the vadose zone. Ground Water Monitoring and Remediation, 25: 59-67.

Werner, D., Grathwohl, P. and Höhener, P., 2004. Review of field methods for the determination of the tortuosity and effective gas-phase diffusivity in the vadose zone. Vadoze Zone Journal, 3: 1240-1249.

Werner, D. and Höhener, P., 2003. In situ method to measure effective and sorption-affected gas-phase diffusion coefficients in soils. Environmental Science and Technology, 37: 2502-2510.

Wiedemeier, T.H., Newell, C.J., Rifai, H.S. and Wilson, J.T., 1999. Natural Attenuation of Fuels and Chlorinated Solvents in the Subsurface. John Wiley & Sons, New York, 617 pp.

Wilkins, P.C., Dalton, H., Samuel, J.C. and Green, J., 1994. Further Evidence for Multiple Pathways in Soluble Methane-Monooxygenase-Catalysed Oxidations from the Measurement of Deuterium Kinetic Isotope Effects. European Journal of Biochemistry(226): 555-560.

Wilson, D.J., 1997. Soil gas volatile organic compound concentration contours for locating vadose zone nonaqueous phase liquid contamination. Environmental Monitoring and Assessment, 48: 73-100.

Wolfsberg, M.J., 1963. Isotope effects on intermolecular interactions and isotopic vapor pressure differences. Journal de Chimie physique et de Physico-chimie biologique., 60(1-2): 15-22.

Yoshizawa, K., 2002. Theoretical study on kinetic isotope effects in the C-H bond activation of alkanes by iron-oxo complexes. Coordination Chemistry Reviews, 226: 251-259.

Zhang, T. and Krooss, B.M., 2001. Experimental investigation on the carbon isotope fractionation of methane during gas migration by diffusion through sedimentary rocks at elevated temperature and pressure. Geochimica et Cosmochimica Acta, 65(16): 2723-2742.

Zhou, E. and Crawford, R.L., 1995. Effects of oxygen, nitrogen and temperature on gasoline biodegradation in soil. Biodegradation, 6: 127-140.

List of symbols

A	Cross-section area	L^2
b	Number of reactive positions	[-]
C_0	Initial concentration of the substrate in the soil air phase	M/L^3
C_a	Concentration of the substrate in the soil air phase	M/L^3
D_m	Diffusion coefficient in the air phase	L^2/T
D_e	Effective diffusion coefficient in the soil air phase	L^2/T
D_s	Sorption-affected diffusion coefficient in the soil air phase	L^2/T
F	Mass flux	$M/(L^2T)$
f	Remaining fraction of the substrate	%
f_{IIa}	Remaining fraction of the subspecies IIa	%
f_{IIb}	Remaining fraction of the subspecies IIb	%
f_a	Mass fraction of the substrate in the soil air phase	%
f_w	Mass fraction of the substrate in the soil water phase	%
f_{oc}	Fraction of organic carbon in soil	%
H	Air-water partitioning coefficient (Henry constant)	$mol\ L^{-3}/mol\ L^{-3}$
KIE	Kinetic isotope effect	[-]
AKIE	Apparent kinetic isotope effect	[-]
^{l}k and k_{app}	Apparent first order biodegradation rate applied to the gaseous phase	T^{-1}
$^{h}k_{2sp}$	Slower first order biodegradation rate for subspecies II	T^{-1}
$^{h}k_{3sp}$	Slower first order biodegradation rate for subspecies IIb	T^{-1}
k_w	first order biodegradation rate applied to the water phase	T^{-1}
K_d	Water-solid partitioning coefficient	$(mol\ M)/(mol\ L^{-3})$
L	Length of the finite system	L
M	Mass of the atom or molecule	M/mol
m	Number of mole of atoms or molecules	mol
n	Number of atoms in the molecule	[-]
p	Complexe Laplace variable	T^{-1}
P	Vapour pressure	atm

∇	Laplace operator	L^{-1}
R	Isotope ratio	[-]
R_0	Initial isotope ratio	[-]
V_g	Gas phase volume	L^3
w	Total quantity of atoms or molecules	M
x	Distance from the source	L
θ_a	Air-filled porosity	L^3 air/L^3 app
θ_w	Water-filled porosity	L^3 water/L^3 app
θ_t	Total porosity	L^3 void/L^3 app
ρ_s	Density of the solid	M solid/L^3 solid
τ	Tortuosity factor	[-]
κ	Force constant of the bond	MT^{-2}
ν	Frequency of vibration	T^{-1}
β	Source depletion rate	T^{-1}
α	Isotope fractionation factor	[-]
ε	Enrichment factor	[-]

Appendix A: Data from the column experiment

Table A-1: Concentrations and isotope ratios measured in the column during the column experiment for pentane, hexane, benzne and isooctane.

		Pentane		Hexane		Benzene		Isooctane	
time	distance	conc.	$\delta^{13}C$	conc.	$\delta^{13}C$	conc.	$\delta^{13}C$	conc.	$\delta^{13}C$
hours	m	mg/L	‰	mg/L	‰	mg/L	‰	mg/L	‰
3	0.215	40.59	-29.98	27.22	-29.89	3.41	-28.01	12.14	-23.47
	0.415	18.95	-31.11	11.80	-30.46	1.35	-29.70	5.64	-25.01
	0.615	4.88	-33.74	2.61	-33.14				
	0.815								
	1.015								
4.25	0.215	40.23	-29.88	28.34	-29.97	4.50	-28.07	15.22	-24.23
	0.415	25.11	-30.52	16.32	-30.13	1.72	-28.68	6.82	-24.14
	0.615	8.78	-32.13	6.36	-31.84			1.94	-24.69
	0.815	1.20	-34.22	1.29	-33.78				
	1.015								
5	0.215	43.69	-29.90	30.27	-29.90	4.24	-27.76	14.08	-23.49
	0.415	29.84	-30.51	19.23	-30.39	2.73	-28.64		
	0.615	14.08	-31.45	7.48	-31.69	0.67	-29.38	2.99	-24.95
	0.815	3.35	-34.24	1.89	-33.12				
	1.015								
6	0.215	50.14	-29.77	35.64	-29.69	4.40	-27.69	17.65	-23.20
	0.415	34.44	-30.37	22.95	-30.25	2.71	-28.46	10.14	-24.52
	0.615	14.63	-30.97	7.80	-31.44	0.77	-29.31	1.70	-24.88
	0.815	3.32	-32.38	1.87	-31.95				
	1.015								
8	0.215	85.14	-30.04	65.00	-29.82	8.81	-27.27	33.74	-23.63
	0.415	77.87	-30.43	55.68	-30.26	6.78	-28.07	27.12	-23.91
	0.615	35.91	-31.14	22.17	-30.85	2.19	-29.06	9.26	-24.67
	0.815	10.77	-32.78	6.25	-32.28			2.21	-24.89
	1.015	1.69	-33.75						
12	0.215	33.72	-28.48	25.26	-28.84	1.90	-28.39	10.57	-23.82
	0.415	44.63	-30.00	31.60	-29.96	4.18	-28.03	14.67	-23.99
	0.615	24.79	-30.51	17.19	-30.49	2.06	-28.62	7.82	-24.38
	0.815	13.84	-31.31	9.02	-31.04			4.04	-24.68
	1.015	5.46	-31.57	3.24	-31.50			1.29	-24.57
25.8	0.215	47.13	-29.38	35.72	-29.61	10.63	-27.02	38.15	-23.83
	0.415	47.36	-29.45	41.74	-29.72	6.24	-27.70	20.97	-23.91
	0.615	49.76	-29.63	39.54	-29.89	6.01	-27.72	22.43	-24.05
	0.815	29.57	-29.68	23.03	-29.95	3.22	-27.74	12.66	-24.04
	1.015	9.29	-29.43	7.17	-29.84	1.05	-27.46	3.40	-23.88

30.75	0.215	45.25	-29.12	30.36	-29.26	13.40	-27.48	44.66	-24.04
	0.415	38.63	-29.16	39.98	-29.49	6.91	-26.45	28.51	-23.52
	0.615	39.02	-29.42	30.87	-29.56	4.39	-27.26	16.76	-23.61
30.75	0.815	19.50	-29.46	14.06	-29.59	3.29	-28.20	9.68	-23.80
	1.015	7.58	-29.29	6.13	-29.40	1.10	-27.48	4.03	-24.17
47.75	0.215	44.63	-28.64	33.59	-28.88	12.54	-26.87	32.12	-23.38
	0.415	36.19	-28.63	41.01	-29.04	9.81	-26.80	26.08	-23.47
	0.615	28.72	-28.75	27.83	-28.77	5.72	-26.73	24.94	-23.57
	0.815	17.80	-28.94	13.07	-28.94	3.31	-26.86	11.08	-23.62
	1.015	6.87	-28.89	6.08	-28.68	1.17	-26.97	4.16	-23.56
57.75	0.215	52.00	-29.00	49.73	-29.42	11.05	-27.00	38.73	-23.83
	0.415	39.19	-28.70	40.47	-29.15	9.79	-26.98	29.51	-23.75
	0.615	27.94	-28.65	19.45	-28.51	6.09	-26.95	15.42	-23.38
	0.815	14.26	-28.54	10.68	-28.28	3.19	-27.09	9.18	-23.20
	1.015	8.22	-28.25	5.14	-28.36	1.08	-26.45	7.58	-23.66
71.45	0.215	44.02	-28.38	38.81	-28.81	12.88	-26.79	40.13	-23.38
	0.415	37.78	-28.20	33.04	-28.58	8.75	-27.00	36.90	-23.54
	0.615	22.75	-27.56	12.62	-27.94	5.37	-27.23	14.62	-23.34
	0.815	15.89	-27.83	7.92	-27.95	2.30	-26.80	9.98	-23.44
	1.015	10.57	-27.71	2.16	-27.26	0.57	-26.83	12.12	-23.34
81.75	0.215	29.15	-28.39	42.43	-28.93	9.04	-26.83	34.07	-23.49
	0.415	32.36	-28.31	22.63	-28.45	7.85	-26.80	23.13	-23.55
	0.615	22.81	-28.23	14.18	-28.08	3.42	-26.83	15.72	-23.46
	0.815	14.05	-28.20	4.38	-27.60	1.73	-26.84	12.65	-23.49
	1.015	6.09	-28.36	2.31	-28.05	0.41	-26.97	4.73	-23.43
96.8	0.035			74.82	-29.38	14.43	-26.56	59.16	-23.88
	0.115			48.87	-29.05	9.56	-26.54	40.22	-23.63
	0.165					12.08	-26.55	51.32	-23.64
	0.215			55.33	-28.83	12.01	-26.68	52.35	-23.58
	0.315					9.19	-26.89		
	0.415			32.28	-28.48	7.18	-26.84	38.11	-23.63
	0.515					5.20	-26.92		
	0.615					4.02	-26.86		
	0.815			6.17	-27.87	1.41	-26.80		
	1.015					0.35	-27.11		
145.3	0.035					14.37	-26.66	63.45	-23.63
	0.165			61.09	-28.77	12.63	-26.62		
	0.215	16.33	-25.91	40.40	-28.29	12.72	-26.83	41.91	-23.48
	0.315					3.15	-26.50		
	0.415	23.52	-27.03	29.40	-28.31	6.86	-26.49	31.23	-23.34
	0.515					6.45	-26.79		
	0.615	23.72	-27.67	26.55	-28.63	5.40	-26.86	29.48	-23.55
	0.815	13.41	-27.42	13.75	-28.43	2.80	-26.57	16.51	-23.29
	1.015	5.78	-28.04	5.28	-28.54	1.11	-26.81	6.68	-23.48

167.8	0.035	37.91	-27.31			12.44	-26.39		
	0.065	37.53	-27.32	61.81	-28.77	12.68	-26.37	58.87	-23.69
	0.115	34.56	-27.19	54.18	-28.58	10.84	-26.35	50.67	-23.46
	0.215	32.77	-27.43	50.30	-28.76	10.34	-26.35	50.30	-23.59
	0.415	22.70	-27.00	34.03	-28.46	6.44	-26.31	36.21	-23.49
	0.615	14.07	-26.53	19.54	-28.15	5.15	-26.88	22.08	-23.24
	0.815	10.85	-27.24	13.68	-28.43	2.95	-26.88	16.51	-23.54
	1.015	4.47	-27.18	5.31	-28.45	1.14	-26.61	6.51	-23.48
191.8	0.035	32.57	-27.14			13.25	-26.44	64.65	-23.51
	0.115	31.94	-27.15			12.64	-26.50		
	0.165	29.12	-26.99			11.43	-26.43	54.49	-23.49
	0.215	20.36	-26.23	37.52	-28.18	11.24	-26.94	41.21	-23.71
	0.315	26.15	-27.10	45.36	-28.66	9.78	-26.44	47.84	-23.57
	0.415	21.27	-26.61	36.11	-28.23	7.51	-26.19	39.11	-23.40
	0.515						-26.77		
	0.615	12.98	-26.51	20.59	-28.23	4.25	-26.12	23.43	-23.41
	0.815	9.08	-26.97	13.17	-28.28	2.73	-26.39	16.28	-23.35
	1.015	3.84	-27.36	5.19	-28.53	1.20	-26.55	6.86	-23.63
263.75	0.035	17.66	-25.75	47.46	-28.04	9.00	-26.00	61.15	-23.64
	0.065	18.91	-25.02	53.08	-28.17	10.10	-25.71	64.87	-23.32
	0.115	17.16	-24.86	46.89	-28.14	9.29	-26.00	58.85	-23.39
	0.165	15.48	-25.45	43.21	-28.08	8.52	-25.90	53.91	-23.39
	0.215	18.17	-24.36	51.77	-27.19	12.65	-24.28	72.32	-22.94
	0.315						-25.85		
	0.415	56.61	-25.71		-28.26	28.50	-25.87		-23.13
	0.615	5.57	-24.98	12.70	-27.40	2.98	-25.15	20.19	-23.09
	0.815	3.98	-25.43	7.97	-27.67	2.10	-25.64	15.37	-23.46
	1.015	1.33	-25.46	2.38	-27.36	0.85	-25.75	6.04	-23.48
311.6	0.035	10.02	-25.04	40.07	-28.19	8.92	-26.30	59.45	-24.26
	0.065	10.39	-24.76	41.60	-28.09	9.03	-25.88	61.63	-23.76
	0.115	9.17	-24.76	35.41	-28.07	7.67	-25.83	53.06	-23.68
	0.165	8.98	-24.91	33.47	-28.00	7.24	-25.84	50.07	-23.68
	0.215	5.96	-24.04	15.23	-27.58	4.67	-25.13	23.57	-23.26
	0.315	8.06	-25.26			6.52	-26.14		
	0.415	5.80	-24.95	12.49	-27.61	4.38	-25.44	21.31	-23.48
	0.615	4.36	-25.77	12.53	-27.60	3.63	-25.68	26.42	-23.54
	0.815	1.93	-24.92	4.76	-27.12	2.02	-25.49	15.67	-23.46
	1.015	0.41		0.93	-26.38	0.79	-25.76	6.00	-23.44
336.1	0.035	9.12	-25.04	41.13	-28.04	9.34	-25.83	64.80	-23.74
	0.065	10.36	-25.10	45.40	-28.02	10.04	-25.70	69.18	-23.70
	0.115	8.00	-24.33	37.45	-27.93	8.61	-25.82	61.68	-23.72
	0.165	8.95	-25.09	38.22	-27.86	8.92	-25.80	63.85	-23.61
	0.215	5.27	-23.56	25.86	-27.50	5.10	-25.19	46.03	-23.36
	0.315	6.21	-24.81			6.04	-25.58		
	0.415	4.41	-24.06	18.53	-27.52	4.19	-25.35	37.70	-23.42
	0.615	3.26	-25.11	10.70	-27.40	3.70	-25.68	30.16	-23.48
	0.815	1.26	-25.69	3.41	-26.77	2.17	-25.56	17.15	-23.47
	1.015			0.57	-25.96	1.10	-26.06	7.45	-23.73

Table A-2: Concentrations and isotope ratios measured in the column during the column experiment for methyl-cyclohexane (MCH), toluene, octane and *m*-xylene.

		MCH		Toluene		Octane		*m*-Xylene	
time	distance	conc.	$\delta^{13}C$	conc.	$\delta^{13}C$	conc.	$\delta^{13}C$	conc.	$\delta^{13}C$
hours	m	mg/L	‰	mg/L	‰	mg/L	‰	mg/L	‰
3	0.215	8.87	-26.33	1.07	-29.01	1.83	-30.12	0.21	-26.93
	0.415	4.50	-27.29			0.70	-31.67		
	0.615								
	0.815								
	1.015								
4.25	0.215	11.22	-26.39	1.29	-28.89	2.94	-30.18	0.28	-26.81
	0.415	5.30	-26.74			1.48	-31.10		
	0.615	1.63	-27.23						
	0.815								
	1.015								
5	0.215			1.38	-28.72	2.30	-30.34	0.32	-27.37
	0.415	7.30	-26.89	0.79	-29.48	1.53	-30.72		
	0.615	2.29	-27.05			0.41	-31.97		
	0.815								
	1.015								
6	0.215	10.91	-26.34	1.45	-29.10	2.30	-30.59	0.34	-27.36
	0.415	6.83	-26.64	0.72	-29.51	1.49	-31.01	0.33	-27.69
	0.615	2.47	-27.16			0.41	-31.10		
	0.815								
	1.015								
8	0.215	23.35	-25.68	2.79	-28.65	5.15	-30.67	0.86	-29.05
	0.415	19.48	-25.79	1.80	-29.70	4.15	-31.05	0.30	-27.73
	0.615	6.61	-26.86			1.02	-30.86		
	0.815	1.89	-27.36						
	1.015								
12	0.215	4.99	-26.46			0.86	-30.58		
	0.415	9.76	-26.60	1.33	-29.36	2.14	-30.92	0.55	-27.42
	0.615	5.36	-26.99			0.90	-30.83		
	0.815	2.88	-26.99			0.40	-31.37		
	1.015	0.97	-28.19						
25.8	0.215	25.69	-25.98	4.46	-28.67	7.37	-30.53	2.00	-26.67
	0.415	15.15	-25.90	1.80	-29.25	4.12	-31.07	0.42	-27.25
	0.615	15.35	-26.11			3.48	-32.54		
	0.815	8.79	-26.22	0.80	-32.69	1.28	-31.50	0.18	-30.64
	1.015	2.41	-26.05	0.43	-30.61	0.94	-29.90	0.12	-28.07
30.75	0.215	30.15	-26.23	5.78	-28.95	8.88	-31.11	2.59	-27.45
	0.415	20.50	-25.53	2.62	-28.83	4.21	-30.86	1.05	-26.72
	0.615	10.79	-25.99	1.15	-29.29	2.05	-31.45	0.46	-27.17
	0.815	7.04	-25.96	0.99	-29.53	1.43	-31.19	0.17	-29.75
	1.015	2.98	-26.14			0.61	-29.75		

47.75	0.215	30.89	-25.73	5.59	-28.34	7.62	-30.61	2.16	-26.81
	0.415	25.19	-25.71	4.18	-28.36	4.76	-31.06		
	0.615	15.11	-25.71	1.52	-27.66	1.12	-29.94		
	0.815	6.99	-25.81	0.78	-27.90				
	1.015	2.71	-25.66	0.28	-28.06	0.12	-28.24		
57.75	0.215	26.24	-25.89	5.88	-28.81	6.12	-31.44	2.38	-27.77
	0.415	19.04	-26.07	4.02	-28.68	3.41	-31.38		
	0.615	9.51	-25.90	1.75	-27.84	0.57	-29.55		
	0.815	5.89	-25.68	0.65	-28.00				
	1.015	4.56	-25.69	0.47	-28.23	1.33	-29.38	0.26	-25.87
71.45	0.215	26.27	-25.67	5.92	-28.54	6.20	-31.03	2.03	-27.14
	0.415	20.96	-25.76	3.48	-29.46				
	0.615	9.25	-25.51	1.42	-28.71	0.54	-31.56		
	0.815	7.71	-25.84	0.40	-28.37				
	1.015								
81.75	0.215	22.93	-26.06	5.48	-28.80	5.23	-31.21	2.00	-27.00
	0.415	13.97	-26.02	2.68	-27.99	1.26	-29.71	0.39	-26.85
	0.615	9.62	-25.71	1.15	-28.57				
	0.815	7.70	-25.91	0.32	-28.11				
	1.015	3.18	-25.47	0.05	-28.12				
96.8	0.035	38.31	-25.78	6.93	-28.16	10.13	-30.76	3.18	-26.77
	0.115	25.96	-25.80	4.38	-28.24	5.17	-30.57	1.74	-26.87
	0.165	32.89	-25.71	5.53	-28.31	5.47	-31.16	1.92	-26.84
	0.215	34.45	-25.71	6.20	-28.51	5.51	-30.54	2.49	-26.94
	0.315			3.46	-28.17	2.04	-29.57	0.93	-28.05
	0.415	24.43	-25.74	2.88	-28.44	1.13	-29.84	0.57	-28.12
	0.515			1.84	-28.08	1.20	-29.21	0.61	-27.84
	0.615	14.92	-25.79	1.21	-28.06	0.34	-28.90		
	0.815	8.62	-25.87	0.32	-29.17				
	1.015			0.04	-28.76				
145.3	0.035	41.53	-25.87	7.85	-27.97	11.55	-30.29	3.87	-27.12
	0.165	35.64	-25.77	6.47	-28.25	6.93	-30.45	2.71	-26.94
	0.215	26.77	-25.66	7.94	-28.84	4.98	-30.15	3.83	-27.98
	0.315	8.33	-25.61	1.15	-28.30	0.77	-30.87	0.23	-26.57
	0.415	19.29	-25.45	3.07	-28.32	1.93	-30.51	0.91	-27.32
	0.515			2.55	-28.32	1.45	-29.85	0.71	-27.84
	0.615	17.90	-25.80	2.08	-28.55	0.88	-29.99	0.47	-29.04
	0.815	10.18	-25.97	0.87	-28.65				
	1.015	3.83	-25.91	0.25	-28.88				
167.8	0.035	38.32	-25.90	7.03	-28.32	10.44	-30.51	3.24	-26.92
	0.065	37.93	-25.80	7.35	-28.51	10.63	-30.62	3.64	-26.84
	0.115	31.91	-25.66	5.56	-28.18	6.80	-30.34	2.33	-26.71
	0.215	31.88	-25.79	5.65	-28.50	6.26	-30.69	2.64	-26.83
	0.415	22.58	-25.65	3.03	-28.28	2.32	-30.06	6.73	-26.81
	0.615	13.36	-25.45	1.97	-28.54	1.01	-30.88	0.47	-29.77
	0.815	10.05	-26.08	0.86	-28.53	0.25	-31.81		
	1.015	3.70	-25.83	0.25	-28.81				

191.8	0.035	41.72	-25.82	8.85	-28.37	13.92	-30.29	4.80	-27.11
	0.115	38.01	-25.86	7.97	-28.42	10.62	-30.54	4.07	-26.70
	0.165	34.84	-25.84	7.09	-28.57	8.81	-30.50	3.48	-27.47
	0.215	25.74	-25.78	4.78	-28.58	5.63	-30.60	2.28	-27.04
	0.315	30.77	-25.84	5.78	-28.57	5.84	-30.87	2.80	-27.21
	0.415	24.61	-25.55	4.03	-28.03	3.57	-30.50	1.69	-26.71
	0.515				-28.46	1.47	-29.98		-27.02
	0.615	14.35	-25.71						
	0.815	9.37	-25.79	0.69	-28.29				
	1.015	3.88	-25.92						
263.75	0.035	48.60	-25.94	6.47	-28.99	12.86	-32.46	4.91	-29.86
	0.065	43.52	-25.51	7.23	-28.42	13.28	-31.33	4.74	-26.65
	0.115	39.33	-25.58	6.42	-28.61	11.34	-31.66	3.88	-26.14
	0.165	35.44	-25.59	5.49	-28.74	8.56	-32.05	2.79	-26.23
	0.215	42.33	-24.77		-27.43	8.30	-31.17	2.47	-25.55
	0.315			15.17	-27.97	17.11	-30.46	5.39	-26.57
	0.415			12.37	-28.07	11.69	-30.91	3.91	-26.48
	0.615	11.63	-25.23	0.93	-27.84				
	0.815	8.30	-25.35						
	1.015	3.01	-25.30						
311.6	0.035	40.63	-26.80	7.63	-29.10	13.72	-31.56	4.63	-27.85
	0.065	40.86	-25.71	7.74	-28.76	14.47	-30.97	5.19	-27.12
	0.115	34.67	-25.73	6.11	-28.78	10.37	-31.90	3.77	-26.76
	0.165	31.89	-25.68	5.28	-28.85	8.01	-31.65	2.72	-26.51
	0.215	14.70	-25.18	2.75	-27.54	3.25	-30.10	1.17	-26.69
	0.315			3.50	-28.42	3.88	-30.38	1.47	-29.06
	0.415	13.01	-25.56	2.03	-27.87	1.94	-30.20	0.65	-26.40
	0.615	14.22	-25.48	1.05	-28.25	0.51	-32.25		
	0.815	7.17	-25.17						
	1.015	1.98	-25.10						
336.1	0.035	42.24	-25.78	7.68	-27.90	13.90	-29.91	5.10	-27.10
	0.065	43.73	-25.54	7.33	-28.01	11.84	-30.14	3.82	-26.90
	0.115	39.20	-25.55	6.96	-28.06	12.00	-30.23	4.63	-26.99
	0.165	40.24	-25.44	6.72	-27.98	10.77	-30.20	4.16	-27.00
	0.215	27.95	-25.36	3.38	-27.60	4.98	-29.87	1.76	-26.48
	0.315			3.13	-27.74	3.50	-29.83	1.19	-26.64
	0.415	21.54	-25.38	2.23	-27.94	2.02	-30.44	0.90	-26.63
	0.615	14.47	-25.40	0.92	-28.28				
	0.815	6.29	-25.08						
	1.015	6.07	-24.31						

Table A-3: Concentrations and isotope ratios measured in the source chamber during the column experiment.

		pentane		hexane	
	time	conc	$\delta^{13}C$	conc	$\delta^{13}C$
	hours	mg/L	‰	mg/L	‰
Initial	0	129.24	-29.50	77.45	-29.51
source1	5	90.10	-29.41	65.07	-29.36
source2	12	74.65	-29.37	59.57	-29.45
source3	78	75.13	-28.63	83.30	-29.32
source4	102	58.77	-28.33	68.67	-29.18
source5	148	46.50	-27.74	72.05	-29.07
source6	168	38.56	-27.46	60.59	-28.85
source7	192	29.28	-26.81	56.39	-28.78
source8	264	13.59	-25.13	37.25	-28.39
source9	312	9.47	-24.27	37.69	-28.14
source10	336	7.44	-24.22	35.08	-27.79

		benzene		toluene	
	time	conc	$\delta^{13}C$	conc	$\delta^{13}C$
	hours	mg/L	‰	mg/L	‰
Initial	0	13.52	-26.81	6.11	-28.25
source1	5	11.29	-26.54	4.06	-27.16
source2	12	10.78	-26.95	4.43	-28.61
source3	78	21.13	-26.91	10.98	-28.55
source4	102	14.65	-26.82	7.46	-28.72
source5	148	14.35	-26.57	8.33	-28.56
source6	168	11.37	-26.53	6.02	-28.43
source7	192	11.01	-26.36	6.47	-28.57
source8	264	6.87	-25.81	3.49	-28.54
source9	312	7.66	-25.75	5.10	-28.18
source10	336	7.42	-25.60	5.45	-28.01

		isooctane		methyl-cyclohexane	
	time	conc	$\delta^{13}C$	conc	$\delta^{13}C$
	hours	mg/L	‰	mg/L	‰
Initial	0	42.12	-23.50	27.99	-25.88
source1	5	35.31	-23.53	23.68	-25.38
source2	12	32.70	-23.44	22.76	-25.30
source3	78	71.25	-23.50	49.62	-25.83
source4	102	54.89	-23.74	37.72	-25.94
source5	148	62.58	-23.62	40.38	-25.83
source6	168	49.86	-23.40	31.21	-25.67
source7	192	51.35	-23.52	31.85	-25.84
source8	264	34.37	-23.42	21.65	-25.40
source9	312	47.86	-23.66	29.75	-25.63
source10	336	50.61	-23.44	31.75	-25.45

		octane		m-xylene	
	time hours	conc mg/L	$\delta^{13}C$ ‰	conc mg/L	$\delta^{13}C$ ‰
Initial	0	7.92	-30.68	2.52	-27.13
Source 1	5	6.17	-29.82	1.61	-26.04
Source 2	12	6.78	-29.76	1.58	-27.03
Source 3	78	16.57	-30.67	4.65	-27.03
Source 4	102	11.91	-30.72	3.49	-27.17
Source 5	148	13.48	-30.77	4.20	-27.12
Source 6	168	9.29	-30.74	2.49	-26.92
Source 7	192	10.44	-30.65	2.92	-27.02
Source 8	264	4.74	-30.58	1.29	-25.89
Source 9	312	8.41	-30.02	2.39	-26.82
Source 10	336	9.70	-29.94	2.81	-26.75

Appendix B: Data from the field experiment

Table B-1: Isotope ratios measured during the field experiment at Vaerlose Airbase, Denmark

Hexane

Distance (m)	3 days	6 days	22 days	45 days	114 days
0	-30.5	-30.4			
0.55		-30.4	-29.1		
0.75	-30.8	-29.9	-29.3		-21.2
0.85		-30.5	-29.9		-21.4
1	-30.9	-30.8	-29.2	-28.5	-21.4
1.25		-30.8	-28.8	-27.9	-21.7
1.5	-32.6	-31.0	-28.9	-27.7	-21.1
2	-32.7	-30.9	-28.6	-26.8	
3	-35.5	-31.8	-28.7		

Methylcyclopentane

Distance (m)	3 days	6 days	22 days	45 days	114 days
0	-34.8	-34.9			
0.55		-35.1	-34.2		
0.75	-35.2	-34.2	-34.3	-34.1	-27.1
0.85		-35.4	-35.6	-33.0	-27.4
1	-35.6	-35.3	-34.7	-32.2	-27.2
1.25		-35.6		-32.4	-27.8
1.5	-36.8	-35.5	-34.1	-33.4	-27.0
2	-37.2	-35.7	-34.4	-32.0	-26.9
3	-40.5	-36.4	-33.9	-27.6	

3-Methylpentane

Distance (m)	3 days	6 days	22 days	45 days	114 days
0	-30.3	-30.20			
0.55		-30.10	-28.80		
0.75	-30.8	-29.80	-29.00		-19.65
0.85		-30.40	-29.70		
1	-30.8	-30.50	-29.00	-28.30	
1.25		-30.90		-27.80	
1.5	-31.9	-31.00	-29.10	-27.30	
2	-32.5	-31.00	-29.20	-26.80	
3	-34.4	-32.00	-28.90	-23.70	

Methylcyclohexane

Distance (m)	3 days	6 days	22 days	45 days	114 days	184 days	237 days
0	-28.1	-28.3			-26.5		
0.55		-28.2	-28.0		-26.1	-25.2	-25.3
0.75	-28.4	-28.1	-28.1	-27.3	-25.5	-25.3	-23.7
0.85		-28.2	-28.0	-27.6	-25.5	-25.2	-24.7
1	-28.4	-28.2	-28.0	-27.0	-25.6	-24.5	-24.5
1.25		-28.7	-28.1	-27.3	-25.6	-25.6	
1.5	-28.9	-28.5	-28.3	-27.1	-25.9	-25.0	
2	-31.9	-28.5	-28.1	-26.6	-26.4	-25.4	
3	-31.4	-29.6	-28.0				
5				-26.8		-27.1	

Toluene

Distance (m)	3 days	6 days	22 days	45 days	114 days	184 days
0	-26.7	-27.1			-24.2	
0.55		-27.2	-26.3			-23.8
0.75	-27.0	-26.5	-27.2	-25.9	-23.5	-21.8
0.85		-26.9	-28.0	-25.2	-23.7	-23.8
1	-26.9		-27.1	-26.1	-23.5	-23.1
1.25		-25.9	-27.1	-25.3	-23.7	-24.4
1.5	-28.3	-28.3	-27.2	-25.5	-25.0	-24.0
2	-30.1	-27.6		-25.1	-24.9	-23.4

m-Xylene

Distance (m)	3 days	6 days	22 days	45 days	114 days	184 days
0	-27.0	-26.5			-26.5	
0.55		-26.8	-26.4		-26.7	-26.3
0.75	-26.9		-26.7	-26.2	-26.0	-25.7
0.85		-26.3	-26.9	-26.3	-25.9	-26.4
1	-27.1		-26.8	-26.5	-25.5	-26.0
1.25		-25.8	-26.8	-26.3	-26.0	-26.6
1.5	-28.9	-26.0	-27.0	-26.5	-25.8	-25.8
2		-27.4	-27.3	-26.1	-26.5	-25.5

Octane

Distance (m)	3 days	6 days	22 days	45 days	114 days	184 days
0	-29.3	-29.4	-29.5			
0.55		-29.5	-29.5		-29.1	
0.75	-29.8	-28.9	-29.4	-29.7	-28.9	-28.8
0.85		-29.3	-29.5	-29.8	-28.8	
1	-29.7	-29.4	-29.7	-29.6	-29.7	
1.25		-29.6	-29.5	-29.1	-29.0	
1.5	-30.3	-29.8	-29.4	-29.4	-28.8	
2	-31.2		-29.6	-29.8	-29.7	-28.6
3		-30.4				

Isooctane

Distance (m)	3 days	6 days	22 days	45 days	114 days	184 days	237 days
0	-24.7	-25.2			-22.9		
0.55		-24.8	-23.8		-22.2	-21.6	-22.1
0.75	-24.7	-25.0	-23.9	-23.9	-22.1	-21.5	-20.5
0.85		-24.8	-23.8	-23.9	-21.9	-21.1	-21.2
1	-24.6	-24.9	-23.9	-23.8	-22.1	-21.0	-21.1
1.25		-24.9	-23.8	-23.9	-22.0	-21.7	-19.3
1.5	-25.1	-25.0		-23.7	-22.1	-22.0	
2	-25.7	-25.0		-23.1	-22.5	-21.7	
3	-27.7	-25.7	-23.9	-20.7	-21.7		
5			-23.6	-22.6		-20.9	

1,2,4-TMB

Distance (m)	3 days	6 days	22 days	45 days	114 days
0	-26.5	-26.5			-26.4
0.55		-26.5	-27.0		-27.2
0.75	-27.2		-26.7	-26.9	-27.1
0.85		-26.5	-26.6	-27.3	-27.0
1	-26.9		-26.8	-27.0	-27.6
1.25		-26.8	-26.5	-27.0	-27.1
1.5		-27.2		-26.9	-27.3
2		-28.6	-27.1	-26.6	-27.2

CO_2

Distance (m)	3 days	6 days	22 days	45 days	114 days	184 days
0	-23.2	-22.7				
0.55		-23.3				
0.75	-23.3	-21.6	-21.1		-25.8	
0.85		-22.6	-20.4		-25.6	
1	-23.4		-20.5		-24.8	
1.25		-23.2	-20.5		-25.8	-26.2
1.5	-24.0	-23.4	-18.4		-25.4	-23.7
2	-24.8	-23.4	-20.4		-25.7	-26.9
3		-24.8		-25.9	-25.1	
5				-27.6	-22.9	-22.9